INTERACTION BETWEEN LANDSCAPE AND POLLUTION ALONG A DAM CASCADE

Wei Ouyang

Examining committee:

Prof.dr. V.G. Jetten	University of Twente / ITC
Prof.dr. Z. Su	University of Twente / ITC
Prof.dr.ir. M.F.P. Bierkens	University of Utrecht
Prof.dr.ir. E.M.A. Smaling	University of Twente / ITC

ITC dissertation number 179
ITC, P.O. Box 217, 7500 AE Enschede, The Netherlands

ISBN 978-90-6164-300-5
Cover designed by Benno Masselink
Printed by ITC Printing Department

INTERACTION BETWEEN LANDSCAPE AND POLLUTION ALONG A DAM CASCADE

DISSERTATION

to obtain
the degree of doctor at the University of Twente,
on the authority of the Rector Magnificus,
prof.dr. H. Brinksma,
on account of the decision of the graduation committee,
to be publicly defended
on Friday 18 February 2011 at 14:45 hrs

by

Wei Ouyang

born on 16 October 1980

in Jiangxi, P.R.China

This thesis is approved by

Prof. dr. Andrew Skidmore, promotor
Dr. A.G. Toxopeus, assistant promotor
Dr. Tiejun Wang, assistant promotor

Dedicated to my wife and family

Acknowledgements

When I began writing the acknowledgements, I knew my PhD research at ITC (Faculty of Geo-Information Science and Earth Observation (ITC), University of Twente) really was coming to the end. The period in Enschede was so impressive and peaceful. It is difficult to find the proper words to express my appreciation to ITC and the people who have helped me in some ways or the other to complete this work, but I want to take this opportunity to use simple words to describe my deepest gratitude.

First of all I am grateful to the excellent supervisors behind me: Prof. Andrew K. Skidmore, Dr. Toxopeus A.G. and Dr. Wang Tiejun of ITC. Prof. Skidmore shared with me his innovative ideas, scientific attitude, invaluable guidance and encouragement throughout my research period. Without your support none of this was possible. The conversations between regular meetings yielded many innovative ideas.

Special gratitude goes to Prof. Hao Fanghua of School of Environment Beijing Normal University for her invaluable suggestions towards my research and the support of my professional career.

I thank ITC, University of Twente, for its financial support, which allowed me to peruse this research in the Netherlands. During this period, I also had discussions with many faculty members of ITC, and they gave me lots of invaluable suggestions and help. Dr. Ali Abkar, Dr. Kees de Bie, Dr. Thomas Groen, Dr. Martin Schlerf, Prof. Eric Smaling, Prof. Zongbo Su, Dr. Chris Mannaerts, Dr. David Rossiter, Mr. Anas Fauzi, Mr. Atkilt Girma, Dr. Nicky Knox, Ms. Tyas Mutiara Basuki and others, thank all of you.

I also thank my organization: School of Environment, Beijing Normal University for the supporting this study. Thanks also to the Forestry Academy of Qinghai Province, Data Center for Resources and Environmental Sciences Chinese Academy of Sciences (RESDC) for their help in data sharing and fieldwork.

I thank Prof. Martin Hale, Dr Paul van Dijk and Ms. Loes Colenbrander, who ensured that I had excellent research administration. I also express my gratitude to the education affairs department, financial department, library, information technology department and international hotel of ITC for their dynamic support. I also owe a great deal to Ms. Esther Hondebrink for her support.

I express my special gratitude to Prof. Srinivasan Raghavan of Spatial Sciences Laboratory Texas A&M University; Prof. Qi Ye from School of public management, Tsinghua University; Dr. Jan de Leeuw of International Livestock Research Institute; Associate Prof. Chen

Hongguan from School of Environment, Beijing Normal University; Prof. David C Duffy from Department of Botany, University of Hawaii at Manoa; Prof. Yang Shengtian of School of Geography, Beijing Normal University; Prof. Robert Wenger from Department of Natural and Applied Sciences, University of Wisconsin-Green Bay; Engineer Jeffrey G. Arnold Grassland Soil and Water Research Laboratory USDA-ARS; Prof. Nicola Fohrer of Dep. of Hydrology, Ecology, Kiel University, Germany; Prof. Allan C. Jones of Texas Water Resources Institute, Texas A&M University; Prof. Liang Xu from Department of Civil and Environmental Engineering, University of Pittsburgh.

Life at ITC was supportive, especially from Wang Tiejun, Wu Guofeng, Yang Zhengshan, Tian Xin, Li Longhui, Wang Guangyi, Qin Chanbo, Pu Shi, Zeng Yu, Zeng Yijian, Zhong Lei, Si Yali, Fei Teng, Bian Meng, Gao Wenxiu. When I stepped down the train, your smiling faces gave me much inspiration and encouragement.

I thank my family as they always support and encourage me. Last but not the least my deepest gratitude goes to my wife, Wang Xuelei, for her support and love.

Ouyang, Wei
ITC, Netherlands
2010

Table of Contents

List of figures

List of tables

x

Chapter 1 Introduction

1.1 Problem statement

Soil erosion and non-point source nutrient pollution are key issues that require serious attention for regional aquatic environmental protection. Soil erosion is an environmental issue in many countries, and specifically affects an area of 3.6×10^6 km^2 in China, which is about 37% of the land area in China (Ni et al., 2008). Generally, no significant improvement has been observed in Chinese water quality during the last several decades in spite of considerable efforts to reduce point source pollution. This may be due to the contribution of non-point sources (NPS) of pollution in both developed and developing countries (Leone et al., 2007). The major NPS pollutants are nitrogen (N) and phosphorus (P), and they are the major causes of water degradation in rivers and lakes. Non-point source nutrient pollution losses from farmland, grassland and forest are important factors limiting water quality (Ribarova et al., 2008; Munodawafa, 2007), which may influence the sustainable developments of the whole basin. Changes of land cover and landscape have direct connections with the formation and transportation of soil erosion and NPS nutrient pollution, which influence the watershed water quantity and quality (Eric et al., 2006).

At the watershed scale remote sensing may be used to observe the long-term land cover dynamics and the response of vegetation to disturbance from natural and human activities (Prasad et al., 2007). With series of Landsat and MODIS images, the temporal-spatial variation of land cover can be analysed with higher resolution.

Regular field monitoring cannot provide sufficient data for watershed soil erosion and NPS pollution analysis (Siegrist, et al., 1998). So, modelling is an alternative option to implement the particular study using local weather variables, soil properties, topography, vegetation and land management scenarios. Modelling has become the first choice for soil erosion and NPS pollution analysis and prevention (Tripathi et al., 2003).

Identifying the pollution source is a priority for the environmental management at a watershed scale. With the application of remote sensing and geographical methods, the interaction between the area of pollution loading and vegetation status was analysed (Vienneau et al., 2009). The critical pollution area can be identified by vegetation data, which can be calculated effectively with remote sensing images.

The study area is part of the upper catchments of the Yellow River. The local terrestrial environment is sensitive to the increasing burden of human disturbance. The exploitation of the hydroelectric cascade is the major human activity in this area and it is interesting to investigate the interaction of land use and landscape pattern on the accumulated impact of hydropower exploitation. The varied land cover and landscape pattern specifically alter the NPS pollution loading within the dam cascade. With

the hydrological model, the pollution loading is simulated and the interactions are identified, which is the key content in the thesis.

1.2 Research objectives

This study is designed to identify how land cover and landscape pattern varied during the last three decades. This is carried out using remote sensing data and the FRAGSTATS model. Also, the feedback of landscape and land cover on soil erosion and the concentration of NPS nutrient pollutants were examined. The aims of this study are as follows:

(1) to express the temporal-spatial dynamics of regional vegetation with MODIS images and analyse their relationship with climate;
(2) to identify the long-term land cover variation using Landsat Multispectral Scanner (MSS) in 1977, the national land cover database in 1996 and 2000, and Thematic Mapper (TM) in 2006
(3) to analyse the variation in landscape pattern and its correlation with exploitation of a cascade of hydroelectric dams in the period of 1977-2006.
(4) to simulate the regional soil erosion loading, sediment yield and NPS nutrient pollutant loading, and identify their response to the long-term variation of land cover and landscape pattern.
(5) to explore the relationship between the temporal-spatial dynamics of vegetation NDVI status with the corresponding soil erosion, sediment yield and NPS nutrient pollution.

1.3 Study area description

Considering the research problems and the characteristics in this study, and the available materials, the study was conducted at Longliu section in the upper catchments of the Yellow River basin, China.

The study area is the main catchment of the upper catchments of the Yellow River (Fig. 1-1). The climate of this area is continental, which is cold, dry and having an obvious seasonal variation. The average annual precipitation is about 411 mm, mainly falling as snow or rainfall, and the average yearly temperature is about -2.3°C, that includes a frost-free season (Feng et al., 2005). Grassland, which covers about 60% of the whole watershed area, is the principal land cover. The villages and farmland are concentrated along the main stream and reservoirs. Forest, woodland and grassland are found in areas of different elevation. In recent decades, a drying trend is the main environmental degradation concern in this region and poses a great threat to regional environmental stability (Wang et al., 2006).

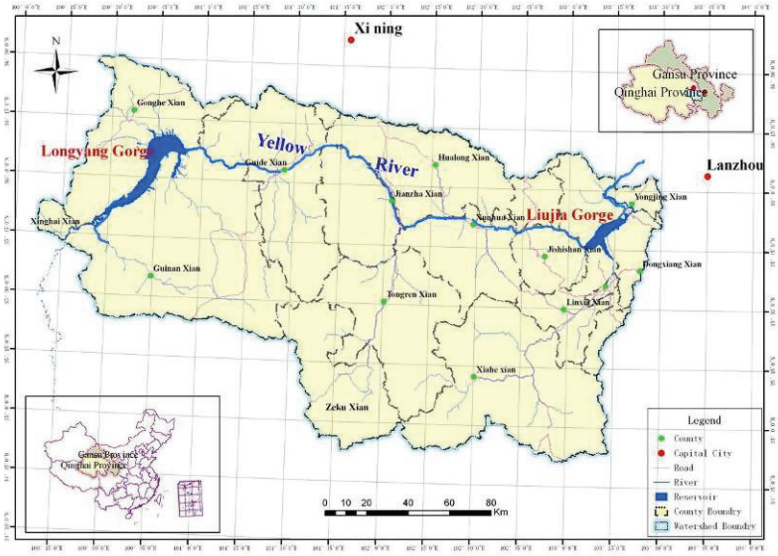

Fig.1-1 Study area of Longliu Section in the upper catchments of Yellow River

This area is economically under-developed and there is almost no industry. As part of Yellow River, with plenty of hydrological resource, the Longliu section is intensely exploited with regard to hydropower and has the longest history of hydropower exploitation. The Liujiaxia Reservoir was the first constructed in this section and is located at the outlet of the study watershed. Following that, the Longyangxia Reservoir lying at the inlet of this section was constructed from 1978. There are another six dams that came into service during the last ten years, located between the Liujiaxia and Longyangxia Reservoirs. The accumulated reservoir capacity is 32.5 billion cubic meters and the total dam height is 800.7 meter. The accumulated 6864 million Walt (MW) hydropower generators can provide 25.9 billion Kw•h electricity every year.

1.4 Thesis outline

Following this introduction, the other chapters were prepared as individual papers linked by the themes outlined in the section 1.2. The main content in Chapter 2 and Chapter 3 concerns land cover variation. The landscape pattern is discussion is Chapter 4. Then, the interactions of soil erosion with land cover and landscape are analyzed in Chapter 5 and Chapter 6, respectively. The final two chapters discuss the interrelationships of non-point source pollution with land cover and landscape. These papers have been published or submitted to the peer-reviewed international journals. The structure of this thesis is as follows:

Chapter 1 covers the research background, defines the research objectives, and describes the study area and presents the study outline.

The MODIS images and climatic data from local weather stations were analyzed in Chapter 2 and regional vegetation dynamics and climatic features were summarized.

Chapter 3 analyzes the long-term land cover variation during three decades using Landsat images and the national land cover database.

Chapter 4 explores the long-term landscape pattern variation and their interactions with exploitation of hydroelectric dams in the same period.

In Chapter 5, a SWAT database is constructed and model system validated. The influence of land cover transformation on soil erosion during three decades is discussed. The effectiveness of landscape services on soil conservation is assessed.

Chapter 6 links the dynamics of temporal-spatial vegetation with the corresponding soil erosion and river sediment yields. The response of various vegetation cover on soil erosion is explored.

Chapter 7 covers the interaction of landscape transformation with simulated NPS nitrogen and phosphorus loadings. The influence of vegetation cover on NPS pollution and transportation is identified.

Chapter 8 investigates the dynamics of NPS nutrient pollution and the temporal-spatial changes of vegetation. The pollution loading response to different vegetation NDVI and slope is analyzed.

Chapter 9 summarizes the results and conclusions of Chapter 2 to Chapter 8 and states the interactions of these chapters and requirements for future work.

The soil erosion and nutrient pollution simulation is based on the same database and model system, which was introduced in detail in Chapter 5. The references used in each chapter have some overlap, so all references are listed together.

Chapter 2 Regional vegetation dynamics with climatic feature

Abstract

Vegetation in the upper catchments of the Yellow River is critical for the ecological stability of the whole watershed. The dominant vegetation cover types in this region are grassland and forest which can influence strongly the eco-environmental quality of the whole watershed. The normalized difference vegetation index (NDVI) for grassland and forest has been calculated and its daily regression models in three years were deduced by using MODIS products on twelve dates in 2000, 2003, and 2006. The responses of the NDVI values of the inter-annual grassland and forest to three climatic indices (i.e. yearly precipitation, highest and lowest temperature) were analysed showing that, except for the lowest temperature, the yearly precipitation and highest temperature had strong correlations with the NDVI values of the two vegetation communities. The correlation coefficients of exponential regression equations ranged from 0.815 to 0.951. Furthermore, the interactions of the NDVI values of the vegetation with the climatic indicators at monthly interval were analysed. The NDVI of vegetation and the three climatic indices had strong positive correlations (larger than 0.733). The monthly correlations also provided the threshold values for the three climatic indictors, to be used for simulating vegetation growth in the regional grassland and forest under different climate variables, which is essential for the assessment of future quality of the vegetation and for regional environmental management.

Published as:

Ouyang Wei, Skidmore A.K., Toxopeus A.G., Hao Fanghua. Vegetation NDVI linked to temperature and precipitation in the Upper Catchments of the Yellow River. Revision submitted to Environmental Modelling and Assessment.

Parts of figures were posted in ISPRS 2008 Comm. VIII, WG VIII/3. Beijing 2008.

2.1 Introduction

The Yellow River is the second longest river in China and influences the ecological stability of northern China (Zhang et al., 2006). The eco-environmental quality, especially the vegetation coverage status in the upper catchment, is essential for the whole watershed (Neal et al., 2003; Xu and Yan, 2005). The local ecosystem is sensitive to fluctuations or changes in the typical continental climate. The dominant land cover types are grassland and forest, which influence strongly the water quality, quantity and sediment load (Wang et al., 2003; Zeng et al., 2003). Despite advances in the understanding of regional climate variation and its interactions with land cover processes, an accurate study of local vegetation dynamics using NDVI and climate-vegetation interaction in China has not been systematically undertaken.

Climatic and intensive human activities have influenced land cover condition and eco-environment quality (McAlpine et al., 2007). The vegetation growth in the upper catchments of the Yellow River is sensitive to temperature and it is an important indicator for monitoring possible climate variation (Zhou et al., 2007). Vegetation degeneration and wetland disappearance have resulted from human disturbance and global warming. The area of desertified land in the upper-stream region of the Yellow River is increasing at an annual rate of 1.83% (Qian et al., 2004). The water flow quantity in the Yellow River has experienced a steady decrease since the 1970s (Huang et al., 2009). The fluctuations in water flow have affected vegetation distribution and consequently a number of alpine meadows, resulting in the alpine meadows being threatened (Chen et al., 2003). Grassland degradation has been one of the important environmental concerns over the last several decades in the whole watershed (Yang et al., 2006). Although there have been some studies on climate variables in upper catchments of the Yellow River, few studies have connected climate variables with the monthly and annual vegetation dynamics. It is thus important to analyse vegetation dynamics in relation to the impact of climate.

The impacts of climate on regional ecosystem processes can be demonstrated by the response of vegetation to climate variables with the application of remote sensing technologies (RS). RS has the potential to monitor and detect land cover change at a variety of spatial and temporal scales, especially with high temporal resolution satellite data (Carlson and Arthur, 2000). The NDVI is calculated by the amount of reflectance in near infrared (NIR) and red (RED) portions of the electromagnetic spectrum and is an efficient indicator for the amount of green biomass in a landscape (Seaquist et al., 2003). The NDVI has been applied to measure biomass variables of land cover characteristics (Fensholt et al., 2004).

The temporal and spatial resolution of the RS data is an essential issue for many applications. In the last century, time-series AVHRR NDVI data with 1 km or 8 km spatial resolution have been widely used to classify land cover patterns at regional or continental scale. However, the coarse spatial resolution of the data has limited many applications (Hansen et al., 2002). From 2000 onwards, the Moderate Resolution Imaging Spectroradiometer (MODIS) instrument on board NASA's Terra satellite can scan 36 spectral bands is available, having a spectral range from the visible to thermal infrared wavelengths. The first seven bands are designed primarily for remote sensing of the land surface with a spatial resolution of 250m and the other bands are commonly referred to as 250 and 500 m (Running et al., 1994). The MODIS can provide moderate spatial and high temporal resolution data specify, which offers a good opportunity to monitor and analyse regional land surface processes. MODIS data has been commonly applied in diverse missions because of its advantages of providing daily data, and has offered new possibilities for studies over a large area (Loboda and Csiszar, 2007; Pflugmacher et al., 2007). The NDVI information from the MODIS 250m product has been applied in China already and has shown significant relationship with vegetation properties (Piao et al., 2006).

2.2 Material and methods

2.2.1 Study area

The study area is in the upper part of the Yellow River basin and is the connection of Qinghai–Tibet Plateau and Loess Plateau (Fig. 2-1). This region is the important water holding area for the whole Yellow River watershed and nearly 49.2% of its water flow comes from the region. The typical continental climate in this area is cold, dry, and its yearly average temperature is -2.3 °C. The vegetation consists of alpine meadow- and alpine steppe species, which are typical for the pasturelands in southern Qinghai Plateau. The deciduous forests are locates in the mountainous areas and the villages are mainly locates near the river and the reservoirs. Steppe widely appears in watershed and the desert steppe occurs in the west of the research area (Wang et al., 2006).

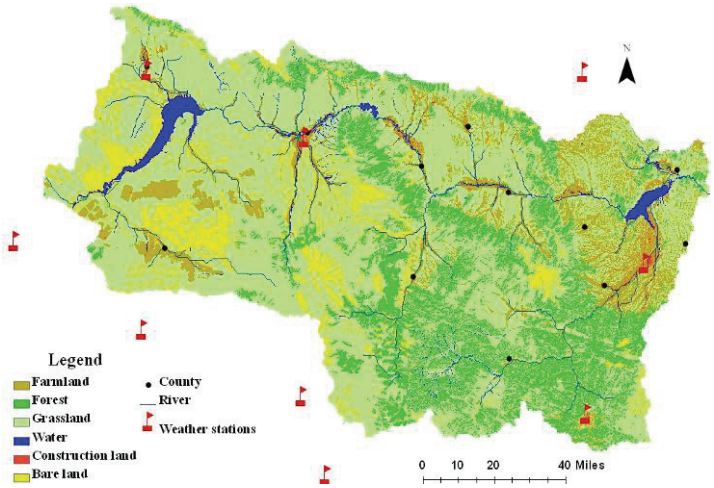

Fig. 2-1 Study area location, land cover and weather station distribution in the upper catchments of Yellow River

2.2.2 MODIS image processing

The NDVI data were extracted from the MODIS NDVI product (MOD13Q1), which were obtained from the land processes distributed active archive centre, NASA. The MODIS NDVI was calculated from the MODIS surface reflectance of the red band (610–680 nm) and near infrared band (780–890 nm), which were corrected with molecular scattering, ozone absorption and aerosols. This 250 m spatial resolution NDVI dataset has a temporal resolution of 16 days (Pontus et al., 2007). According to local land cover and climatic characteristics, a twelve series of MODIS NDVI data, starting from February 18 to December 18 in 2000, 2003 and 2006 were ordered using the EOS data gateway website. Data were required from the MODIS tile (h26 v05) for state-wide coverage. Then the NDVI images were mosaicked and geo-referenced to the Universal Transverse Mercator (UTM) projection system by using nearest-neighbour re-sampling method (William and Maik, 2005).

2.2.3 Regional meteorological processing

Precipitation is the a direct factor influencing vegetation primary productivity, especially in arid and semi-arid environments, but other climatic indicators, such as solar radiation, temperature and wind, have also impact on vegetation productivity (Okin et al., 2001). In order to analyse the relationship between vegetation biomass and climate, daily precipitation, highest temperature and lowest temperature were selected to express regional climatic characteristics. Weather information, monitored daily, was collected from nine local weather stations located in or around the study area (Fig. 1). The altitude of the stations ranged from 1814 m to 3500 m.

The yearly and monthly average rainfall, highest temperature and lowest temperature in 2000, 2003 and 2006 were used to explore the correlation with NDVI of vegetation. Three climatic variables were interpolated using ordinary Kriging method with latitude, longitude and elevation as independent variables. The ordinary Kriging includes the local variation as it uses a local neighbourhood centred on the location being estimated. This method considers the trend component to be stationary, thus the linear estimation is expressed as a linear combination (Belda and Melia, 2000; Carrera-Hernandez and Gaskin, 2007). Elevation was expressed in meters; latitude and longitude were expressed in units of degree. The spatial variation of the three selected climatic variables was expressed at a grid resolution of 250m, which was considered to be appropriate in order to represent the variation in the topographically dependent variables and having the same resolution of NDVI data from MODIS (Jeffrey et al., 2001).

2.3 Results

2.3.1 Vegetation NDVI characteristic

The regional land cover characteristics were analysed using the national land cover database in 2000 from the Data Center for Resources & Environmental Sciences, CAS (Fig. 2-1). The dominant land cover type was grassland, which occupied 59.57% of the whole area. Forest and farmland were accounting for 15.49% and 12.82% of the study area, respectively. Forest was mainly scattered in mountain area and with latitude higher than 2800 m. Construction areas, water and bare land occupied the remaining 12.13%. The grassland and forest together, which are considered to be the main part of land cover, covered nearly 75% of the whole study area. As especially these cover types have strong influence on the soil erosion and water holding capacity in the area, it was decided to selected these cover types to study the variation in land cover characteristics in upper steam of the Yellow River.

Thirty-six 250 m NDVI distribution maps of the indicated three years (2000, 2003 and 2006) were generated with monthly MODIS imageries. The regional NDVI data on Julian day 241 in 2006 were cited in Fig.2-2. There was a trend for the NDVI to increase from west to east. Moreover, there was a climbing trend presented along the southern plateau boundary and in the central-east region. In the area around the reservoir located in the west, especially the west bank, the dominant land cover was bare land and the NDVI value was low. There was also a large patch of bare land in the south-eastern part, close-to this reservoir and its NDVI value did not change much during the whole year. In the north-eastern part of the study area the NDVI varied intensively over time. During field investigations it was found out that this area was farmland and the major crops were wheat and maize.

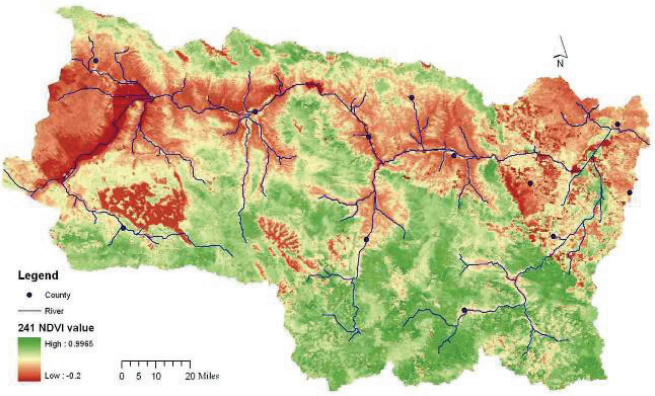

Fig.2-2 The studied watershed with the NDVI values from MODIS data (Julian day 241 in 2006)

Referring to land cover data, the NDVI values of the two dominant vegetation communities in the three selected years were derived and averaged from the MODIS images (Weiss et al. 2003). The mean NDVI of grassland and forest on twelve days in 2000, 2003 and 2006 were calculated to present the monthly growth dynamics. The NDVI values for the vegetation of all thirty-six days were statistically analysed by SPSS and the results are listed in Table 2-1. The NDVI values of the grassland fluctuated from a minimum (min) of 0.123 on the 49th day in 2000 to a maximum (max) of 0.528 on the 225th day in 2003. The NDVI values of the forest ranged from 0.146 to 0.711 in three years. The NDVI value for grassland in 2003 was 0.375, which was bigger than those in the two other years. The NDVI range of forest in 2003 was the lowest one. Despite different climatic conditions, the minimum NDVI values for grassland and forest were recorded on the 353rd day in 2000 and on the 49th day in 2006. However, the maximum NDVI seemed to have a different pattern. The maximum NDVI values in 2003 and 2006 were recorded on the 255th day and on the 177th day in 2000, respectively. The mean NDVI demonstrated that the NDVI values for both the grassland and forest increased from 2000 to 2006.

Table 2-1 Statistical analysis of NDVI of grassland and forest in 2000, 2003 and 2006

Index \ Year	Grassland			Forest		
	2000	2003	2006	2000	2003	2006
Range	0.356	0.375	0.313	0.566	0.439	0.566
Min	0.130	0.153	0.190	0.146	0.255	0.254
Min Day	49	353	49	49	353	49
Max	0.486	0.528	0.503	0.712	0.694	0.676
Max Day	177	225	225	177	225	225
Mean	0.307	0.323	0.345	0.433	0.448	0.463
Std. De	0.137	0.142	0.126	0.208	0.179	0.169

The monthly NDVI variations of the two vegetation communities could be shown more clearly from Fig. 2-3. The NDVI value of the vegetation began to drop from the middle of August. The NDVI value of the vegetation in 2003 and 2006 were overlaid for most of the period. The vegetation did not grow obviously during the first three months of 2003 and 2006, but had a higher NDVI in the middle of the year. The NDVI value of vegetation in spring of 2000 was much lower than that of the other two years and the maximum value occurred a month earlier than in normal occasions. With the standard deviation (Std. De) analysis, the NDVI value of vegetation became more concentrated from 2000 to 2006.

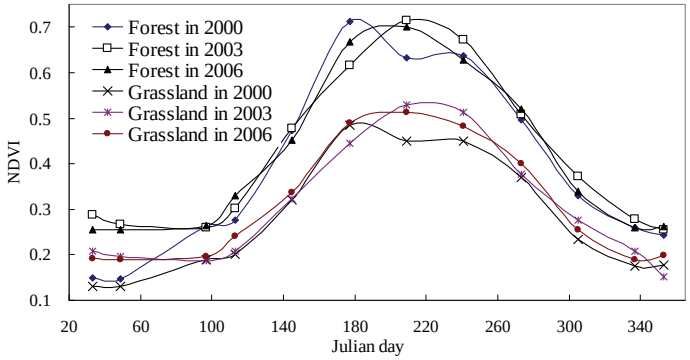

Fig.2-3 NDVI variation of grassland and forest in the years 2000, 2003 and 2006

Time series regression models of the NDVI variations of grasslands and forest in these three years were deduced (Table 2-2). All these exponential dynamic models had a strong coefficient of correlation determination (R^2), which ranged from 0.815 to 0.951. The higher R^2 value indicates that the models can objectively describe the daily variation of NDVI values in the vegetation. All the forest regression models are more significant than the grassland models. The regional NDVI value of vegetation could be calculated and assessed daily by using

these models. The NDVI of vegetation is an important index for environmental simulation and assessment. With simulated NDVI under similar climatic condition, the daily vegetation quality can be quantified conveniently, which can indicate regional eco-environmental quality. So, these analyses help regional environmental management.

Table 2-2 Regression models of NDVI of grassland and forest in three years

Year	Land cover	Regression model	R^2
2000	Grassland	$y = 0.0813*e^{0.0095x}$	0.951
	Forest	$y = 0.0969*e^{0.0106x}$	0.949
2003	Grassland	$y = 0.1068*e^{0.0079x}$	0.815
	Forest	$y = 0.1645*e^{0.0071x}$	0.828
2006	Grassland	$y = 0.1262*e^{0.0072x}$	0.874
	Forest	$y = 0.1688*e^{0.0073x}$	0.885

Note: When Julian day (d)≤210, x=d; when d> 210, x=420-d

2.3.2 Climatic data calculation

The interpolated yearly precipitation distributions of three years are mapped in Fig. 2-4 A. There is a similar rainfall distribution trend in three years. The precipitation becomes less from south-east to north-west. Much rainfall occurred in 2006, which was 671.77 mm. The interpolated regional annual highest and lowest temperature in three years has a same distribution trend, but is different from the precipitation (Fig. 2-4 B and C). In the north-eastern of study region, there are warmer than the west-southern. The highest annual highest temperature was 5528.67 degree in 2006. Moreover, the same year had the least lowest temperature, which was 856.76 degree. The yearly highest temperature in the coldest 2000 was 5234.63 degree and the yearly lowest temperature was -356.44 degree.

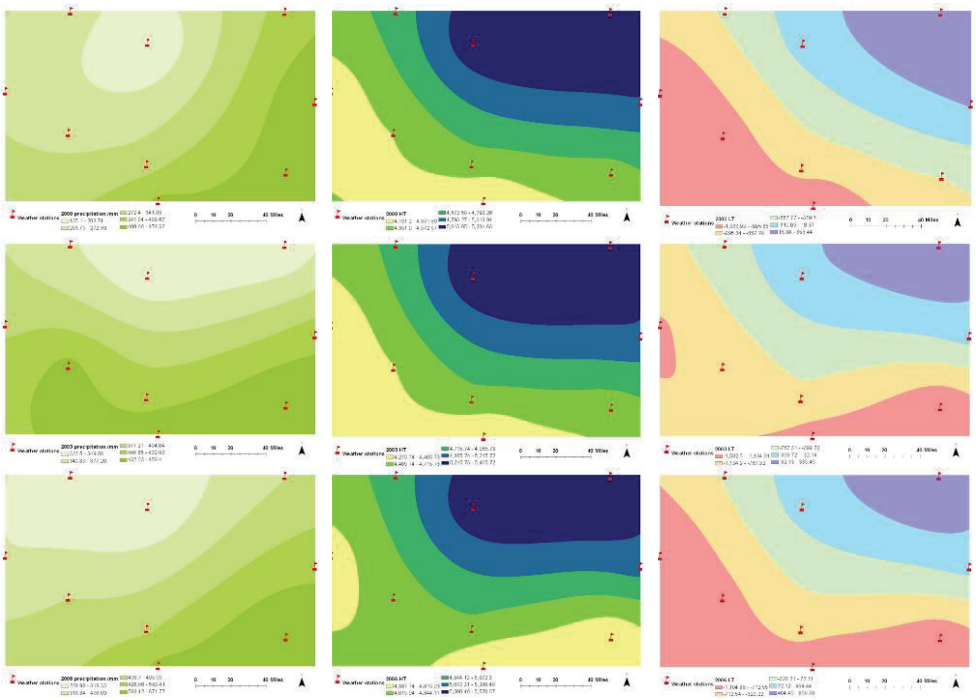

A Precipitation B Highest temperature (HT) C Lowest temperature (LT)

Fig.2-4 The annual climatic index distribution after interpolation

Based on the interpolated data, the watershed yearly climatic information in 2000, 2003 and 2006 were averaged. The annual precipitation in three years is 301.80, 396.04 and 426.03 mm, respectively. The yearly highest and lowest temperatures are also listed in Table 2-3. The highest and lowest temperature both climbed from 2000 to 2006, which demonstrated a warmer climate. The temperature increased much more from 2003 to 2006 than 2000 to 2003. The meteorological index was also calculated by simple average method from nine weather stations. The averaged value is much close to the interpolated value. The principal absolute difference of annual precipitation is just 19.39 mm (6%). The difference of yearly lowest temperature is the biggest and the relatively difference is 12.4%. The average yearly highest temperature is close to the interpolated value and the biggest relative difference is only 1.5%. Overall, the interpolated value of three climatic indices is similar to the averaged data. So, in the process of monthly correlation analysis, the watershed monthly precipitation, highest and lowest temperatures are just averaged of daily monitoring data from all nine stations.

Table 2-3 Comparison of meteorological index after interpolation with directly averaged

Index	Yearly precipitation /mm			Yearly HT/°C	
Year	2000	2003	2006	2000	2003
Averaged	321.19	398.77	437.67	4641.81	4780.56
Interpolated	301.80	396.04	426.03	4698.51	4851.53
Difference	19.39	2.72	11.64	56.70	70.98
Error Percent	6.0%	0.7%	2.7%	1.2%	1.5%
Index	Yearly LT /°C			Yearly HT/°C	
Year	2000	2000	2000	2006	
Averaged	-633.91	-633.91	-633.91	4885.69	
Interpolated	-596.19	-596.19	-596.19	4942.84	
Difference	37.72	37.72	37.72	57.15	
Error Percent	6.0%	6.0%	6.0%	1.2%	

2.3.3 Yearly correlation analysis

It is hypothesized that significant positive relationships may appear between climatic variables and the NDVI value of vegetation. In order to explore inter-annual correlation between them, the annual mean NDVI in each year was selected to present the greenness growth. The precipitation and the highest- and lowest temperature were employed to describe climatic features. The correlation between NDVI of vegetation and precipitation is shown in Table 2-4. The NDVI of the grassland and forest increased with the precipitation and the R^2 value between them were 0.869 and 0.914, respectively. When annual precipitation increased from 301.8 mm in 2000 to 426.0 mm in 2006, the NDVI value of grassland climbed from 0.307 to 0.345. At same time, the NDVI value of forest increased to 0.463. The analyses proved that more precipitation would definitely cause higher NDVI value of vegetation.

The NDVI of vegetation also had a strong positive linkage with the yearly highest temperature, so higher temperature led to higher NDVI value of vegetation. Although forest had a stronger relationship with NDVI of vegetation than grassland, the yearly lowest temperature did not have a close correlation with NDVI of vegetation.

Table 2-4 Correlation between climatic index and vegetation NDVI

Dependent (X)	Regression equation	R^2
Yearly precipitation	$NDVI_{Grassland} = 0.0003 * X + 0.2215$	0.869
	$NDVI_{Forest} = 0.0002 * X + 0.3672$	0.914
Yearly highest temperature	$NDVI_{Grassland} = 0.0002 * X - 0.4094$	0.950
	$NDVI_{Forest} = 0.0001 * X - 0.1172$	0.977

2.3.4 Monthly correlation analysis

Analysis of the correlation between annual climatic index and NDVI of vegetation showed that the lowest temperature did not have strong relationship with greenness growth. In order to examine this correlation in more detail, correlations were calculated between monthly climatic variables and NDVI of grassland and forest. The same three climatic variables were correlated with the monthly NDVI of vegetation, and the results of the analyses are presented in Fig. 2-5. The NDVI of grassland and forest were exponentially correlated with monthly lowest temperature and the R^2 values were 0.862 and 0.838 respectively. The monthly highest temperature was less strongly correlated with NDVI of vegetation, as the R^2 value with grassland and forest were 0.823 and 0.816, respectively. The NDVI of forest had the lowest interaction with precipitation, but the R^2 value was still 0.733. The widely distributed grassland had a higher R^2 value with climatic indicators than forest, which meant that grassland was more sensitive to the variations in the weather. The expectation of a positive correlation between the climatic index and NDVI of vegetation has been confirmed.

Fig.2-5 also demonstrates that the monthly climatic indicators are concentrated in two zones (left zone and right zone). In the left zone of the two temperature indices, the vegetation NDVI just fluctuated a little, but increased rapidly in the right zone with higher temperature condition. The conjunction point of two zones was the threshold value of the temperature, beyond which vegetation began to grow. Furthermore, the threshold values of the lowest and highest temperature for the two vegetation zones were the same, 0 and 13 respectively. Although the NDVI of vegetation increased in the left zone when relating it to precipitation, beyond the threshold point (14 mm), vegetation NDVI climbed into a higher step, but remained steady stage. Summarizing, analyses of the correlation between the monthly climatic variation and NDVI of vegetation provided threshold data of precipitation and temperature for inducing the growth of the vegetation.

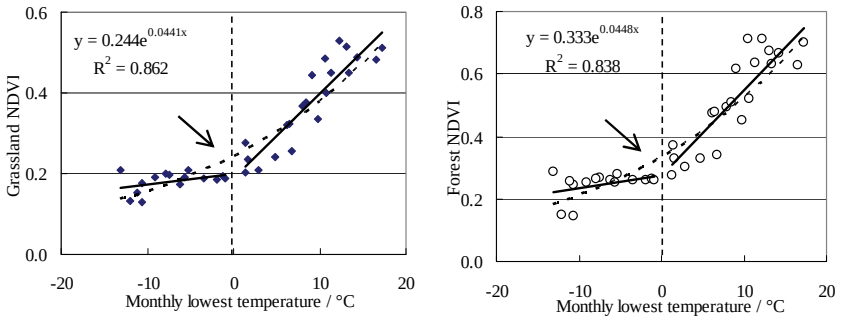

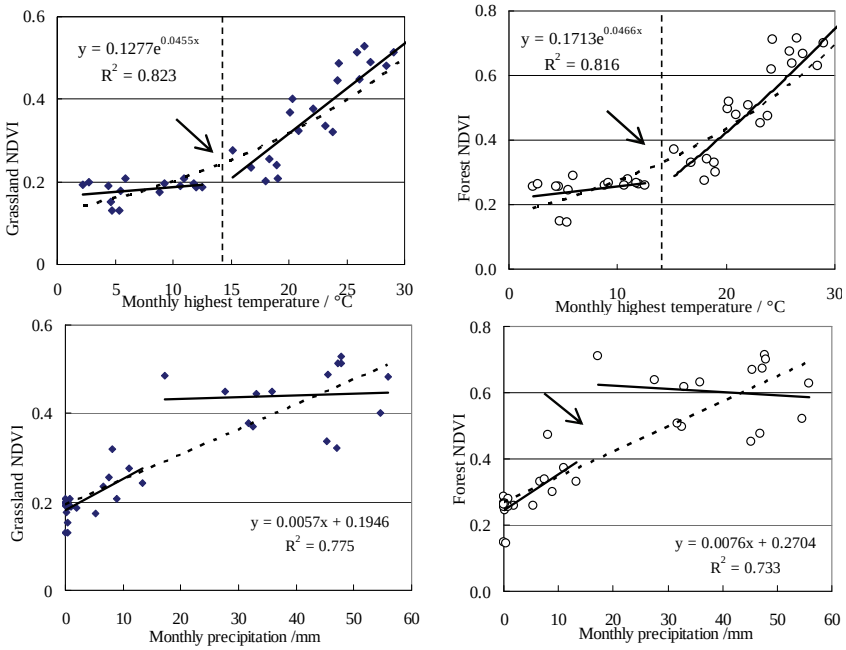

Fig.2-5 Correlation model between grassland, forest NDVI and monthly meteorological variation

(General regression trend line---, group regression trend line⁻, threshold point →)

2.4 Discussion

2.4.1 Correlation of NDVI and climatic indicators

Our inter-annual correlation equations show that the grassland and forest NDVI could increase by 0.003 and 0.002, respectively by 10 mm more precipitation. The sensitiveness for the highest temperature was less significant than that of the precipitation, but still had a high R^2 value. The R^2 values of the three monthly climatic indices with NDVI are higher than 0.733, which demonstrates strong interactions between them.

The increased NDVI of vegetation can improve local ecosystem stability. Dense vegetation cover can reduce soil erosion, resulting in better water quality (Arsenault and Bonn, 2005). Furthermore, as the NDVI of regional vegetation can be predicted using climatic parameters, future NDVI of vegetation can be predicted when consideration possible climate variation, which, in turn, can improve the efficiency of environmental management. The lowest temperature, not precipitation, is much correlated with NDVI, as might have not been anticipated from previous studies (Lin et al., 1996). The correlations between climatic indicators and NDVI of vegetation have been observed for a long period, which demonstrates complex relationships between vegetation growth and

climate variables (Fritts, 1974). In a similar arid region, Weiss (2004) also proved that precipitation was not principally correlated with NDVI change of vegetation. Climate change across Qinghai-Tibet Plateau has been modulated on decadal-century time-scales. The scientists have predicted that the temperature in the whole Qinghai–Tibet Plateau will increase with 0.20 every century (Long et al., 2006). The regional severe drought periods have happened in recent decades. Consequently, the correlation model between climatic index and NDVI can be used to simulate regional NDVI variations of vegetation.

2.4.2 Application in regional environmental management

Vegetation cover had significant interactions with diffuse pollution formation and transportation. In this paper, the temporal interactions between vegetation and climatic indicators were analysed. The climatic data has been monitored every hour at local stations, which are a reliable data source for analyses of regional environmental processes. With the correlations achieved in this paper, the vegetation status can be simulated effectively at a higher resolution of temporal scale. Furthermore, with the help of the finding of this study also the other eco-environmental index (i.e. soil erosion, non-point source pollution) can be estimated and or predicted in a much better way, which is an essential starting point for regional environmental management. With China's Westward Development Plan, the regional economic development will impose more pressure on local environmental quality conservation. The water resource in the upper catchments of the Yellow River will attract more attention, as eight dams already have been constructed in this area, which will have a direct influence on the regional landscape pattern. In future, even more dams are planned to be constructed in the upper catchments of the Yellow River. The findings in this study will be applicable and fundamental in the process of preserving land cover and minimizing negative environmental impact.

2.5 Conclusions

By applying NDVI and climatic data from 2000 through 2006, time series of grassland and forest communities NDVI simulation models were developed for the upper catchments of the Yellow River. The results confirm the utility of NDVI as an index to express vegetation variability in a watershed with continental climate at high latitude and with little precipitation. The findings also added knowledge of complex understanding about climate and vegetation. The inter-annual and monthly relationships between grassland and forest NDVI with climatic variables have been estimated. The correlation coefficients confirmed the strong relationships between NDVI of vegetation and climate characteristics. The strongest inter-annual correlation between climatic variables and NDVI of vegetation were precipitation and the highest temperature, which were completely different from the monthly correlation pattern. Overall, the research results indicate that the

monthly lowest temperature has the pronounced impact on land cover change. The monthly highest temperature and precipitation also remarkably affect NDVI value of vegetation. By using monthly correlation analyses, the threshold values of three climatic indictors can also be calculated.

As stated in this study, correlations between NDVI of vegetation with climatic variables have implications for research on climate and vegetation in the upper catchments of the Yellow River. With the results from the present study, the daily variation of the regional vegetation can be predicted under similar climatic conditions. The response of NDVI of regional vegetation to climate variables can be assessed much more accurately by using climatic data, which is important for vegetation assessments. The other eco-environmental factors can be calculated further from vegetation quality simulation and prediction.

Chapter 3 Long-term land cover variation analysis

Abstract

The eco-environmental impacts for dam constructions, especially successive dam constructions and operations, are the main concerns in regional environmental management. However, there is a widespread lack of detailed data to support the systematic assessment of the impacts of hydropower cascade exploitation over long periods. During the period of 1977–2006, the variations of land cover in the upper catchments of Yellow River for successively eight dam constructions were investigated using remote sensing data. Landsat Multispectral Scanner (MSS) and Thematic Mapper (TM) data were applied to produce land cover maps for the years 1977 and 2006. In combination with data from the national land cover database in 1996 and 2000, the data in these four years were applied to analyse land cover dynamics over three decades. The six first-level types land cover change principles were concluded after matrix calculation. The grassland was a extensively converted type, which reduced from 2162346 ha (63.07%) in 1977 to 2041691 ha (59.57%) in 2006. The other five categories land cover area increased over the three decades. Furthermore, the conversion area was mapped out by transformation matrix analysis, which can assess the impact range for the dam disturbances.

Published as:
Ouyang Wei; Hao FangHua; Li Gang; Shi Xuying. Land cover variation for hydropower cascade exploitation in the Yellow River Basin in 1977-2006. International Conference on Earth Observation Data Processing and Analysis (ICEODPA). Proc. SPIE, Vol. 7285, 72854Y (2008); DOI: 10.1117/12.812376.

3.1 Introduction

There are more than 40000 large dams on the world's rivers and to date, nearly 29000 dams have been constructed in China (Wang et al., 2007). These dams can provide extensive economic benefits, but they also disturb the fluvial processes of rivers and impact upon the environmental characteristics of the watershed. The eco-environment aggradations have taken place in many rivers (Wang et al., 2007; Jiao et al., 2007). In recent decades, the Yellow River has experienced a dramatically decreasing water flow discharge since the construction and operation of large reservoirs, which are mainly located in the upstream catchment (Ta et al., 2007). The regional environment is extremely fragile and difficult to recover, the eight successive dams construction deliver impacts on land cover. Studies of the detailed land cover change and its interaction with hydroelectric cascade exploitation can help to explain the spatial extent and the degree of the change itself, but also assist to predict the change directions for future dam construction.

Dams are constructed for diverse purpose, such as to control seasonal flood, to generate hydroelectric power and to provide a better supply of water resources. However, dams also cause negative impacts on natural environment (Sahin and Kurum, 2002; John and Stuart, 2002). Hydropower dam construction affects the regional eco-environment by increasing the area of open water decreasing total suspended solids. The water flow regime has been found to change significantly after the service of the dam (Jørn et al., 2005; Matti and Olli, 2007). After the dam goes into operation, the irrigation condition is improved and the water table depths will increase, which lead to conveniently access of water. As a result, the farmland area will increase and cropping patterns shift (Ashraf et al., 2005). On most occasions, the communities living in close proximity to large dams were often affected by the hydropower resources explorations (Leonard and Thayer, 1999). With the hydrological and social economic impacts, the watershed land cover /land cover will also change consequently, which is the monitoring index in this paper. Whether or not to continue exploit hydropower by dam construction has become an increasingly important topic of widely debate in developing countries, as well as in developed countries (Han et al., 2007). However, those impacts identifications and assessments are mainly about single dam constructions (Pamo and Tchamba, 2001; Gordon and Meentemeyer, 2006). However, there is a widespread lack of detailed data to support systematic assessments of the long-term impacts of hydroelectric cascade exploitation. By the advance of remote sensing technologies, the study about the land cover change by hydroelectric cascade exploitation in watershed has become feasible and reliable.

Studies have demonstrated that remotely sensing (RS) data can provide both actual and spatial information for land cover monitoring and

analysis, especially watershed scale area over long period which is difficult to monitor by conventional techniques (Adel and Ryutaro, 2007). In order to investigate long period land cover transformation principle, the combination of multi-source remote sensing is an effective approach. Fabio (2004) successfully used the NOAA-AVHRR, Landsat TM and ETM+ images to produce long-term NDVI data series for forest assessment in Tuscany (Central Italy). Achim (2005) have proved the Landsat TM and MSS data can be inter-calibrated each other. Geographical Information Systems (GIS) tools treat the information extracted from remotely sensed data and the analysis results can be applied as primary base for regional environmental impact identification and management (Ning et al., 2006, Marc et al., 2007). This paper focuses on the data from integration of Landsat series data. The Landsat MSS data has been widely applied for multi-temporal land cover analyses for its availability for over long period. The MSS image has large area coverage and is highly economic efficiency (Hostert et al., 2003). The later launched Landsat TM data also can provide high quality and frequently time-series data for a wide variety of environmental applications, ranging from regional land cover analyses and vegetation simulation (Lorenzo et al., 2008).

3.2 Material and methods

3.2.1 Study area

The study area is the upper part of the Yellow River watershed (Fig.3-1). Its lower control section is the outlet of Liujiaxia reservoir and the upper control section is the end of Longyangxia reservoir. For this reason, the study area between two sections is named Longliu Section. This area locates in upper catchments of Yellow River basin and is the connection area of Qinghai–Tibet Plateau and Loess Plateau. This region is the important water holding area for the whole watershed and about 49.2% of the water flow comes from here.

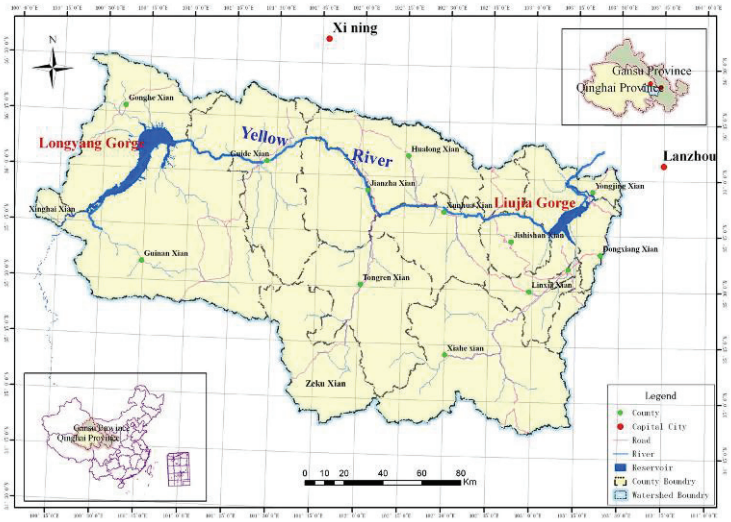

Fig.3-1 Study area of Longliu Section in the upper catchments of Yellow River

3.2.2 Image acquisition and pre-processing

Regional land cover data from 1996 and 2000 were directly extracted from the national land cover database, acquired from Data Center for Resources and Environmental Sciences, Chinese Academy of Sciences (RESDC). These two sets of data were interpreted from Landsat TM series of images. Landsat MSS and TM image data of 1977 and 2006 (Table 3-1) were manually georeferenced, and then interpreted, classified with references to available databases of 1996 and 2000 and also classified into six first level categories: Grassland, Farmland, Construction land, Forest, Water area, Bare land (Table 3-2). The classification procedure is similar to that of the national database scheme, which is designed to minimize system errors during landscape metric calculation (Liu et al., 2005). For the limitations of proper images repetition, we choose the image data according to the same season. Table 3-3 presents the error matrix and accuracy assessment for land cover classification in 2006. The 88 check points were selected randomly across the study area and were located by Global Positioning System (GPS) in August 2007. The overall accuracy of classification is approximately 86.34%.

Table 3-1 Description of Landsat images

Date Track/frame	Landsat 1 MSS	Landsat 5 TM
131/35	04 Jan. 1974	05 Aug. 2006
131/36	14 Jul. 1977	05 Aug. 2006
132/35	15 Jul. 1977	10 Sep. 2005
132/36	15 Jul. 1977	10 Sep. 2005
133/35	22 Feb. 1977	20 Sep. 2006

Table 3-2 Land cover reclassification scheme

First level land cover type	Original land cover type
Grassland	Dense grass, moderate grass, sparse grass
Farmland	Paddy land, dry land
Construction land	Urban built-up, rural settlements
Forest	Forest, shrub, woods
Water area	Stream, river, lake, reservoir and pond
Bare land	Sandy land, swampland, bare soil, bare rock

Table 3-3 Classification accuracy evaluation of land cover in 2006

Class name	Reference totals	Classified totals	Number correct	Producers accuracy	Users accuracy
Farmland	10	13	9	90.00%	69.23%
Forest	12	13	11	91.67%	84.62%
Grassland	32	36	30	93.75%	83.33%
Water area	15	13	11	73.33%	84.62%
Construction land	8	11	7	87.50%	63.64%
Bare land	11	13	9	81.82%	69.23%

3.3 Results

3.3.1 Watershed land cover variation from 1977 to 2006

The land cover distribution in 1977, 1996, 2000, and 2006 were mapped in Fig.3-2 A-D. The natural vegetation, consisting largely of forest and grassland, is the dominant land cover category in the study area. The forest and grassland occupy 15.49% and 59.57% of study area in 2006, respectively. The farmland, which accounts for 12.82% of land cover in 2006, is mainly distributed alone the river and around the reservoirs. In the north-eastern part of study area, the farmland is widely spread. Forests principally are situated in the central and southern parts of the watershed, which is a mountainous area. A high proportion of bare land is located in the western part. By evaluating land cover maps, six kinds of land cover transforming processes in four observed periods were identified and statistics results are presented in Table 3-4.

Table 3-4 Area of six types land cover in Longliu Section from 1977 to 2006

Land cover	1977		1996	
	ha	%	ha	%
Farmland	410355	11.97	384582	11.40
Forest	527936	15.40	491598	14.34
Grassland	2162346	63.07	2136788	62.34
Water area	53919	1.57	60597	1.77
Construction land	2464	0.07	21558	0.45
Bare land	271427	7.92	332419	9.70
Land cover	2000		2006	
	ha	%	ha	%
Farmland	392696	11.46	392696	11.46
Forest	489799	14.29	489799	14.29
Grassland	2125454	62.01	2125454	62.01
Water area	72405	2.11	72405	2.11
Construction land	19701	0.57	19701	0.57
Bare land	327487	9.55	327487	9.55

The grassland percentage reduced intensively from 1977 (63.07%) to 2006 (59.57%), which was the biggest area conversion with 120655 ha grassland disappearing over this period. After the eight reservoirs had come into service, the water area was increased from 53919 ha in 1977 to 78124 ha in 2006. The forest area decreased from 527936 ha in 1997 to 489799 ha in 2000. However, the forest area increased again over the last several years to 530756ha, which was even more than the original area. The reduction in grassland coincides with the increase of other five land cover types. The bare land experienced a remarkable increase from 271427 ha to 332419 ha in the period of 1977-1996. In recent ten years, some policies have been implemented to improve vegetation cover rates and better local ecosystem, so the bare land decreased down to 316043 ha in 2006. But the finally added 44616 ha was the biggest area increase of all six types. The farmland decreased from 1977 to 2000, but increased in the period of 2000-2006. Finally, there were 35076 ha in 2006 more than thirty years ago, which was the second most increased category. The construction land increased dramatically from 2464 ha in 1977 to 21558 ha in 1996. However, it continually declined to 15349 ha from 1996 to 2006.

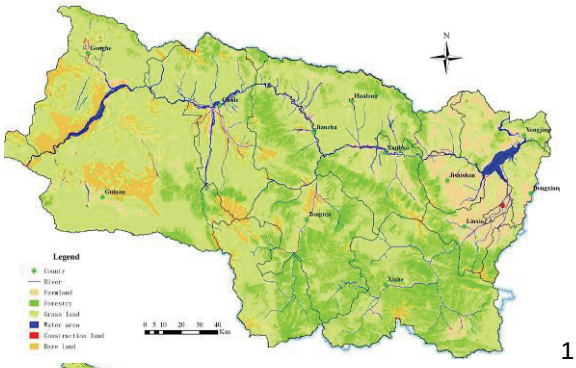

1977 A

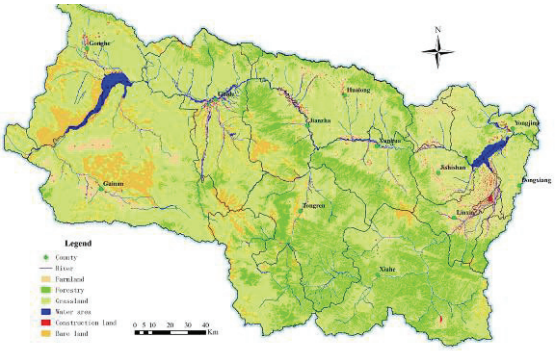

1996 B

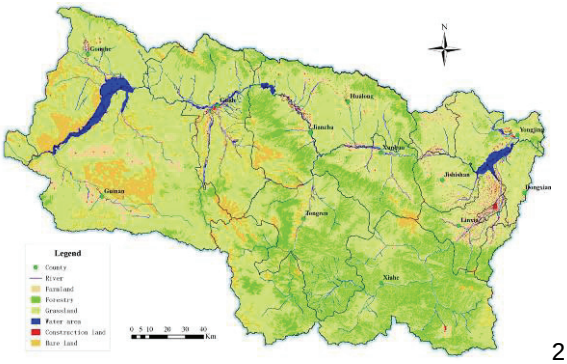

2000 C

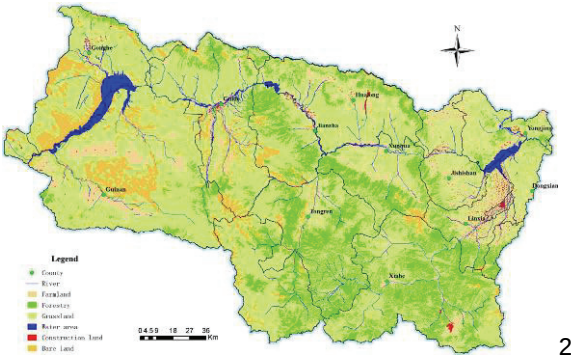

2006 D

Fig.3-2 Time series land cover distribution in 1977, 1996, 2000 and 006

3.3.2 Grassland transformation with other land covers

During the 1977-2006, dramatic land cover changes occurred on the grassland. For this reason, the grassland is selected to explore regional land cover transformation principle with other five types and map variation locations in three analysis periods. Conversion of grassland to other five land cover types from 1977 to 1996 is illustrated in Fig.3-3. In this period, the Longyangxia Reservoir was built and the mainly influenced land cover was the bare land. Only the grassland situated in the river beach was covered by water after two giant dams come into service. Some patches of grassland located in the central mountain area were transformed into forest in the course of the study period. In the south-western area, some farmlands were converted from forest. Referring to digital elevation data, most of forest degradation was detected at the edges of forestry and grassland in the base of slope. Some farmlands were changed into grassland and most of these conversions occurred in the northeast, especially around the Liujiaxia Reservoir. At same time, a large patch of grassland in the north of Guinan was changed into farmland.

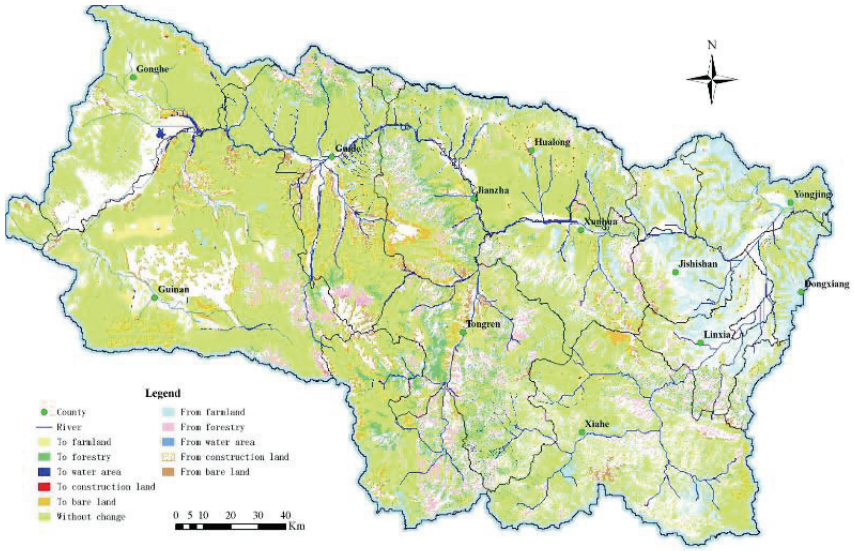

Fig.3-3 Transformations of grassland and other five land covers from 1977 to 1996

Fig.3-4 shows the converted grassland in the study area between 1996 and 2000. In this period, some farmland patches located in eastern (South of Jishishan) and western (Northwest of Guinan) of study region were converted into grassland. Alternatively, some grassland in north of Guinan were cultivated with crops. A small area of grassland in west changed into bare land.

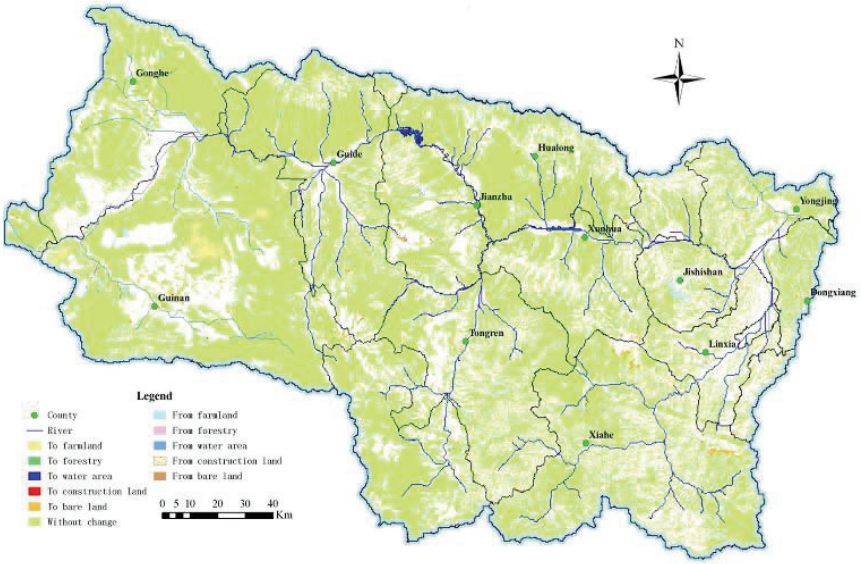

Fig.3-4 Transformations of grassland and other five land covers from 1996 to 2000

The grassland transformation with other five categories of land cover is demonstrated in Fig. 3-5. With dams constructed from 2000 to 20006, the water covered the grassland along the river beach in the middle of study area. Moreover, the original grassland around Longyang Reservoir disappeared for the increased water level. In the mountain area of central study watershed, some patches of grassland were converted into forest. From 2000 to 2006, some bare lands were detected to be transformed into grassland, especially the bare land in southwest of study area has become greenness after the implementations of sandstorm control policies. The farmland around the counties and reservoirs did not change obviously in these seven years. The land cover conversions concentrated in central part of watershed, where was the area that four dams constructed.

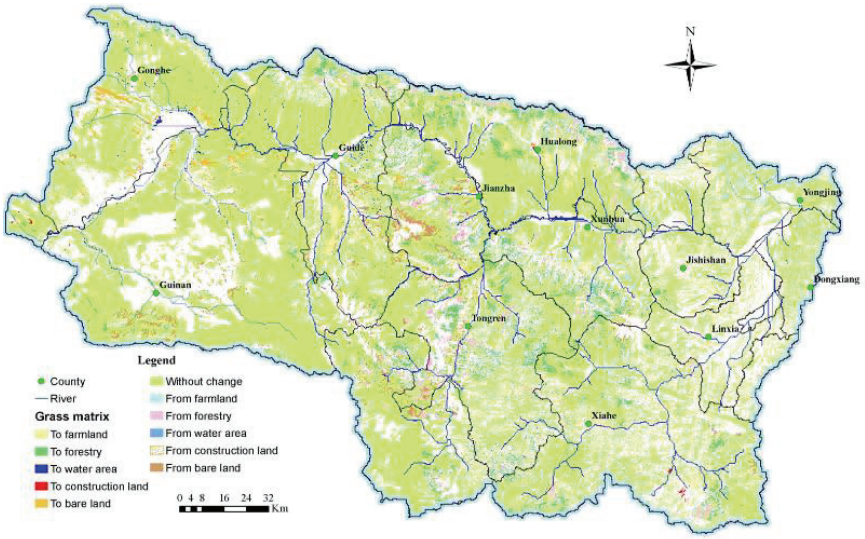

Fig.3-5 Transformations of grassland and other five land covers from 2000 to 2006

3.3.3 Land cover transformation matrix from 1977 to 1996

During this study period, all six categories land cover changed intensively (Fig.3-2). Approximately half of farmland was converted into other land cover and part of them (36.47%) was transformed to grassland from 1977 to 1996. However, the grassland area in 1996 was less than in 1977 and nearly 20% of original grassland was cleared to farmland (6.78%), forest (6.49%) and bare land (5.72%). In the period of 1977-1996, about two thirds of forest area was conserved to other land covers. In the area of changed forest, one third (33.86%) was converted to grassland. After three giant dams come into services, the water area increased from 53919 ha to 60597 ha in the two decades, which is nearly a 40% increase. The new water area was mainly from farmland (9796 ha) and grassland (13312 ha). From 1977 to 1996, the construction land increased from 2464 ha to 21558 ha, which mainly occurred on farmland (14321 ha) and grassland (4310 ha). The expansion of construction land was still the maximum increase. It also demonstrated that the hydroelectric cascade exploitation can secure regional economic development and lead to increased urbanization. According to the results, the urbanization process primary affected the agricultural land. Between 1977 and 1996, about 71% of bare land remained and almost all changed bare lands were converted to grassland (24.52%). However, the bare land area still increased from 271427 ha to 332419 ha after hydropower exploitation. The main reason was that 123583 ha of grassland changed into bare land in this period. (Table 3-5).

Table 3-5 Transition matrix characteristics of six types land cover from 1977 to 1996, 1996 to 2000, 2000 to 2006

1977 to 1996	Farmland ha/%	Forest ha/%	Grassland ha/%	Water area ha/%	Construct-ion land ha/%	Bare land ha/%
Farmland	219345/ 53.46	11436/ 2.79	149643/ 36.47	9796/ 2.39	14321/ 3.49	5785/ 1.41
Forest	4882/ 0.93	333787/ 63.31	178530/ 33.86	1255/ 0.24	65/ 0.01	8733/ 1.66
Grassland	146668/ 6.78	140265/ 6.49	1734261/ 80.20	13312/ 0.62	4310/ 0.20	123584/ 5.72
Water area	9197/ 17.06	772/ 1.43	7902/ 14.66	33483/ 62.12	662/ 1.23	1886/ 3.50
Construction land	319/ 12.95	29/ 1.20	56/ 2.27	2/ 0.08	2056/ 83.47	1/ 0.04
Bare land	4131/ 1.52	5265/ 1.94	66492/ 24.52	2760/ 1.02	152/ 0.06	192429/ 70.95
1996 to 2000						
Farmland	372238/ 96.79	303/ 0.08	10149/ 2.64	606/ 0.16	451/ 0.12	835/ 0.22
Forest	232/ 0.05	487987/ 99.27	2978/ 0.61	44/ 0.01	57/ 0.01	300/ 0.06
Grassland	17194/ 0.80	1225/ 0.06	2107762/ 98.64	2563/ 0.12	4/ 0.00	8040/ 0.38
Water area	570/ 0.94	74/ 0.12	937/ 1.55	58969/ 97.31	0/ 0.00	47/ 0.08
Construction land	2039/ 9.46	18/ 0.08	297/ 1.38	0/ 0.00	19174/ 88.94	30/ 0.14
Bare land	423/ 0.13	192/ 0.06	3331/ 1.00	10223/ 3.08	15/ 0.00	318235/ 95.73
2000 to 2006						
Farmland	358142/ 91.20	2303/ 0.59	27167/ 6.92	3731/ 0.95	826/ 0.21	550/ 0.14
Forest	7307/ 1.49	404693/ 82.59	75797/ 15.47	404/ 0.08	32/ 0.01	1776/ 0.36
Grassland	68585/ 3.23	117993/ 5.55	1889155/ 88.90	5448/ 0.26	655/ 0.03	43301/ 2.04
Water area	3171/ 4.38	336/ 0.46	2926/ 4.04	65366/ 90.30	9/ 0.01	583/ 0.80
Construction land	4732/ 24.02	72/ 0.37	940/ 4.77	156/ 0.79	13788/ 69.98	14/ 0.07
Bare land	3521/ 1.08	5371/ 1.64	45648/ 13.94	3025/ 0.92	37/ 0.01	269833/ 82.41

3.3.4 Land cover transformation matrix from 1996 to 2000

Table 3-5 shows that the transformation in this period was relatively slight and the obvious conversion of grassland was the loss for the construction of Lijiaxia reservoir in the central watershed. The land cover transformation matrix data between 1996 and 2000 indicates that there was no any conversion between water area and construction land in these five years. The conversion between other categories was also very slight. From 1996 to 2000, the area percentage of farmland, forest grassland, water area, construction land and bare land did not change significantly and was 96.79%, 99.27%, 98.64%, 97.31%, 88.94% and 95.73%, respectively. Only 0.73% (3601 ha) of the forest changed, principally to grassland (2978 ha). In this study period, the construction land decreased approximately 11% and most (9.46%) was transformed into farmland. Among the grassland changes (1.36%), 0.80% of it was converted into agricultural land. The main source of newly added water area (3.69%) was the bare land (3.08%).

3.3.5 Land cover transformation matrix from 2000 to 2006

The land cover transformation matrix from 2000 to 2006 is illustrated in Table 3-5. By contrast, the land cover change between 2000 and 2006 was more dramatic than that for the period 1996-2000. In this period, about 68585, 117993, 5448, 655 and 43301 ha of the grassland was converted into farmland, forest, water area, construction land and bare land, respectively. The farmland changed slightly and 91.2% of it was unchanged. Among the 8.8% area varied, most of was converted into grassland. The construction land increased obviously from 2000 to 2006. Almost all of the newly added 1559 ha resulted from the conversion of grassland (655 ha) and farmland (826 ha). After four dams were built in this period, the water area increased from 72405 ha to 78124 ha. The water area mainly covered the farmland (3731 ha) and grassland (5448 ha) along the river beach. Although 75797 ha forest transformed into grassland, the total forest area increased from 489799 ha to 530756 ha. Most of the new forest came from grassland, which meant the conversion between grassland and forest was frequent. The land cover conversion proved the regional ecosystem did not change essentially with the construction of four dams in this period.

3.4 Conclusions

The land cover distribution in Longliu Section from 1977 to 2006 has been compiled from multi-temporal Landsat data and national land cover database. The successful combination of multi-source remote sensing data provides reliable data for long-term land cover transformation analysis. After three decades successive hydropower exploration, the grassland decreased and other all five types of land cover increased. The grassland area had decreased from 63.07% of the investigated area in 1977 to 59.57% in 2006, which was the biggest absolute area decrease.

After eight dams come into operation, the water area increased from 53919 ha to 78124 ha. The largest annual increase rate was construction land, which had an annual increase rate of 17.43%. The forest mainly is located in the mountain area, which did not changed dramatically and had a slight increase after three decades hydroelectric cascade exploitation. The land cover change matrixes in four observation years were calculated. The grassland, the only continually decreasing land cover type, was selected to determine the conversion locations in the period of 1977-2006.

Chapter 4 Long-term landscape pattern variation with hydroelectric cascade exploitation

Abstract

The accumulated impacts of hydroelectric cascade exploitation on the landscape are greater than the simple sum of the impacts from a single dam. The spatial–temporal landscape characteristics resulting from the accumulated impacts of hydroelectric cascade exploitation from 1977 to 2006 in Longliu Watershed, a part of the Yellow River basin, were investigated. In this innovative approach, the FRAGSTATS model was employed to calculate landscape indices, which characterized landscape in term of its fragmentation, shape and diversity. Three fragmentation indicators and four shape indicators were analysed at patch scale for each land cover type in period of 1977–2006. The diversity simulators were calculated also at landscape scale. Furthermore, two hydroelectric cascade exploitation indicators, summed dam heights and hydroelectric generator capacities, were used to explore the correlated impact with landscape pattern. The analysis revealed that landscape fragmentation variations are strongly dependent on the magnitude of exploitation. The correlation coefficients ranged from 0.65 to 0.95. Except for PAFRAC value of water area, all other shape metric variations were closely linked to the level of hydroelectric cascade exploitation and the correlation coefficients ranged from 0.5267 to 0.9514. This study also demonstrated that landscape diversity changes were exponentially related to hydro-exploitation parameters, with correlation coefficients arranging from 0.7487 to 0.9856. The correlation analysis also demonstrated that hydroelectric cascade exploitation a factor determining regional landscape variation. It is concluded that these correlation analysis assist in predicting landscape variation about future hydroelectric cascade exploitation. The findings will also be helpful for regional environmental management and for the understanding expected landscape transformations

Published as:
Ouyang Wei, Skidmore, A.K., Hao Fanghua, Toxopeus A.G., Abkar Ali. Accumulated effects on landscape pattern by hydroelectric cascade exploitation in the Yellow River basin from 1977-2006. Landscape and Urban Planning. 2009, 93: 163–171.

4.1 Introduction

Landscape ecology has been defined as the study of land cover pattern change from the perspective of ecology (Turner, 1989). Bunkei (2006) has stated that human-induced land cover change can cause intense impacts on regional landscape composition and structure, which also have significant impacts on local environmental quality and species diversity. One major landscape change results from hydroelectric cascade exploitation, which is the development of successive dams in a watershed. Landscape-scale information about the effects of hydroelectric cascade exploitation development is currently relatively basic, yet is important for regional environmental management. Due to the difficulty of getting reliable long-term and historical data, this landscape investigation is typically limited to single dam effects (Sahin and Kurum, 2002; Hooke, 2006). Accumulated landscape impact analysis is a systematically approach to identify and assess the impacts of hydroelectric cascade exploitation on local ecosystems. The combination of RS and landscape modelling systems can increase understanding of the accumulated regional landscape changes for a long period (Thwaites and Slater, 2000).

One systematically approach to assess the accumulated impacts of hydroelectric cascade exploitation on ecosystems is to observe the ecosystem pattern changes with methods from landscape ecology (Sternberg, 2006). Two different perspectives of categorical patterns have profoundly influenced the development of landscape metrics and affected the interpretation of individual metrics. One is the island biogeography model, in which emphasis is on the single patch type and disjuncture, viewed as analogous to oceanic islands embedded in an inhospitable or ecologically neutral background (McGarigal et al., 2009). The other framework is the landscape mosaic model. In this model, landscapes are viewed as spatially complex, heterogeneous assemblages of patch types, which cannot be simply categorized into discrete elements such as patches or as a matrix (With et al., 1999). With the advance of RS technology, landscape metrics can be calculated effectively. Since the advent of popular index-calculating software, more landscape indices can be analysed in a short time, even although the behaviour of landscape pattern indices still vary in different contexts or data characteristics, thus complicating interpretation (Corry, 2005). Calculated landscape metrics can simulate the regional land cover characteristics, and also can predict animal movement in binary landscapes (Cumming and Vernier, 2002). The interpretation of these metrics and their ecological significance requires awareness of the landscape context and the openness of landscape relative to the phenomenon under considerations (Weng, 2007).

Quantitative measurements of landscape pattern have been used widely in landscape ecology for nearly two decades. The FRAGSTATS model

system is a popular and effective tool for landscape metrics quantification (Neel et al, 2004). The results of modelling allow diverse research objectives to be achieved efficiently (Coulson et al, 2005). Obtaining accurate time-series land use/cover maps is a key to characterizing a landscape and its dynamics in structure and function. The advance of RS technology and ground measurement for calibration and verification provides increasingly amount of land cover data. Furthermore, the combination of GIS and the FRAGSTATS model greatly improve the efficiency of landscape analysis (Tinker et al, 2003).

With the inherent technical advantages and its economic and environmental benefits, hydroelectric power has made an important contribution to the world's energy mix. It has accounted for a high percentage of the electricity market and develops rapidly in both developing and the developed countries (Yuksek et al., 2006; Kjærland, 2007). Hydropower station construction and operation is a complex process and also result in diverse impacts on ecosystems structures, services and functions (Klaver et al., 2007). Although studies of the influences of hydropower exploitation on landscape properties have covered diverse research points, some studies focus on the impacts of individual station rather than the accumulated impacts of hydroelectric cascade exploitation over a long period (Thórhallsdóttir, 2007; Pinho et al., 2007). The main characteristic of watershed hydroelectric cascade exploitation is that a series of hydroelectric dams will be constructed successively along the river in a short period. The impacts on ecosystems by cascade development are not the simple summation of every dam, which is accumulated, latent and systematically. The accumulated landscape changes analysis about hydroelectric cascade exploitation plan can demonstrate the terri-ecosystem changes from ecological prospect.

4.2 Material and methods

4.2.1 Study area description

The lower section is the outlet of Liujiaxia reservoir and the inlet section is the end of Longyangxia reservoir, So Yellow River basin between these two sections is named Longliu Watershed (Fig. 4-1). In order to summarize the accumulated impacts of successively hydroelectric power exploitations on landscape, results from landscape metric analysis based on regional land cover types were regressed with hydropower exploitations characteristics indexes (summed dam heights and hydroelectric generator capacities) across four time periods.

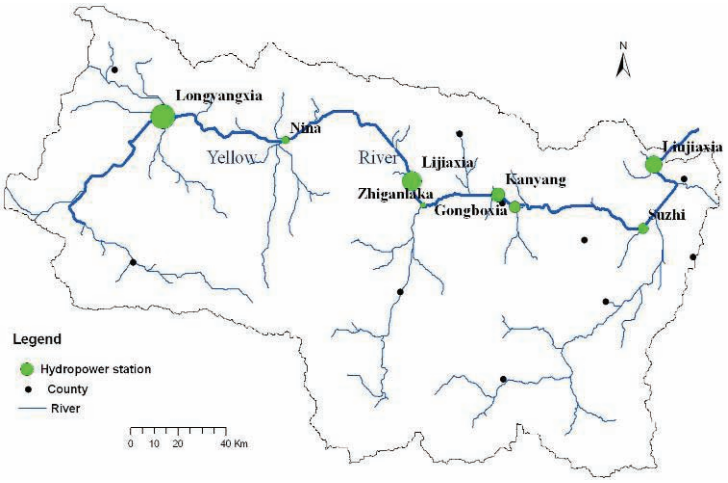

Fig.4-1 Study area of Longliu Watershed in the upper catchments of Yellow River

4.2.2 Landscape simulation

The relationship between landscape metric and hydroelectric cascade exploitation indicators can assist to understand the landscape variation under the hydroelectric cascade exploitation developments in the upper catchments of Yellow River over three decades. The FRAGSTATS model can calculate more than 100 landscape metrics, and some of them are correlated each other. According to the research objectives and experiences from previous studies (Palmer, 2004), three groups of landscape metrics were selected in this study, including landscape fragmentation, shape and diversity indices (Table 4-1). Landscape fragmentation metrics can provide quantitative information on how hydroelectric cascade exploitation breaks up larger patch into smaller patches, which include PD (Patch density), MPS (Mean patch size) and LPI (Largest patch index). Landscape shape analysis can provide information on patch shape and size, which involve ED (Edge density), LSI (Landscape shape index), FD (Fractal dimension index), and PAFRAC (Perimeter-area fractal dimension). The landscape diversity metrics are used to describe the landscape richness (number of patch types) and evenness (distribution areas of different type), which can give the information about the compositional and structural components of diversity. The selected metrics about landscape diversity are CONTAG (Contagion), SHDI (Shannon's diversity index), and SHEI (Shannon's evenness index) (McGarigal et al., 2002).

Land cover data of four periods, originally in shape file format were converted to raster format and then imported into the FRAGSTATS model for metric calculation. The input pixel size has been shown to principally influence the metric analysis results (Fearer et al., 2007; Uuemaa et al., 2007). Hence, the preliminary work was to decide about the pixel size.

Based on the modelling experience and the land cover characteristics, a pixel size of 50 m was chosen. At this pixel size, the land cover details can be kept and the analysis noise can be deleted to the greatest extent. Then, three category sets of landscape pattern changes in thirty years were calculated.

After the calculation, the associations between hydroelectric cascade exploitation characteristics and landscape metrics were analysed by simple regression method. Considering the landscape changes features at class level, the two intensively varied landscapes, grassland and water area are selected. The summed dam heights (SDH) and accumulated hydroelectric generator capacities (AHC) are employed to describe cascade exploitation degree.

Table 4-1 Landscape metrics utilized for landscape pattern characterization

Category	Code/Metrics	Description	Range
Fragmentation character metric	PD/ Patch density	The number of patches per 100 hectares.	PD>1
	MPS/ Mean patch size	The average area of all patches in a landscape.	MPS>0
	LPI/Largest patch index	Area of the largest patch in each class, expressed as a percentage of total landscape area.	0<LPI≤100
Shape character metric	ED/Edge density	Sum of length of all edge segments for the class, divided by total landscape area.	ED≥0
	LSI/Landscape shape index	Average complexity of the landscape as a whole.	LSI≥1
	FD/ Fractal Dimension index	Reflects shape complexity across a range of spatial scales.	FD>0
	PAFRAC/ Perimeter-area fractal dimension	Equals 2 divided by the slope of regression line obtained by regressing the logarithm of patch area against the logarithm of patch perimeter.	1≤PAFRAC≤2
Diversity character metric	CONTAG/ Contagion index	Equals 1 plus sum of proportional abundance of each patch type multiplied by number of adjacencies between cells of that patch type and all other types multiplied by logarithm; divided by 2 times logarithm of number of patch types.	0<CONTAG≤100
	SHDI/ Shannon's diversity index	Equals minus the sum, across all patch types of proportional abundance of each patch type multiplied by proportion.	0≤SHDI<1
	SHEI/ Shannon's evenness index	A measure of patch diversity, which is determined by the distribution of the proportion of different land-use types in a landscape	0≤SHEI≤1

4.3 Results

4.3.1 Landscape fragmentation metric variation

Three metrics derived from landscape fragmentation modelling at patch level are discussed in this section (Fig. 4-2). The largest patch size was grassland, which rose from 1000.16 ha in 1977 to 1126.37 ha in 2000. Thereafter, the grassland MPS decreased dramatically to 684.90 ha, which was lower than the area in 1977. The original farmland MPS (1179.18 ha) was as high as that of grassland, but decreased to about

240 ha in 1996 and remained at the same level over the next decade. The water area MPS decreased to 143.35 ha in 2006, which was much smaller than 374.45 ha in 1977. The construction land MPS remained at a low level, 11.71 ha in 2006, after a 30-year decline. This continual decrease caused the bare land MPS to drop by half from 239.78ha to 154.85 ha. The forest MPS decreased until 2000, but after that date it increased to 146.42 ha in 2006. Nevertheless, it was still lower than 152.45 ha in 1977. The decreasing six categories land cover MPS demonstrated all regional landscapes were transformed into smaller patches and become more fragile.

Forest land had the highest PD, which increased continually from 0.101 in 1977 to 0.106 in 2006. The smallest PD was that of the water area, although this also rose from 0.004 to 0.016. The remarkable change was grassland PD, which increased from 0.002 to 0.087, especially during the last period under investigation. The farmland PD also had a trend similar to that of grassland, but it increased slightly in last six years. Although the construction landscape PD increased in first two decades, it was the only one that decreased in following ten years. Finally, the construction landscape PD decreased to 0.040 in 2006, although this figure is higher than the PD value of 0.003 in 1977. The PD analysis reveals that the patch number increases and becomes fragile, which indicate habitat fragmentation.

The construction land LPI was lowest and increased from 0.02 to 0.03 over the period of three decades. A similar increasing trend was found with the water area LPI, which more than doubled from 0.49 to 1.07. The grassland LPI was the largest, but decreased continually from 74.21 in 1977 to 45.88 in 2006. The farmland LPI also decreased from 6.46 to 2.50 in same period. The bare land LPI increased during the first two decades, but decreased in last ten years of the study period. The forest landscape LPI decreased from 1.65 in 1977 to 0.74 in 2000 and then rose again to 1.23 in 2006. In summary, the LPI analysis showed that the farmland, grassland and forest largest patch area percentages decreased in the period of 1977-2006. At same time, the LPI values of the other three landscapes LPI increased, meaning that the largest patches in these three landscapes were more dominant. In conclusion, analysis of fragmentation metrics indicated that the regional landscapes patch became more fragile in the period from 1977 to 2006. The dramatic conversion occurred in grassland, farmland and water area, and the forest fragmentation had the least change.

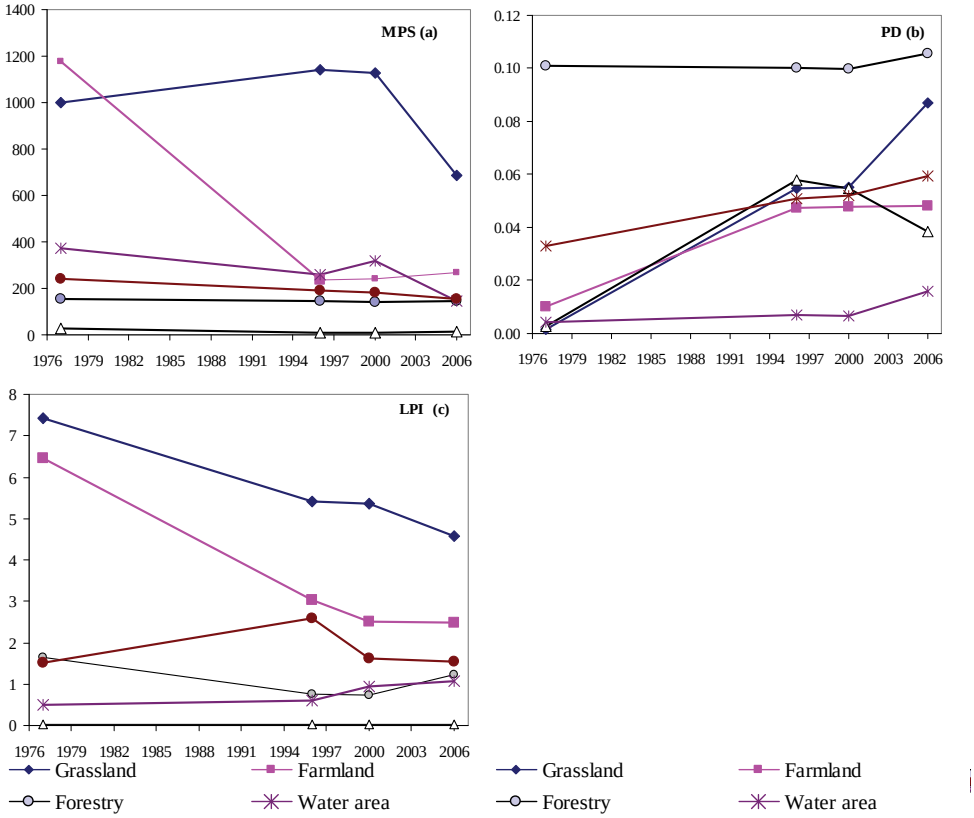

Fig.4-2 Patch level landscape fragmentation metrics variation from 1977-2006. (In order to normalize the metric value, the grassland LPI value in (c) was 10% of the real value)

4.3.2 Landscape shape metric variation

The landscape shape metrics variation at patch level in whole three decades is shown in Fig. 4-3. ED is a simple index which describes the patch edge density of each type of land cover. The water area ED was the only one continually increased, which rose from 1.0 to 1.3. The largest edge density was that of grassland, which increased from 14.5 in 1977 to 20.4 in 2006. The other four of landscapes had similar trend in the variation of their ED values. Although the forest landscape had a larger ED value, it varied over a small range (from 10.1 to 11.1). The construction ED was lowest, but it showed a high relative increase from 0.1 in 1977 to 0.6 in 2006. The ED analysis demonstrated that the regional landscape patch edge density increased and the patch shape become more complex.

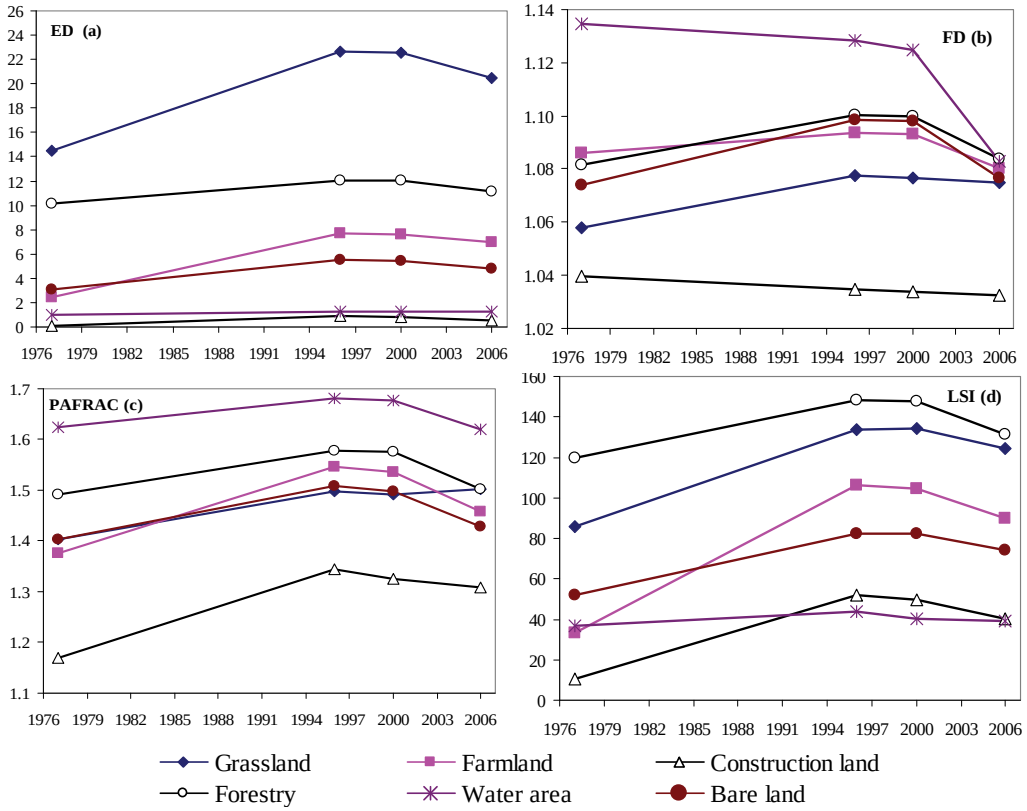

Fig.4-3 Patch level landscape shape metrics variation from 1977-2006

The LSI index can assess patch shape aggregation. All six categories of land cover had the same LSI variation trend. In the first period, the LSI increased dramatically and then continually decreased in the final ten years, which was still bigger than in 1977. The two categories of natural landscapes, grassland and forest, had relatively larger LSI values. On the other hand, the construction land and water area had the lowest values. The analysis of LSI changes showed that the regional land cover landscape shape converted into less aggregated form.

FD reflects shape complexity at patch size. The water area and construction land had similar trend in the variation of FD. Both continually decreased, with the water area showing the biggest drop. The FD of the other four landscapes presented another variation, namely increasing during the first twenty years and then decreasing in the last ten years. Except for construction land, the other five types landscape FD had close value in 2006. The FD analysis demonstrated that the shape complexity of farmland, construction land and water area decreased while the other three kinds land cover patch shape (grassland, forest and bare land) become more complex.

PAFRAC considers both the patch shape complexity and the patch sizes. The grassland PAFRAC increased continually from 1.40 to 1.50, but the PAFRAC value for the other five categories of landscape decreased between 2000 and 2006 following an increase in the period of 1977-2000. The construction landscape had the lowest PAFRAC value, but it also had evident increase (from 1.17 to 1.31) in relative terms. The water area landscape had the highest PAFRAC value, which indicates that it developed into a simpler shape. The forest PAFRAC changed in a similar way to that of grassland. On the other hand, the water area also increased in same period. Therefore, the analysis of the PAFRAC suggests that the patch perimeter increased and the patch shape became more complicated

To summarize, the regional landscape shape characteristic developed more complexity during the three decades considered in the study. The water area landscape remained the feature with the stable patch shape

4.3.3 Landscape diversity metric variation

CONTAG is an index describing the occupancy status of the landscape and also expresses the dispersion and interspersion of patches. Fig.4-4 demonstrates the temporal changes of landscape diversity feature over the three decades. The CONTAG value decreased from 60.3 in 1977 to 54.4 in 2006, which indicates the occupancy of single land cover became lower. The landscape dominance was more diffuse and diverse. The annual decline in the first twenty years was more rapid than in the last ten years, which demonstrates that landscape transformation has become slower in recent years. SHDI is an index which is widely accepted in community ecology as a means to assess landscape diversity. The SHDI increased from 1.1 in 1977 to 1.2 in 2006, meaning that the landscape diversity level become higher. A similar trend was found in the study of SHEI, which expressed the proportion feature of different land covers. SHEI also continually increased from 0.61 to 0.67, which indicates that the proportion of different land cover types became more averaged. The calculation of SHEI also indicated that regional landscape shifted from single type of land cover to a more mixed pattern. In conclusion, the landscape diversity became more diverse in the period from 1977 to 2006.

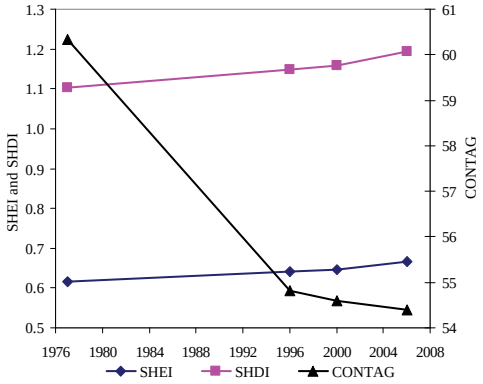

Fig.4-4 Landscape diversity metric variations from 1977-2006

4.4 Discussion

4.4.1 Landscape fragmentation with hydroelectric cascade exploitation

The regression models between grassland and water area fragmentation and hydroelectric cascade exploitation are presented in Table 4-2. The analysis indicated that landscape fragmentation variations had a strong relationship with hydroelectric cascade exploitation. The R^2 value between three fragmentation metrics with two independents ranges from 0.65 to 0.95. The grassland landscape has a closer relationship with SDH than AHC. On most occasions, the grassland landscape metrics have stronger relationship than with water area landscape. The grassland PD has the strongest positive relationship with two indices of hydroelectric cascade exploitation. In contrast, the water area landscape PD and MPS have strong negative relation with hydroelectric cascade exploitation degree. In comparisons, the water area LPI has a positive relationship with degree of exploitation.

Table 4-2 Correlation between landscape fragmentation parameters and hydroelectric cascade exploitation indices

Land cover	Independent	Dependent	Correlation model	R^2
Grass land	SDH	*PD*	$y=138.51*e^{19.707x}$	0.9499
		MPS	$y=0.0084*x^2-16.102*x+7907$	0.9135
		LPI	$y=9278.3*e^{-0.0567x}$	0.9236
	AHC	*PD*	$y=1154*e^{20.06x}$	0.8984
		MPS	$y=0.0717*x^2-137.99*x+67741$	0.8428
		LPI	$y=83676*e^{-0.0578x}$	0.8757
Water area	SDH	*PD*	$y=135.61*e^{118.88x}$	0.7316
		MPS	$y=2000.5e^{-0.0062x}$	0.7304
		LPI	$y=53.156*e^{2.4852x}$	0.8993
	AHC	*PD*	$y=1133.5*e^{120.58x}$	0.6871
		MPS	$y=16562*e^{-0.0061x}$	0.6480
		LPI	$y=390.86*e^{2.6681x}$	0.9462

The generalized models for the landscape fragmentation indices with hydroelectric cascade exploitation indicators are shown in Fig. 4-5. The water area PD, LPI and grassland PD are positively exponentially related to the degree of exploitation. These three metrics values therefore will increase with implementations of the hydroelectric cascade exploitation plan. In contrast, the water area MPS and grassland LPI are negatively exponential regressed with hydroelectric cascade exploitation. As the result, these two indicators will decrease. The different LPI development patterns of the two landscapes are due to the potential impacts on grassland fragmentation and the emergence of a larger water area after the dam was constructed. The grassland MPS is positively second order polynomially related to exploitation index. The mean patch size of grassland increased after it experienced the first period of decline. In conclusion, the grassland landscape was more fragile and the water area fragmentation developed in the converse direction.

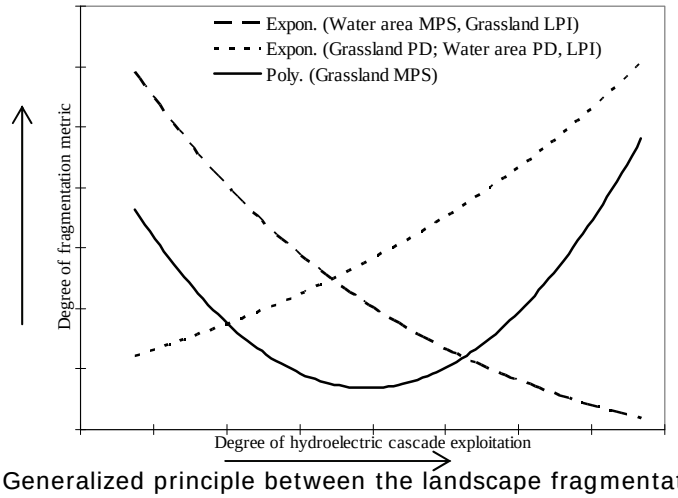

Fig.4-5 Generalized principle between the landscape fragmentation and hydroelectric cascade exploitation degree

4.4.2 Landscape shape with hydroelectric cascade exploitation

Table 4-3 shows the correlation model between landscape shape metrics and hydroelectric cascade exploitation indices. The four grassland shape simulators all had a reliable relationship with SDH and AHC. The correlation coefficients of eight models range from 0.5267 to 0.9514. The grassland ED and PAFRAC have stronger linkage to hydroelectric cascade exploitation degree than the other two shape metrics. The water area shape metrics and the ED, LSI, and FD variations have obviously response to hydroelectric cascade exploitation properties. In contrast, the water area PAFRAC change does not have a close relationship with the hydroelectric cascade exploitation degree. The probable reason for this is that the dominant features in water area landscape are the water areas in the giant reservoirs, not the new water areas in later established small stations.

Table 4-3 Correlation between landscape shape parameters and hydroelectric cascade exploitation indices

Land cover	Indepen-dent	Dependent	Correlation model	R^2
Grass land	SDH	*ED*	$y=-36.521*x^2+1385.4*x-12255$	0.9514
		LSI	$y=23.001*e^{0.0232x}$	0.5541
		FD	$y=2*10^{-26}*e^{60.619x}$	0.6203
		PAFRAC	$y=1*10^{-6}*e^{13.387x}$	0.7676
	AHC	*ED*	$y=-311.1*x^2+11814*x-104604$	0.8949
		LSI	$y=184.27*e^{0.0237x}$	0.5267
		FD	$y=7*10^{-26}*e^{61.499x}$	0.5828
		PAFRAC	$y=6*10^{-6}*e^{13.571x}$	0.7200
Water area	SDH	*ED*	$y=1.3099*e^{4.7126x}$	0.7760
		LSI	$y=-34.542*x^2+2793.5*x-55814$	0.6498
		FD	$y=1*10^{8}+14*e^{-25.361x}$	0.6921
		PAFRAC	$y=756104*x^2-2*10^{6}*x+2*10^{6}$	0.1511
	AHC	*ED*	$y=9.8976*e^{4.8089x}$	0.7376
		LSI	$y=-328.4*x^2+26519*x-529431$	0.7410
		FD	$y=10+16*e^{-25.944x}$	0.6612
		PAFRAC	$y=5*10^{-6}*x^2-2*10^{7}*x+1*10^{7}$	0.0865

Fig. 4-6 assists in the understanding of the changes in water area and grassland patch shape metrics in relation to the degree of hydroelectric cascade exploitation. Because the water area PAFRAC has a very low coefficient, it is not mapped in this figure. The water area PD was negatively exponentially connected to the degree of exploitation. The grassland LSI, FD, PAFARC and water area ED are positively exponentially correlated. However, the grassland ED and water LSI are second order polynomial related to exploitation index. The water area LSI therefore will develop to the original pattern with as more dams are constructed. The number of the largest water patch will be mitigated and the smaller patch number will increase. The decrease of grassland ED and the increase of LSI indicate that the largest grassland patch shape will be more dominant. Some of the grassland patch shape will change into smaller with future hydroelectric cascade exploitation development. The grassland shape will develop in a scattered pattern.

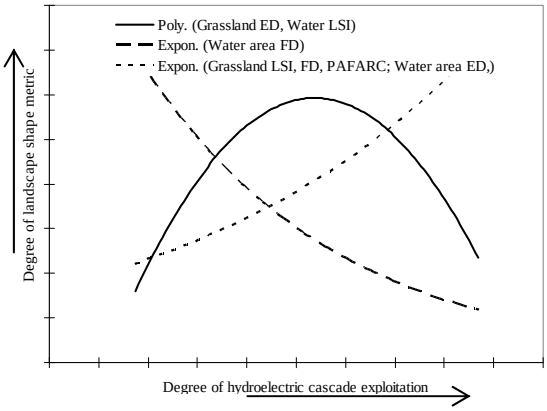

Fig.4-6 Simplified trend of landscape shape metrics variations with degree of hydroelectric cascade exploitation

4.4.3 Landscape diversity with hydroelectric cascade exploitation

Results from landscape diversity metric analysis in the response to hydroelectric cascade exploitation demonstrate that the regional landscape diversity pattern variances have strong relationship with the degree of hydroelectric cascade exploitation (Table 4-4). The six exponential models of the three diversity metrics are logical because of their higher correlation coefficients, which are between 0.75 and 0.99. The SDH mean closer linage between three diversity metrics than the AHC. The landscape SHDI and SHEI patterns have extremely high relation with hydroelectric cascade exploitation degree, and the lowest correlation coefficient being 0.95.

Table 4-4 Correlation between landscape diversity parameters and hydroelectric cascade exploitation indices

Independent	Dependent	Correlation model	R^2
SDH	*CONTAG*	$D=8*10^{7}e^{-0.2203\ x}$	0.7843
	SHDI	$D=7*10^{-8}e^{19.441\ x}$	0.9856
	SHEI	$D=7*10^{-8}e^{34.798\ x}$	0.9856
AHC	*CONTAG*	$P=9*10^{8}e^{-0.2253\ x}$	0.7487
	SHDI	$P=3*10\text{-}^{7}e^{20.008\ x}$	0.9529
	SHEI	$P=3*10^{-7}e^{35.814\ x}$	0.9530

The Fig. 4-7 shows the common direction of variation of three landscape diversity metrics under the hydroelectric cascade exploitation degree. The SHDI and SHEI value increased for the positive relationship with hydroelectric cascade exploitation development plan. The CONTAG has

distinct pattern, but also indicates that the regional landscape diversity pattern will be more diverse as more hydropower stations are constructed. The exponential models also indicate that diversity pattern will experience a relatively slow change in future, less than the last three decades. The landscape diversity development features also can be simulated with the reference to these models.

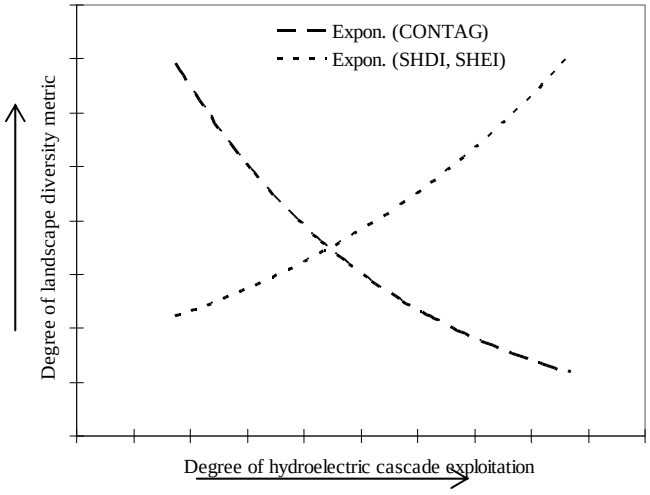

Fig.4-7 General trend of landscape diversity in relationship to the degree of hydroelectric cascade exploitation

In conclusion, there were strong relationships between landscape metric variations with SDH and AHC. As hydroelectric cascade exploitation advanced, the grassland landscape fragmentation indices (MPS and PD) and diversity metrics (SHDI and SHEI) continually increased. This proves that the hydroelectric cascade exploitation will cause regional landscapes to become more fragile. The water area LSI and grassland ED value firstly increased and then decreased after three decades of exploitation. The reason for this is the appearance of huge water area that was created after the hydroelectric cascade exploitation. In general, the landscape shape will become more complicated.

4.4.4 Application for hydroelectric cascade exploitation Environmental Impact Assessment

One challenge to regional environmental management is to identify and predict the landscape change resulting from the hydroelectric cascade exploitation development plan. The demand for hydroelectric power is increasing due to rapid economic development and the higher living standard in China. In Longliu Watershed five hydropower stations will be constructed, which will create more pressure on the regional landscape

management. The results from this paper can be used to predict future landscape patterns

Correlation models can simulate the landscape metrics under different magnitudes of hydroelectric cascade exploitation development. The metrics value has the advantage on the landscape quantification, which is the basis for assessing the impact of an exploitation plan. Landscape prediction is the main concern in the regional landscape impact assessment. The mean patch area, patch density, which are simple indicators, can act as an important meter in the decision making process of environmental assessment. Landscape modelling is a systematically effective approach to derive the regional spatial and temporal landscape pattern. Input data, however, is the base for modelling results. Therefore, land cover classification, pixel size, and metric selection need to be considered carefully. The selection of these factors will significantly influence the simulation results.

4.5 Conclusions

The impacts of single dams on the landscape have been widely researched, but the accumulated landscape impacts over long periods are still little studied for cascade dams in a watershed. Advances in RS/GIS techniques speed and modify the quantification of the landscape variation. With the land cover data in a time-series of four dates from 1977 to 2006, the landscape temporal and spatial characteristics in Longliu Watershed were analysed. According to the fragmentation metrics analysis, the regional landscape changed into more fragile zones, especially the grassland, farmland and water area. The regional landscape shape characteristics were concluded to be more complex after three decades. The three landscape diversity simulators proved that regional landscape diversity levels have become more diverse in the period of 1977-2006.

The study of the temporal landscape pattern changes in Longliu Watershed is the primary basis for understanding the accumulated impacts of hydroelectric cascade exploitation development. The grassland and water area were selected as the typical landscapes to describe the response to hydroelectric cascade exploitation. Correspondingly, the SDH and AHC were selected to indicate hydroelectric cascade exploitation degree from 1977 to 2006. The regression models between these two categories of indicator revealed that the landscape fragmentation metrics had strong relationship with hydroelectric cascade exploitation. The correlation coefficient between three landscape fragmentation metrics and two independents ranged from 0.65 to 0.95. Except for water PAFRAC, all landscape shape metrics variations were closely linked to the degree of hydroelectric cascade exploitation development, the correlation coefficients varying from 0.53 to 0.95. The six exponential models of

three diversity metrics gave logical results because of their high correlation coefficients between 0.75 and 0.99.

In conclusion, landscape fragmentation, shape and diversity were identified have strong connection with degree of hydroelectric cascade exploitation development. The landscape metrics can be predicted under different types of hydroelectric cascade exploitation development plans. The simulated landscape patterns can facilitate decision makers in preparing different scenarios analysis, which is of great importance for regional environmental management.

Chapter 5 Soil erosion dynamics response to landscape pattern

Abstract

Simulating soil erosion variation with a temporal land cover database reveals long-term fluctuations in landscape patterns, as well as priority needs for soil erosion conservation. The application of a multi-year land cover database in support of a Soil Water Assessment Tool (SWAT) led to an accurate assessment, from 1977 to 2006, of erosion in the upper watershed of the Yellow River. At same time, the impacts of land cover and landscape service features on soil erosion load were assessed. A series of supervised land cover classifications of Landsat images characterized variations in land cover and landscape patterns over three decades. The SWAT database was constructed with soil properties, climate and elevation data. Using water flow and sand density data as parameters, regional soil erosion load was simulated. A numerical statistical model was used to relate soil erosion to land cover and landscape. The results indicated that decadal decrease of grassland areas did not pose a significant threat to soil erosion, while the continual increase of bare land, water area and farmland increased soil erosion. Regional landscape variation also had a strong relationship with erosion. Patch level landscape analyses demonstrated that larger water areas led to more soil erosion. The patch correlation indicated that contagious grassland patches reduced soil erosion yield. The increased grassland patches led to more patch edges, in turn increasing the sediment transportation from the patch edges. The findings increase understanding of the temporal variation in soil erosion processes, which is the basis for preventing local pollution.

Published as:
Ouyang Wei, Skidmore, A.K., Hao Fanghua, Wang Tiejun. Soil erosion dynamics response to landscape pattern. Science of the Total Environment, 2010, 408(6):1358-1366.

5.1 Introduction

As a result of rapid socio-economic development during the last several decades, land cover in the upper Yellow River has been significantly affected. Soil erosion is the direct result and has become a key concern for environmental management in this basin, which is known for its severe soil erosion and sandy soils. Regional landscape variation often results from transformation of land cover and hydrological conditions, which affect the amount of soil erosion initiation and transportation to the water body (Bakker et al., 2008). Understanding the spatial distribution and long-term dynamic principles of soil erosion is the basis for effective regional land cover management and soil erosion prevention (Irvem et al., 2007).

Soil erosion is soil quality degradation in an irreversible direction and soil loss to river is considered as important environmental problem (Munro et al., 2008). The transportation of sediment to water bodies is accompanied by loss of nutrients, which lead to eutrophication and turbidity (Vanacker et al., 2003).

The Yellow River basin is an excellent natural laboratory for soil erosion studies in arid and semi-arid loess hilly area. The erosion from the middle and upper catchments contributes the principal sediment to the Yellow River basin (Huang et al., 2007). Many studies have shown that soil erosion formation and transportation are influenced by numerous factors (Hartanto et al., 2003). Wang (2008) examined the characteristics of soil particle size distribution under different land cover types. Ruysschaert (2007) observed soil loss due to harvesting of various crop types in contrasting agro-ecological environments. The soil erosion response to different land cover has been carefully examined. However, there is little known about the relationship between soil erosion and landscape pattern.

Soil erosion research requires regular field experimentation or long-term monitoring, which is expensive and time consuming (Siegrist, et al., 1998). Since soil erosion is affected by diverse factors, regular monitoring cannot provide reliable data because of difficulties in controlling these factors. In this context, the application of a watershed simulation model may be useful. A physically based watershed modelling approach may consider many factors, leading to the temporal and spatial quantification of soil erosion load. Among soil erosion models, the Soil and Water Assessment Tool (SWAT) can consider watershed weather variables, soil properties, topography, vegetation and land management scenarios by including water flow, sediment transport, crop growth, and nutrient cycling at different temporal scales (Mulungu and Munishi, 2007). SWAT can be used to identify the main sub-watersheds for soil conservation management and also characterize the response of different land cover condition (Tripathi et al., 2003).

Land cover characteristics have long been recognized as major factor for soil erosion. However, little attention has been paid to longer term regional soil erosion dynamics, especially with respect to land cover, landscape variation in large scale watershed. This paper uses the SWAT model system to explore the relationship between watershed land cover and landscape characteristics with soil erosion. The findings of this study may assist our understanding of soil erosion dynamics and the relation with landscape characteristics.

5.2 Material and methods

5.2.1 Study area description

The study area includes the main catchments of the upper catchments of the Yellow River and is the connection of the Qinghai–Tibet Plateau and the Loess Plateau (Fig. 5-1).

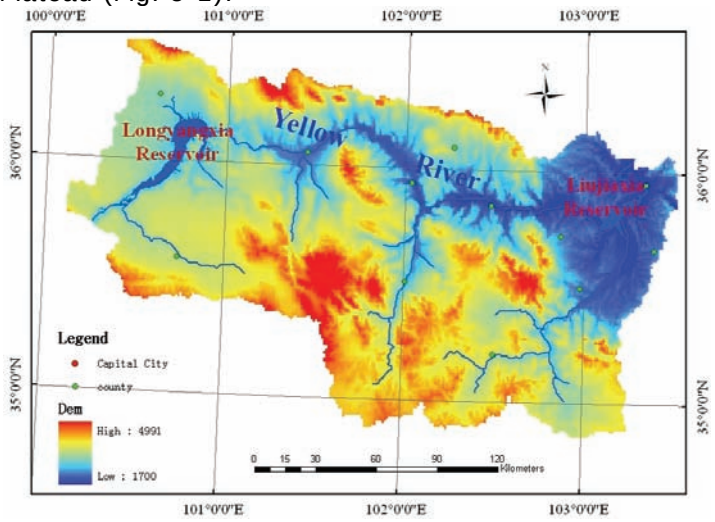

Fig. 5-1 The topography in the upper catchments of Yellow River basin

5.2.2 SWAT modelling database setup

5.2.2.1 Model description

Using input databases, SWAT simulates hydrology, soil erosion, and nutrient loading. Hydrological process modelling is the first step for nutrient pollution modelling and follows the water balance equation, consisting of four parts (i.e. surface runoff, evapotranspiration, soil water, and groundwater). Soil erosion is simulated with the Modified Universal Soil Loss Equation (MUSLE), which takes into consideration factors such as runoff, peak runoff rate, soil erodibility, soil management, support practices, topography and coarse fragments (Williams, 1995). During nitrogen cycle simulation, SWAT identifies the transformation of five forms of nitrogen and estimates their yield, respectively. In this

paper, the nitrogen is separated into two groups, soluble and organic. Soluble N is the inorganic form of nitrogen, NH_4^+ and NO_3^-. Organic N relates mainly to soil humus, crop residue, and microbial biomass. In regard to phosphorus cycle simulation, the model can estimate six forms and categorize them into organic P and sediment P. The organic P, including fresh, active, and stable organic P, comes from crop residue, soil humus, and microbial biomass. The sediment P is the amount of P discharged into water with the sediment. In consideration of correlation analysis and application in regional environmental management, the temporal-spatial variations of total nitrogen (TN) and total phosphorus (TP) were also calculated (Arnold et al., 1998).

5.2.2.2 Model input

The necessary input databases for SWAT simulation are prepared (Table 5-1). The spatial databases regarding topography, land cover, and soil properties were developed and reclassified by the model. The watershed management information was applied to improve modelling accuracy. The characteristics of the watershed climate were simulated with daily, historical monitoring data from 1990 through 2006, collected from nine weather stations around study area (Fig. 5-1).

Table 5-1 Data type scale and data description

Data type	Scale	Data description
Topography	1:250,000	Elevation, overland and channel slopes and lengths
Land cover	1:1,000,000	Land cover classifications
Soil properties	1:1,000,000	Soil physical and chemical properties
Weather	9 stations	Daily precipitation, wind, solar radiation, and temperature
Land management	_	Fertilizer application, planting, and harvesting

Fig. 5-2 shows the observed land cover distribution of the watershed in 2000. There is more vegetation cover in the eastern and southern areas than in the western and northern areas. Most barren lands appear in the western area, while forests and dense grassland are widespread in the southern basin. The agricultural land is close to water and around the reservoir in the eastern portion and along the main stream of the Yellow River. Grassland is the principal land cover and constitutes about 62.01% of the study area. Forests and farmland cover 14.29% and 11.46%, respectively.

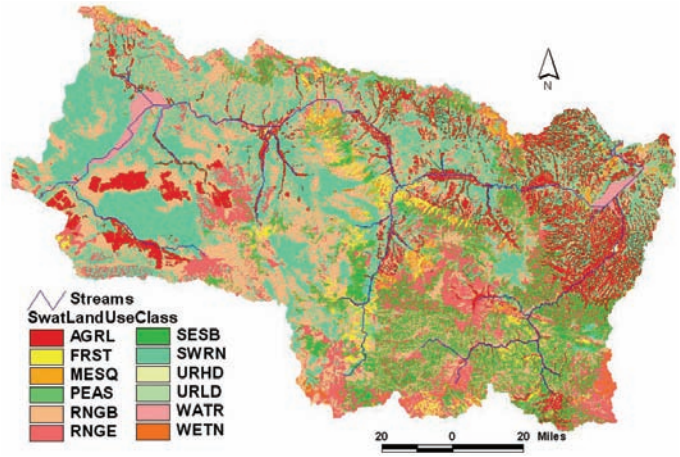

Fig. 5-2 Land cover distribution in study area

Soil property is another key factor for nutrient formation and loading, although it did not change for several decades. There are thirteen categories of soil in this research basin (Fig. 5-3). The soil property indices include area, percentage, coarse sand, fine sand, silt, clay, organic carbon, TN, TP and total potassium. The dominant soil types in this area are *Chestnut soil* and *Meadow chernozem*. The *Chestnut soil* occupies nearly half of the area and its TN, TP content is 0.18% and 0.08% respectively. The *Meadow chernozem* dominates another 23.55% of the area and has a higher content of TN (0.25%). The *Grey desert soil* spreads along the main stream of the Yellow River, which has direct impact on water quality. The TN and TP contents of this soil are 0.07% and 0.10% respectively.

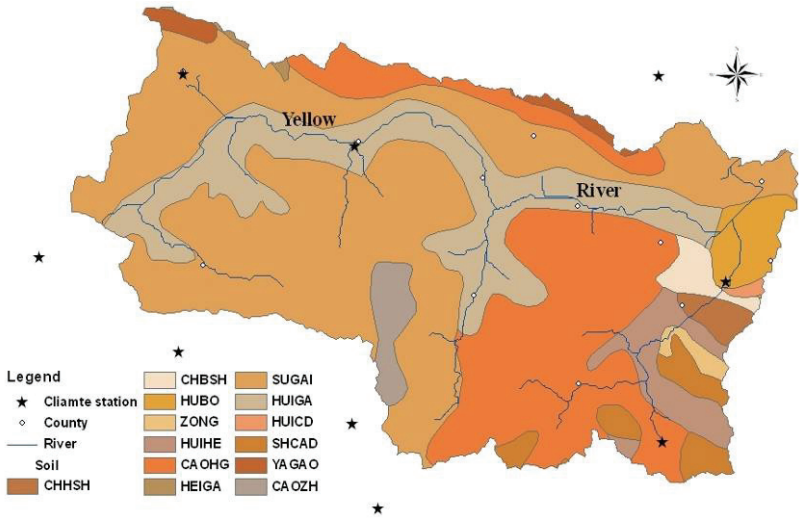

Fig. 5-3 Distribution of watershed soil types and weather stations

5.2.2.3 Model calibration

Expert advice and historical water quality and stream flow monitoring data were used to calibrate the SWAT model (Table 5-2) (Ouyang et al., 2008). Only limited observed flow and sediment data were available for this study. First sensitivity analysis was performed for the study watershed and only the sensitive parameters were selected to perform additional manual calibration. The process lasted from Jan. 2000 to Dec. 2002. Six stream flow related parameters were adjusted to correct for water flow overestimation. The sand density and water flow data at the outlet of the study area were used to calibrate six more soil erosion related parameters. Considering that there were three main land covers, *canmx* and C_{USLE} indicies were used for the three leading vegetation leading to more accurate modelling result.

Table 5-2 SWAT model parameters for model calibration

Parameter description	Calibration value
Curve number (*CN_2*)	61
Plant water uptake compensation factor (*SOL_AWC*)	0.04
Soil evaporation compensation factor (*ESCO*)	0.41
Groundwater delay coefficient (*GW_DELAY*)	30.1
Amount of shallow aquifer water that moved into the soil profile (*GW_REVAP*)	0.1
Maximum canopy storage (*canmx*)	Grassland: 3.5, Farmland: 2.2 Forest: 4.2
Threshold depth of water in shallow aquifer for "revap" or percolation to deep aquifer (*REVAPMN*)	200
Base flow alpha factor (*ALPHA_BF*)	0.03
Average slope steepness (*SLOPE*)	0.129
Average slope length (*SLSUBBSN*)	26.15
Maximum amount of sediment (*SPCON*)	0.001
Sediment restrained in channel (*SPEXP*)	1.21
Universal Soil Loss Equation factor (*C_{USLE}*)	Grassland: 0.08 Farmland: 0.25 Forest: 0.10
Initial humic organic N in soil layer (*SOL_ORGN*)	5000
Initial humic organic P in soil layer (*SOL_ORGP*)	1500
Initial NO_3 concentration in soil layer (*SOL_NO_3*)	3500
Nitrate percolation coefficient (*NPERCO*)	0.25
P percolation coefficient (*PPERCO*)	12.5
P soil partitioning coefficient (*PHOSKD*)	160
Biological mixing efficiency (*BIOMIX*)	0.25

Fig. 5-4A shows a comparison between the observed and simulated monthly water flow. The coefficient of correlation (0.7261) indicates that the simulated data is close to the observed value. In general, the

intersection (0.7472) shows that the simulated water flow was under simulated as compared to the observed data. Fig. 5-4B demonstrates the difference between the simulated and observed monthly soil erosion. The improved coefficient of correlation indicates the soil erosion simulation is more accurate than the water flow. However, the lower intersection means that the simulated soil erosion load was still underestimated. This may be due to the under prediction of water flow. Given the limited amount of observed data, the simulation of water flow and soil erosion is reasonable.

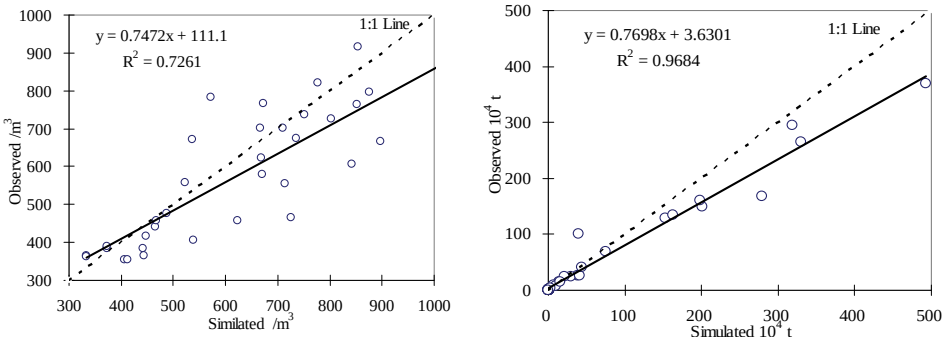

Fig. 5-4 Comparison of simulated and observed monthly water flow and soil erosion from 2000-2002

After validating the water flow and soil erosion, the next step was to calibrate nutrient parameters, which was difficult for lack of monitoring data. Seven principle N and P discharge parameters are listed in Table 5-2 after sensitive analysis. However, there was no regular organic or inorganic N or P monitoring in this area. Consequently, the TN monitoring data were applied in N calibration (Misgana and John, 2005). With TN monitoring data from Zhang et al., the monthly TN yield was validated first (Zhang, et al., 2003). The comparison of simulated and recorded TN is given in Fig. 5-5 A. It was also noted that there is a ratio between NPS nitrogen and phosphorus yield in a predefined basin (Ouyang et al., 2008). In the Yellow River watershed, Yang (2006) has calculated the yield ratio of TP and TN resulting in a value of 0.1304. The P simulation parameters were validated with this ratio. The monthly yield ratio ranged from 0.16 and 0.08 and the average ratio was 0.12 (Fig. 5-5 B). Based on the limited data and acceptable results, the model system was validated and ready for simulation.

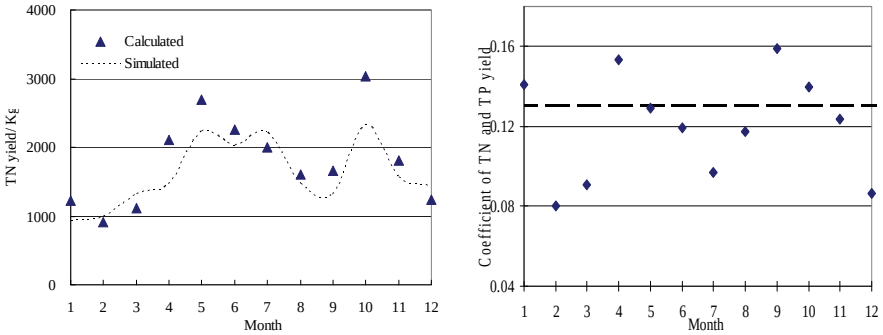

Fig. 5-5 Comparison of simulated and calculated monthly total nitrogen and total phosphorus yield

5.2.3 Data analysis

To identify the relationships between land cover variations and soil erosion, the correlation of simulated soil erosion and six types of land-use were examined in the initial phase. According to the theory of MUSLE, there are five dominant factors for soil erosion. Despite the land cover, precipitation is the principal and variable contributor to soil erosion. The other three factors, (i.e. practice, topographic and coarse fragment) did not vary over decades, and were assumed to be constant. Consequently, the soil erosion load was standardized with the same period precipitation and to highlight the impact of land cover variations. The original simulated load was divided by the yearly precipitation, and then was imported into correlation analyses. The land cover data were treated as a dependent variable, and the treated load was used as independent variable.

In order to explore the connection between landscape pattern and soil erosion, twelve landscape indicators were treated as dependent variables, and the yearly soil erosion with precipitation consideration was used as independent variables. The individual dependent variable was correlated against load in SPSS to produce the model. Furthermore, the landscape pattern at patch level was also correlated with soil erosion. The patch level of all six types of land cover would lead to ambiguous results as there are many interrelationships between them. To overcome this problem, principal component analysis was applied on six land cover variables. The data of six types of landscape pattern at patch level were manipulated in SPSS 10 package for Windows for statistical analysis. The orthogonal rotation was calculated using the varimax rotation method of Factor procedure, which is used to rotate the axes so that they fit better through the variable cluster (Zaharescu et al., 2009).

5.3 Results

5.3.1 Watershed yearly soil erosion

The simulated distribution of annual soil erosion loads provided a similar pattern from one year to another (Fig. 5-6). The highest soil erosion load which occurred in 1977, 1996, 2000, and 2006 was 160, 81, 85, and 67 t/ha/y, respectively. The main soil erosion came from agricultural land in the eastern area. The northern and central part of the study area experienced relatively slight soil erosion, perhaps because its dominant land cover was forest and grassland in steep mountain areas. The simulations showed that the watershed averaged soil erosion loads were 9, 10, 7, 8 t/ha/y, respectively for the four year study period.

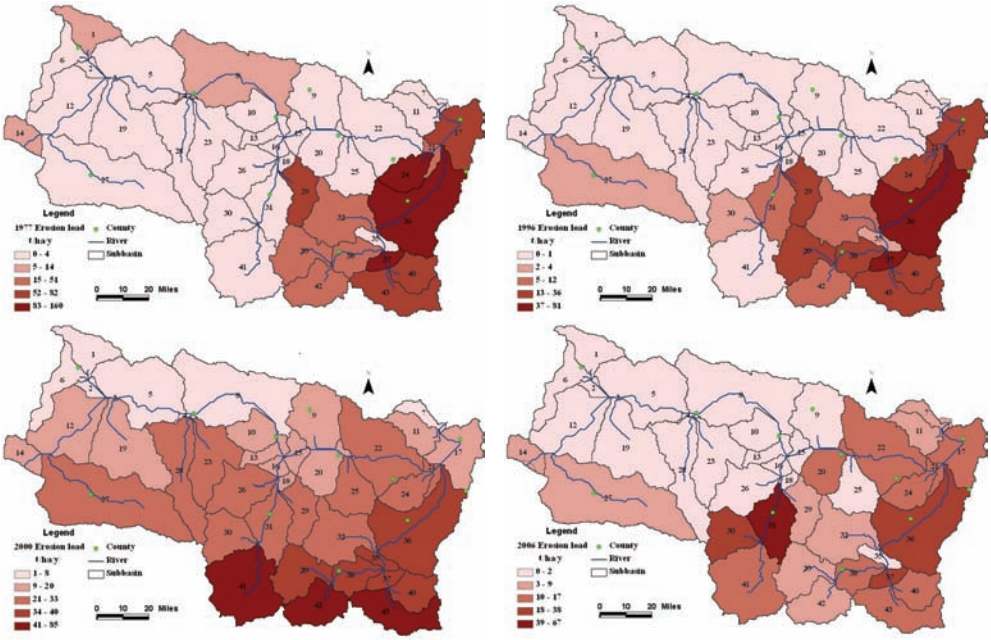

Fig. 5-6 Regional soil erosion load distribution in four simulated years

5.3.2 Monthly soil erosion

After analysing the watershed soil erosion spatial distribution, the temporal variation at a monthly scale is summarized in Fig. 5-7. Most of the soil erosion occurred in the summer period, from Apr. to Sep., especially Jun. Jul. and Aug. The maximum averaged monthly soil erosion load in four simulated years was 3.14, 3.86, 3.92 and 2.37 t/ha/m, respectively. It should be noted that the peak monthly soil erosion occurred in Jun. 2000, the year with least annual precipitation. The soil erosion amounts in other months were slight, with an average load less than 0.5 t/ha/m.

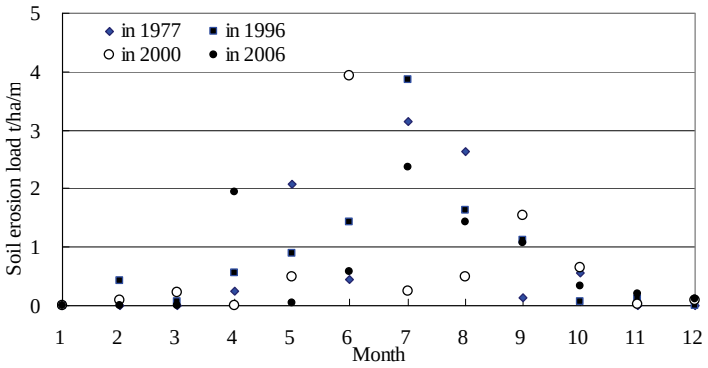

Fig. 5-7 Monthly soil erosion load in four simulated years and the seasonal trend line

Table 5-3 summarizes the statistical feature of all forty-eight-month soil erosion loads. The monthly soil erosion for the four years was 0.77, 0.85, 0.65, and 0.68 t/ha/m, respectively and varied in the similar trend with yearly load. The monthly load in 2006 was not the lowest one, but had the smallest standard (Std.) error and Variance value, which indicates the monthly difference in this year is the slightest.

Table 5-3 Statistical analysis of monthly soil erosion load (t/ha/m)

Year	Min	Max	Sum	Mean	Std. Error	Variance
1977	0.0	3.14	9.26	0.77	0.33	1.32
1996	0.0	3.86	10.15	0.85	0.32	1.24
2000	0.0	3.92	7.77	0.65	0.32	1.25
2006	0.0	2.37	8.10	0.68	0.24	0.70

5.3.3 Soil erosion with land cover

The relation of soil erosion and land cover is listed in Table 5-4. The directly simulated soil erosion had poor relation with land cover and the highest R^2 value was 0.471. After considering the precipitation, except the forest, the significance of other vegetation increased obviously and the highest R^2 value increased to 0.978. The *t*-test was applied to evaluate the correlation difference between these two sets of correlation analysis. At level of 0.05, the significance is 0.023, which indicated the precipitation is a significant factor. In order to distinguish the impact of precipitation, the soil erosion in following section is the value after considered with precipitation.

The spatial and temporal variation of land cover was found to considerably across the watershed. As the direct consequence, land cover change substantially influenced the soil erosion. Decreasing of grassland expansion of farmland has been widespread change over the last 30 years. The grassland and water area had the strongest relation with the

soil erosion, which showed strong interaction with soil erosion. Apart from these two, other four types of land cover types had moderate relation with soil erosion. The forest, the least area ratio land cover, had the slightest R^2 value, which indicated the forest area variation did not make substantial contribution to soil erosion.

Table 5-4 Interaction between regional land cover characteristics and soil erosion (S)

Condition	Dependent	Correlation model	R^2
Direct simulated soil erosion load	Farmland	S=-2E-05x + 17.16	0.156
	Forest	S=-8E-06x + 12.703	0.015
	Grassland	S=1E-05x - 15.194	0.175
	Water area	S=-9E-05x + 14.565	0.471
	Construction land	S=6E-07x + 8.724	0.001
	Bare land	S=-2E-06x + 9.2003	0.001
Soil erosion load after considering precipitation	Farmland	S=-1E-05x + 9.0228	0.232
	Forest	S=1E-06x + 2.698	0.010
	Grassland	S=1E-05x - 25.567	0.810
	Water area	S=-7E-05x + 7.9731	0.978
	Construction land	S=-6E-05x + 4.0874	0.371
	Bare land	S=-2E-05x + 9.0521	0.426

5.3.4 Soil erosion with landscape pattern

The analysis result of landscape indicators and soil erosion is showed in Table 5-5. All landscape variables were significantly correlated with soil erosion and achieved similar second order polynomial models. The correlation analysis indicated that watershed landscape pattern had strong impact on soil erosion. Among these models, the FRAC and SHAPE were the positively interacted with soil erosion. The analysis also showed significant correlations

Table 5-5 Interaction between regional landscape characteristics and soil erosion (S)

Dependent	Correlation model	R^2
PD	$S= -62.194x^2 + 17.856x + 3.2509$	0.916
LPI	$S = -0.0369x^2 + 4.7723x - 147.17$	0.986
ED	$S= -0.0106x^2 + 0.2617x + 2.7213$	0.916
LSI	$S= -0.0005x^2 + 0.0584x + 2.6148$	0.916
SHAPE	$S= 25.717x^2 - 104.74x + 108.92$	0.921
FRAC	$S= 24663x^2 - 53381x + 28888$	0.927
PAFRAC	$S= -75.794x^2 + 211.76x - 143.54$	0.887
CONTAG	$S= -0.0161x^2 + 2.1388x - 66.087$	0.947
SHDI	$S= -96.102x^2 + 184.2x - 81.975$	0.993
MSIDI	$S= -149.07x^2 + 193.6x - 54.505$	0.991
SHEI	$S= -308.5x^2 + 330x - 81.959$	0.993
MSIEI	$S= -478.39x^2 + 346.73x - 54.478$	0.991

5.3.5 Soil erosion with patch landscape feature

As mentioned above, there was a significant relation between regional landscape variables and soil erosion. The analysis at patch level of all six land covers will lead to a confusing result. So, after analysing six land cover types with the principal component analysis in SPSS, the water area and grassland were identified as key landscapes in this area. The statistical analysis of soil erosion with patch landscape pattern is listed in Table 5-6. All eight grassland landscape indicators had close interaction with soil erosion. The PAFRAC and PD of grassland were negatively correlated with soil erosion. The relationships between grassland and water area patch landscape variables in watershed exhibit some differences. About the water area, except the PAFRAC of water area, the other metrics had strong relationship with soil erosion characteristic. Their results showed that grassland, water area patch landscape pattern had significant positive correlation with soil erosion.

Table 5-6 Interaction between patch landscape of grassland and water area with soil erosion (S)

	Dependent	Correlation model	R^2
Grassland	PD	$S = -6033.5x^2 + 829.88x-24.141$	0.878
	LPI	$S = 0.0362x^2 - 3.5028x +86.966$	0.947
	ED	$S = 0.0858x^2 - 3.3048x +34.097$	0.910
	LSI	$S = 0.0027x^2 - 0.6124x +36.976$	0.898
	SHAPE	$S= 45.066x^2 - 155.41x + 136.31$	0.965
	FRAC	$S= 25937x^2 - 55421x + 29608$	0.984
	PAFRAC	$S = -513.7x^2 + 1476.3x - 1055.9$	0.744
Water area	PD	$S = 25863x^2 - 676.21x + 6.6034$	0.896
	LPI	$S= 1.8329x^2 - 5.6934x + 6.4807$	0.955
	ED	$S=-223.79x^2 + 500.85x - 272.63$	0.975
	LSI	$S= 0.1086x^2 - 8.8153x + 181.45$	0.823
	SHAPE	$S = 2.9972x^2 -13.345x +16.912$	0.986
	FRAC	$S = 2265.1x^2 - 4986.5x + 2746$	0.990
	PAFRAC	$S= -1657.7x^2 + 5470.7x - 4509$	0.067

5.4 Discussion

5.4.1 Relationship between soil erosion and land cover

With the correlation of six land cover types with soil erosion, the response of land cover variation on erosion loading can be estimated. Spatial distribution of soil erosion in Fig.6 and land cover distribution in Fig.2 showed that farmland contributed the most of erosion load. 35000 ha farmland were added during the three decades of the study, which should intensively increase soil erosion loading. However, the moderate correlation of farmland also exhibited that the farmland area variation did not intensively affect the load. So, at watershed scale, the impact of single land cover can be affected by other land cover types. Construction land and bare land had a positive trend, indicated that an increase of area caused more soil erosion. The grassland was positively correlated with erosion, but the water area was negatively correlated. In most cases, less grassland area contributed more sediment, but there was lower soil erosion load in this study under the condition of 4% of grassland disappeared. The main reason was that the converted grassland did not intensify the erosion and maybe the new vegetation patch pattern mitigated the soil erosion discharging. The study of Siepel also showed that the vegetation landscape had the function in adjusting hydrological conditions and affecting particles transportation (Siepel et al., 2002).The close correlation of six types of land cover indicated that

watershed soil erosion was the combined result of all categories of land cover. In brief, the findings suggested that the watershed land cover variation had close relationship with soil erosion load and appeared to be able to indicate soil erosion load.

The nature of regression of land cover and soil erosion is the consequences of land cover change on soil erosion exports. There are reasonable amounts of studies about export coefficient and several models have been widely applied (Worrall and Burt, 2001). In this study, this part of analysis was aimed to highlight the influence of precipitation. Similarly, the main uncertainty of regional study is the limited data about regional land cover change, which is come from remote sensing imagery. In the previous cases, the three or four year's data were the common situation. Based on three-year data, Ierodiaconou estimated exports variation (Ierodiaconou et al., 2005). With four-year imageries, the relation of landscape pattern with pollution was identified (Xiao and Ji, 2007). In this watershed scale study, the inevitable difficulty was to collect the long-term imageries and we got four-year data. At last, the relationship of soil erosion with land cover and landscape was concluded, which was alternative method for watershed soil conservation prediction.

5.4.2 Relationship between soil erosion and landscape pattern

(1) Relationship between soil erosion and landscape pattern

The statistical analysis suggested that landscape variation pattern was strongly related to soil erosion loading. Among the landscape indicators, the indices of diversity had higher R^2 values, which reflected that landscape diversity status affected more directly than other landscape indices. Higher diversity of landscape pattern led to decrease of soil erosion formation and transportation. So the higher abundance and distribution of land cover proportion contributed to soil erosion conservation.

The positive relation with SHAPE and FRAC showed that landscape shape size has a negative impact on soil erosion load at watershed scale. The other landscape shape indices, LSI and PAFRAC, had a negative correlation with soil erosion. The results reflected that the larger shape can intensify the erosion, which was the same conclusion as the other two shape indicators. The other eight landscape indices were negatively correlated with soil erosion. The four landscape fragmentation indictors had similar correlation equations and indicated that proper fragile landscape status can prevent soil yield by disturbing the formation and transportation. In brief, the correlation models suggested that regional landscape metrics were helpful in assessing soil erosion load and landscape characteristics should be considered in soil erosion conservation.

(2) Landscape connection with soil erosion at patch level

The correlation models of patch pattern of water area and grassland landscapes with soil erosion were similar second order polynomial equations, but there were still some differences. The grassland patch density was negatively correlated with soil erosion, but water area was positively correlated, which indicated the higher grassland patch density caused less erosion and that lower density of water area patch intensified soil erosion. In a defined area, higher density of grassland patch meant smaller area of patch and more patch edge. The ED analysis proved that patch density analysis and higher grassland patch edge density benefited soil erosion prevention. The lower patch density, also the bigger water area shape characteristic led to more soil erosion. The reason was that more water area meant more streamflow, so that more soil erosion can be formatted and transported. The grassland PD and ED analysis demonstrated that the smaller patch size and higher patch edge caused lower load. During three decades, the grassland area decreased nearly 120000 ha, which was the most significant land cover change. With the landscape metric calculation results, the continual increased PD indicated grassland patch numbers increased and patch size became smaller. The proper mechanism for this was that the grassland patch conserved the soil erosion principally by patch edge, not the whole patch area. The grassland correlation analyses demonstrated that more complicated patch can reduce soil erosion yield and more patch edge prevented soil erosion. The results were consistent with the land cover area analysis and provided an explanation to why soil erosion load deceased with less grassland area.

5.5 Conclusions

The main finding was that landscape pattern status played an important role in soil erosion formation and transportation in Longliu watershed. At the watershed landscape scale, the correlation model of twelve landscape metrics and soil erosion had significant R^2 values and the landscape diversity status was the dominant dependent. The principal component analysis proved that grassland and water area were the principal variable dependents in six landscapes. Correlation of their patch level characteristics with soil erosion was also analysed. The grassland PD and ED analysis demonstrated that the smaller patch size and more patch edge lead to lower load because erosion was a function of patch edge, not the whole patch area.

The correlation of six land cover types with soil erosion indicated that no single type of land cover exhibited significant relationship with directly simulated erosion load. When the impact of precipitation was considered, the land cover types had significant relationship with treated soil erosion. Forest and grassland fit a positive correlation model while the other four types fit negative equations. Most of land cover types had close relation

with soil erosion, which concluded watershed erosion loading was the integrated result of diverse land cover types.

With the application of multiple year land cover data in SWAT, the temporal-spatial feature of soil erosion variation was achieved. The watershed average soil erosion loads in four years were estimated and the main soil erosion come from agricultural land in the eastern area. Most of soil erosion occurred during the summer period, from Apr. to Sep., especially in Jun. Jul. and Aug. The temporal and spatial soil erosion distribution is the basis for regional land cover and environmental management. The simulation demonstrated that the main soil erosion sources were the eastern areas, where the soil and water conservation practices should be focused. The temporal variation also provides guidelines for regional soil erosion conservation practices. Finally, the correlation model of soil erosion response to land cover and landscape dynamics can be applied in watershed soil erosion prediction.

Chapter 6 Modelling soil erosion and sediment yield by SWAT and interaction with vegetation NDVI in basin and sub-basin scale

Abstract

Soil erosion is a significant concern when considering regional environmental protection, especially in the Yellow River watershed of China. This study evaluated the temporal-spatial interaction of land cover status with soil erosion characteristics simulated in the Longliu Basin of China, using the Soil and Water Assessment Tool (SWAT) mode. SWAT is a physical hydrological model which uses the RUSLE equation as a sediment algorithm. Considering the spatial and temporal scale of the interaction between soil erosion and sediment yield, simulations were undertaken at monthly and annual temporal scales and basin and sub-basin spatial scales. The corresponding temporal and spatial Normalized Different Vegetation Index (NDVI) information was summarized from MODIS data, which can integrate regional land cover and climatic features. The SWAT simulation revealed that the annual soil erosion and sediment yield showed similar spatial distribution patterns, but the monthly variation fluctuated significantly. The monthly basin soil erosion varied from almost no erosion load to 3.92 t/ha and the maximum monthly sediment yield was 47540 tonnes. The inter-annual simulation focused on the spatial difference and interaction with the corresponding vegetation NDVI value for every sub-basin. It is concluded that, for this continental monsoon climate basin, the higher NDVI vegetation zones prevented sediment transportation, but at the same time they also contributed considerable soil erosion. The monthly basin soil erosion and sediment yield both correlated with NDVI, and the determination coefficients of their exponential correlation model were 0.446 and 0.426, respectively. The relationships between soil erosion and sediment yield with vegetation NDVI indicated that the vegetation status has a significant impact on sediment formation and transportation. The achieved findings can be applied not only in soil erosion conservation, but also lead to a new prospect in understanding soil erosion.

Submitted as:
Ouyang Wei, Skidmore A.K., Toxopeus A.G., Hao Fanghua. Modelling soil erosion and sediment yield by SWAT and interaction with vegetation NDVI in basin and sub-basin scale. Science of the Total Environment. Under review.

6.1 Introduction

Soil erosion is a matter of worldwide concern. It is the primary environmental issue in the Yellow River watershed, China as a result serious aggravating factors, such as hilly topography, erosion-prone soil properties, land cover condition, climate and inappropriate agricultural practices (İrvema et al., 2007; Hessel and Jetten, 2007). This widespread problem threatens water quality and sustainable development in the Yellow River watershed. Consequently, many investigations have been carried out to observe soil erosion mechanisms in the hope of developing methods that prevent sediment transport to water bodies (De Vente et al., 2007). In this paper, we focus on temporal-spatial soil erosion, sediment yield dynamics and their interaction with vegetation (as measured by NDVI), which could provide an innovative prospect for soil erosion studies.

Soil erosion can occur in areas when the soil is erodible, the terrain is sloping and high-intensity rainfall coincides with limited vegetation cover (Vrieling et al., 2007). Soil erosion evaluation is an important for identification of vulnerable areas and for the assessment of sediment yield. The temporal and spatial distribution of erosion is the basis for sustainable land cover management and soil conservation. The widely applied methods of simulating the average soil erosion rate and sediment yield load is the Revised Universal Soil Loss Equation (RUSLE) (Renard et al., 1997; Nyakatawa et al., 2007). This equations consider the dominating factors, such as surface runoff volume, runoff rate, soil erodibility, land cover and management practices, topography and, coarse soil particle fraction (Koulouri and Giourga, 2007).

Soil erosion and sediment yield are important indicators and can be applied to surface water quality control. Soil erosion is considered to deteriorate on-site soil quality in an irreversible way and is quantified by the average amount of soil removed from a defined area over a given period. Sediment yield is the amount of soil removed to rivers and lakes in a given period over a defined area, which is an important process in catchment soil erosion (Tripathi et al., 2003; Sutherland and Ziegler, 2007). Non point nutrient pollutants, heavy metals and pesticides are also transported with the soil particles, so higher sediment yields will lead to water eutrophication and the disturbance of fragile aquatic ecosystems (Wilson et al., 2008). Intensive soil erosion and excessive sedimentation exported to rivers or reservoirs will disturb aquatic life and diminish environmental quality.

Among the factors influencing soil erosion, soil properties and topography can be considered constant in the short term, so that land cover and climatic features are the dominant variables influencing the erosion process in the short term (Marques et al., 2007). Land cover dynamics in the Yellow River watershed over the past decades has been extensively

studied with new technologies and in particular by remote sensing. Land cover temporal dynamics are significantly correlated with climatic change, especially with precipitation and temperature (Lin et al., 1996). Consequently, a vegetation index (like NDVI) can be used to integrate land cover and climatic features, which are the factors for watershed soil erosion and sediment yield. The introduction and application of a series of vegetation indices (like NDVI, Leaf area index, and net primary productivity) depends the study of vegetation depending on remote sensing data (Seaquist et al., 2003; Rasmus and Eva, 2008).

In this study, monthly and annual watershed NDVI information was calculated with data from the Moderate Resolution Imaging Spectroradiometer (MODIS). The MODIS instrument on-board NASA's Terra satellite is designed primarily for remote sensing of the land surface with spatial resolutions of 250 m (Running et al., 1994). MODIS provides good spatial and temporal-resolution data, which gives a reliable opportunity to monitor and analyse vegetation processes. It has been widely applied in diverse missions for large areas (Loboda et al., 2007).

6.2 Material and methods

6.2.1 Research framework

The general framework in this paper consists of four parts. Firstly, a SWAT geographical database was compiled, which included land cover, topography, soil properties and climate data. Secondly, the model parameters for water flow and sand density were calibrated and validated. After that, the regional soil erosion and sediment yield temporal dynamics over three years were simulated. Thirdly, monthly MODIS NDVI data for the same three years were analysed and summarized at the basin and sub-basin scale. With the SPSS statistical tool, correlations between soil erosion and NDVI, and sediment yield and NDVI at different tempo-spatial scales were analysed.

6.2.2 Data procedure

The land cover NDVI data were extracted from MODIS images (MOD13Q1, h26 v05), which were downloaded from the Land Processes Distributed Active Archive Center at NASA. The NDVI values were calculated with reflectance of red band (610–680 nm) and near infrared band (780–890 nm), which have been corrected for molecular scattering, ozone absorption, and aerosols. The 250m spatial resolution NDVI images were repeated over a cycle of 16 days (Pontus et al., 2007). According to local land cover and climatic characteristics, a monthly series of MODIS images were taken from February 18 to December 18 in 2000, 2003 and 2006 and were implemented to express land cover variation. The original MODIS images were mosaicked and georeferenced to the Universal Transverse Mercator (UTM) projection system by the nearest-neighbour resampling method (William and Maik, 2005). With

ArcGIS 9.2, the basin and sub-basin NDVI tempo-spatial variation characteristics were calculated. The monthly NDVI was the average value of the whole watershed. The yearly NDVI of every sub-basin was calculated by first summing and averaging the 12 monthly images of basin NDVI were after which the average sub-basin value was extracted using the zonal statistics tool (Ouyang et al., 2009).

After getting the NDVI and simulated the soil erosion data, their relationship was explained using an exponential correlated model. The exponential model can simulate the temporal dynamics of soil erosion process, especially the erosion formation and transportation (Kinnell, 2009).

6.3 Results

6.3.1 Soil erosion and sediment yield simulation

(1) Yearly sub-basin soil erosion and sediment yield

With the SWAT model, the annual soil erosion and sediment yield distributions in the three studied years were simulated (Fig. 6-1). The soil erosion showed similar spatial distributions in three years and the intensively eroded sub-basins were found to be situated in the eastern part of the study area. The soil erosion in the central mountain area also had a higher erosion load because of its steeper slopes. The sediment yield of the sub-basin is the amount of sediment moved out of the sub-basin and not all eroded soil was transported out. The sediment yield of single sub-basins varied intensively, but the inter-annual distribution at the basin scale did not vary significantly.

The yearly sediment yield of the forty-one sub-basins in three years were statistically analysed (Table 6-1). The maximum sub-basin load of soil erosion in 2000, 2003, and 2006 occurred in sub-basins 24, 24 and 29 respectively. Each of these basins is in mountain areas and covered by farmland. The maximum sediment yields in 2000 and 2006 both were located in the 27 sub-basin 27. Although the averaged erosion load in 2003 was not considerable, the yearly sediment yield was remarkable. The explanation for this is that an intense rain storm occurred in the southern basin in 2003, resulting in considerable sediment transported from the southern mountain area.

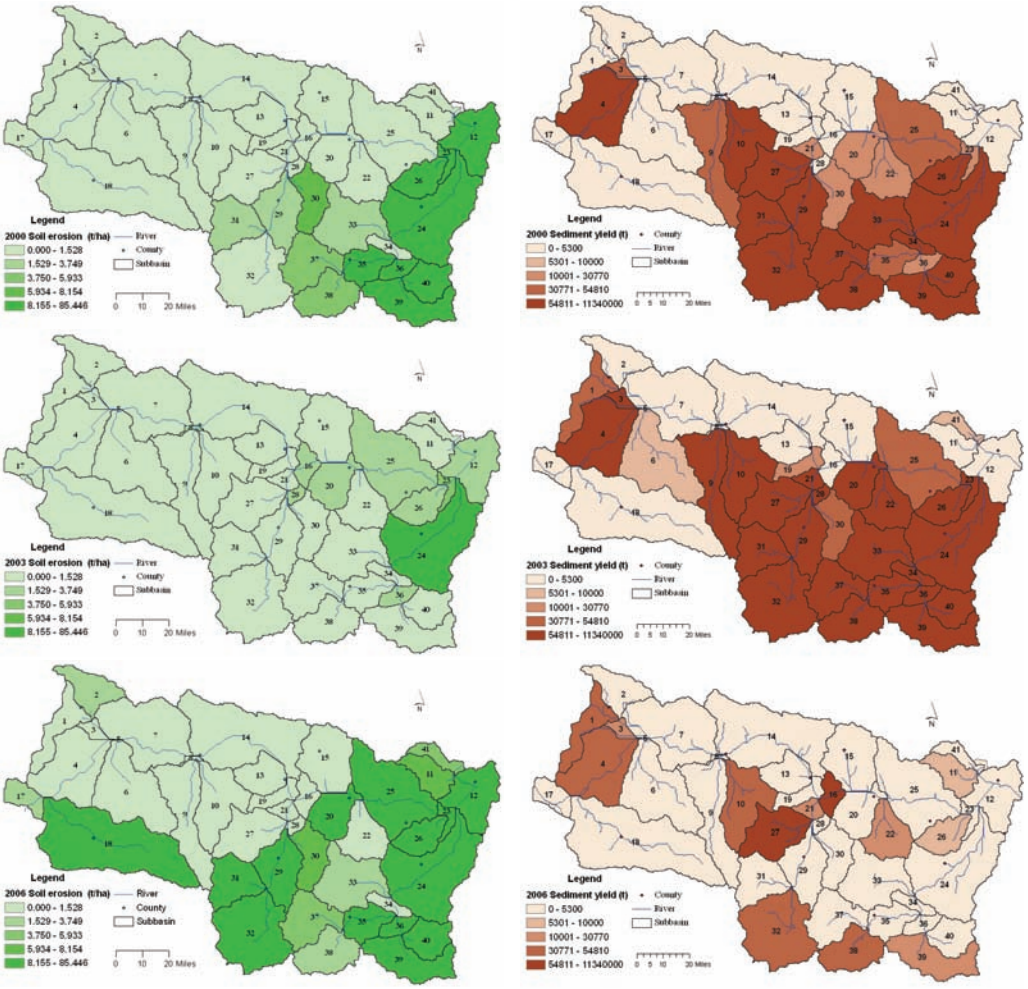

Fig. 6-1 Soil erosion and sediment yield distribution of each sub-basin in three years

Table 6-1 Statistical characteristic of annual sediment yield and soil erosion of sub-basins

Index	Year	Min	Max	Mean	Std. D
Sediment yield (t)	2000	334	3165000.0	200578.5	530619.2
	2003	838	11340000.0	1138347.2	2505003.2
	2006	40	105200.0	14127.2	24570.2
Soil erosion (t/ha)	2000	0.001	85.45	7.28	17.33
	2003	0.000	9.17	1.10	1.82
	2006	0.003	66.51	8.03	13.03

(2) Monthly basin soil erosion and sediment yield

Table 6-2 summarizes the monthly sediment yield and soil erosion loads in 2000, 2003, and 2006. The simulated data of soil erosion and sediment yields presented similar seasonal variation patterns, which had their maximum values in summer periods. There was almost no soil erosion in the spring. The yearly averaged sediment yield in three years was 4845.2, 10539.9, and 7709.1 ton respectively. The annual erosion load did not vary intensively and the mean values in three years were 0.648, 0.925, and 0.675 t/ha, respectively.

Table 6-2 Monthly sediment yield and soil erosion of whole basin

	Sediment yield (t)			Soil erosion (t/ha)		
Month	2000	2003	2006	2000	2003	2006
1	0.0	0.0	0.0	0.00	0.00	0.00
2	103.5	0.0	0.0	0.10	0.01	0.00
3	156.2	96.5	0.0	0.22	0.14	0.00
4	0.1	437.6	349.8	0.01	0.34	1.95
5	70.9	7019.0	71.0	0.50	0.63	0.04
6	18590.0	4470.0	180.8	3.92	0.17	0.58
7	2683.0	39680.0	16490.0	0.26	3.61	2.37
8	7064.0	34250.0	47540.0	0.48	2.41	1.44
9	17490.0	25770.0	13510.0	1.54	1.43	1.07
10	11060.0	13720.0	2437.0	0.64	2.28	0.33
11	544.0	985.8	9208.0	0.02	0.07	0.21
12	381.1	49.3	2722.0	0.08	0.01	0.11

6.3.2 Basin and sub-basin NDVI

(1) Yearly sub-basin NDVI

The spatial distribution of NDVI at a basin scale did not show variation over the observation period (Fig. 6-1). The vegetation in the western study area and along the main stream distinguished the relative lower NDVI and the vegetation of higher NDVI which occurs mainly in the south-eastern area. The common land cover around the reservoir in the north-east of the basin was farmland, which had a moderate NDVI value. At sub-basin scale, the averaged sub-basin NDVI in 2003 had the smallest NDVI range and Std. Deviation (Std. D), which indicated the NDVI in 2003 had smaller spatial differences than in the other two years (Table 6-3). Sub-basin NDVI data was used as a proxy, integrating vegetation status and precipitation, which was then used to investigate the relation of these two with soil erosion.

Table 6-3 Statistical characteristics of averaged sub-basins NDVI

Index	Year	Min	Max	Range	Mean	Std. D
NDVI	2000	-0.057	0.478	0.535	0.117	0.014
	2003	-0.018	0.451	0.469	0.102	0.010
	2006	-0.048	0.468	0.516	0.111	0.012

(2) Monthly basin NDVI variation

The monthly averaged NDVI of the whole watershed in three years was calculated with MODIS data, which presented temporal variation feature of land cover at basin scale. The averaged NDVI showed similar monthly patterns during the three years, describing the vegetation status. The NDVI increased dramatically from April, reached a maximum in July, and then decreased slowly. The inter-annual differences of maximum NDVI in 2000, 2003, and 2006 were not significant and their yearly values were 0.490, 0.518, and 0.489, respectively.

6.3.3 Sub-basin yearly interactions

(1) NDVI interaction with soil erosion

Using the annual modelling results, the relationship between soil erosion and sediment yield with NDVI at the sub-basin scale is demonstrated in Fig. 6-2 and Fig. 6-3, which describe the spatial vegetation distribution and its impact on soil erosion and transportation. The NDVI and corresponding soil erosion in all 41 sub-basins of three simulated years is shown in Figure 8. The schematic plots concentrated in four main zones. In zone 1, erosion was low, as was the NDVI (less than 0.15). These sub-basins were mainly bare land in the western basin. In zone 2, the NDVI was relatively low (ranging from 0.15 to 0.25), but this zone experienced considerable soil erosion. These sub-basins were mainly cultivated with crops and were near the main stream of the Yellow River. In zone 3, the NDVI increased to 0.30, but the erosion load decreased. The land covers in these sub-basins were dominantly grassland. The most significant erosion occurred in the highest NDVI area (greater than 0.30), which were mainly covered with forest and dense grass.

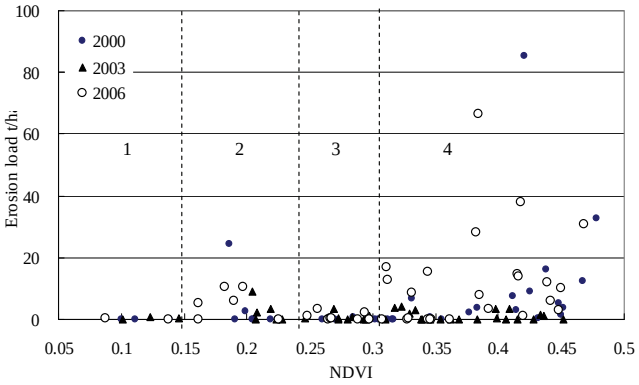

Fig. 6-2 Scatterplot of monthly sub-basin NDVI with soil erosion

(2) NDVI interaction with sediment yield

The sediment yield is definitely related to sub-basin area, but there is still a clear linkage with corresponding NDVI values (Fig. 6-3). Similar to the distribution pattern in Fig. 6-2, the plots of 41 sub-basins in every year were divided into four zones. Although the soil erosion load in zone 1 was lower (less than 0.15 t/ha), the amount of sediment yield was higher for the larger sub-basin areas and areas with almost no vegetative cover. On the contrary, the farmland (NDVI between 0.15 and 0.25) was more erosive, but yielded less sediment (zone B). The main reason was that the dominant crop in this basin was winter wheat, which was cultivated in terraces, which prevented sediment movement. The grassland area in zone C (NDVI ranged 0.25-0.30), as expected, contributed low amounts of sediment into the water body. The main sediment in the studied basin originated from the higher NDVI area (greater than 0.30), especially the forested area. However, in zone D, some sub-basins had higher NDVI, but did not contribute significant sediment yields.

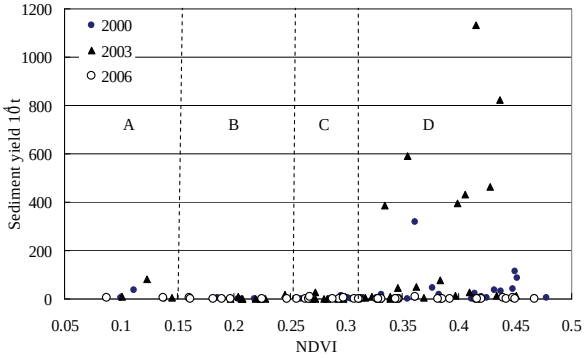

Fig. 6-3 Interaction of annual sub-basin NDVI with sediment yield

6.3.4 Monthly basin interactions

(1) NDVI interaction with soil erosion

After analysing the spatial relationship between NDVI and soil erosion, the temporal interaction between them was correlated. The interactions between NDVI and soil erosion of whole basins in all 36 months were examined and shown in Fig. 6-4. The correlation equations in three years were analysed respectively. The coefficients of determination (R^2) in 2000, 2003, and 2006 were 0.540, 0.461 and 0.500 respectively. Considering the precipitation in these three years presented the drought, normal and rainy conditions, a general correlation model was explored ($y=71.481x^{5.1986}$, $R^2=0.4460$). With the equation, the basin soil erosion load can be estimated using NDVI. With the general trend line of correlation models of all estimated months, it was found that there is a threshold at which the erosion load varied significantly. When the basin's mean NDVI was less than 0.30, the soil erosion load was fewer low. Once the basin NDVI climbed up to 0.35, soil erosion rose intensively.

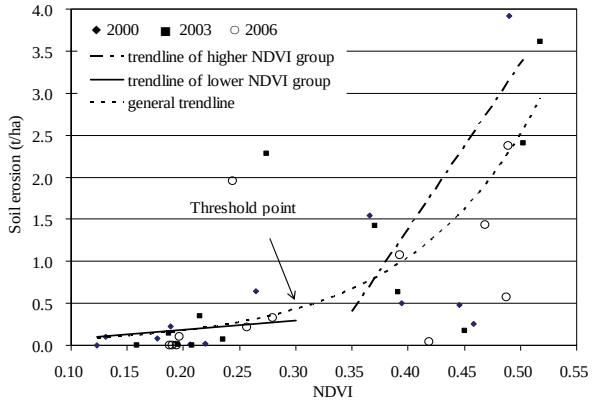

Fig. 6-4 Interaction of monthly basin NDVI with soil erosion

(2) NDVI interaction with sediment yield

The linkage between monthly basin NDVI and corresponding sediment yield also was analysed (Fig. 6-5). The R^2 values of exponential correlation equations in three observed years were 0.419, 0.515, and 0.447, respectively. The R^2 value of the general correlation equation of the total 36 simulated months was 0.4264 and the exponential model was $y = 0.0277e^{7.1258x}$. With the figure, the plots were found distributed in two groups and there was a definite NDVI gap around 0.30-0.35. During the winter period, the vegetation NDVI was lower than 0.35, which accompanied slight sediment transportations. During the summer period, the vegetation has grown and the land was well covered for soil erosion conservation, but most of sediment transported in this period with rainfall. When the averaged NDVI of whole basin was higher than

0.35, the sediment yield increased significantly. This threshold point indicated that when the vegetation NDVI is bigger than 0.32, it was also the period to prevent sediment movement by the engineering methods. This temporal principles can assist simulate sediment yield with vegetation status, which play an important role in water quality prediction and control.

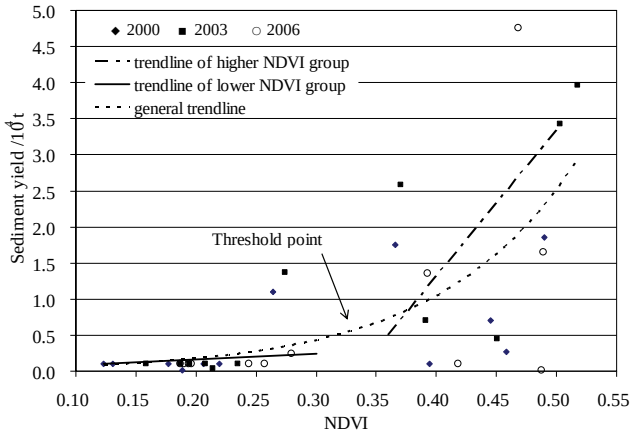

Fig. 6-5 Interaction of monthly basin NDVI with sediment yield

6.3.5 Interaction of NDVI, slope with soil erosion

With the finding in Fig. 6-2 and Fig. 6-3, the bare land had lower NDVI values and was more erosive, but the simulated erosion load was much lower. In order to explain this, and the embodied impact of slope, the interrelationship of slope, annual NDVI, with respectively soil erosion and yield sediment were analysed (Fig. 6-6). The forested mountain area with the steepest slope was a leading soil erosion source. The forested sub-basins with slopes of 10-12 degrees experienced the most serious soil erosion. The bare land with lower NDVI and lower slope also showed moderate soil erosion loading. The main sediment yield areas had a slope less than 8 degree with an NDVI ranging from 0.35 to 0.43. However, there was another zone that had a remarkable yield with an NDVI around 0.3 and a slope of 12 degree.

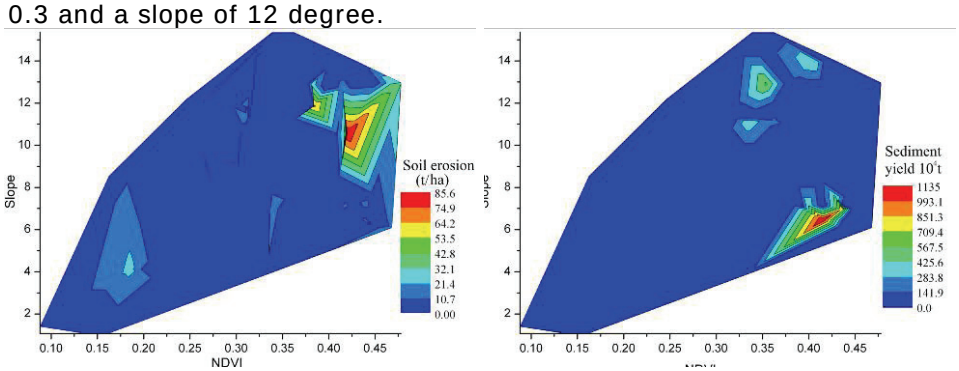

Fig. 6-6 Interaction of sub-basin NDVI and slope with soil erosion

6.4 Discussion

6.4.1 Spatial interaction

With the interaction of NDVI with soil erosion and sediment yield at sub-basin scale, the spatial correlation of soil erosion with vegetation NDVI feature was summarized. The findings helped to assess the spatial distribution of soil erosion and sediment yield with NDVI characteristics, which can be extracted from remote sensing data. The interaction also provided a new prospect to identify soil erosion sources. There are a number of studies showing that bare land significantly contributes to sediment yield (del Mar Lopez et al., 1998). However, the simulation in this paper demonstrated that the erosion loading of bare land is not the highest. Agricultural land had moderate erosion loading, but the sediment discharging is not correspondingly high. The tillage practice is conducive for soil conservation (Engel et al., 2009). In comparison, the sediment yield of grassland is not as sustainable as the erosion loading. Although grassland has widely been recognized as structural mechanism to bind soil and slow erosion (Melville and Morgan, 2001), it also contributes to some amount of sediment. The spatial correlation analysis indicated that even when land cover in some sub-basins was covered with vegetation; it remained the main source area for soil erosion in the study area. Arnaev (2004) also noted that the forest had the statistically significant effect on runoff and erosion. In brief, this study showed that only improving land cover is not best option for soil erosion conservation.

6.4.2 Temporal interaction

Understanding the temporal variation is the beginning for soil conservation (Hogarth et al., 2004). With the relationship of monthly basin NDVI with soil erosion and sediment yield, the temporally correlation of soil erosion with vegetation feature was achieved. The analysis demonstrated that the NDVI summit period was also the prime time for soil erosion conservation activity (sand-blocking dam, gully erosion control; slope formation works, intercepting ditch on sloping land). When the land cover has an NDVI higher than 0.35, the soil erosion will become more serious. The higher vegetation NDVI was also the time with sustainable erosion loads, which indicated that increase land cover area alone cannot conserve soil erosion effectively. Engineering methods should be carried out to reduce erosion load and to prevent sediment movement (McConchie and Ma, 2002). With the exponential correlation models, the basin soil erosion and sediment yield was assessed with NDVI characteristics, which can be extracted from remote sensing data with higher temporal resolution (Garrigues et al., 2008). The main reason for a lower R^2 value was that most of the rain falls in short-term periods, which can cause the erosion load to increase sharply (Davison et al., 2005).

6.4.3 Slope, NDVI and soil erosion

Slope was a direct cause of erosion (Fox and Bryan, 2000). Consequently, the analysis in Fig. 6 demonstrated that slope is an important factor for soil erosion formation and sediment transportation. The slope condition had more direct impact on soil erosion loading than the NDVI status. This outcome was similar to the simulation results by EROSION 3D (Schob et al., 2006). The sediment yield was much more complicated and the slope was not as sensitive as NDVI. The analyses showed that most of the sediment originated from moderately steep, forested areas and dense grassland. The well-preserved, highest NDVI in mountain area was not the main contributor to sediment yield. By comparison, it was found that the higher NDVI area with steep slopes suffered the most serious soil erosion, but did not contribute to sediment yield.

6.5 Conclusion

With the application of SWAT model, soil erosion and sediment yield in month and year temporal scale, in basin and sub-basin spatial scale were simulated in upper catchments of the Yellow River. The temporal-spatial correlations of soil erosion and NDVI were calculated at different scales. It was concluded that the vegetation NDVI can act as an indicator that combines land cover status and climatic situations at the same time. Consequently, the interaction between basin and sub-basin NDVI with its soil erosion load and sediment yield provide a new prospect with which to observe the soil erosion dynamics.

The annual sub-basin analysis focused on their spatial interactions, which helped to assess the soil erosion and sediment yields in every sub-basin and to identify the essential erosion areas through their NDVI characteristics. The difference of erosion load and sediment yields from different sub-basins was demonstrated by corresponding NDVI values. After considering the slope of the sub-basins, it was found that the higher NDVI area with steep slopes suffered the most serious soil erosion, but did not contribute most sediment yield under this continental monsoon climate.

Using the monthly simulation results, the temporal interaction of soil erosion and sediment transportation amount with vegetation feature also was summarized. The correlation analysis indicated that the vegetation NDVI peak period was the best time for the implementation of soil erosion conservation efforts. Based on the exponential correlation equations, the temporal dynamics of basin soil erosion and sediment yield can be assessed by means of real time NDVI characteristics. With the threshold point in the trend line of general correlation equations, soil erosion and sediment transportation can be assessed and be conserved effectively. Storm water run-off has intense impacts on soil erosion processes, but cannot be expressed in the slow NDVI variation, which

decreased the coefficient of determination. With the vegetation NDVI characteristics, the temporal-spatial variation features of basin soil erosion and sediment yield can be simulated. The basin vegetation NDVI can be conveniently calculated with diverse remote sensing data with higher temporal resolution.

The proposed methodology was successfully applied in soil erosion simulations in the upper catchments of the Yellow River. Based on the outcomes of the present modelling, it appears that regional soil erosion was concentrated on eastern farmland and southern mountain areas. The monthly simulation results demonstrated that the soil erosion becomes serious during June to August.

Chapter 7 Landscape transformation and non point source nutrients pollution interaction

Abstract

Grassland, forest, and farmland are the dominant land covers in upper catchments of the Yellow River and their landscape status has direct connection with dynamics of non-point source (NPS) pollution. Understanding the correlations between landscape variables and different formats of NPS nutrients pollutants is a priority in order to assess pollutants loading and predicting the impact on surface water quality. The regional vegetative cover in 1977, 1996, 2000 and 2006 was determined by classifying historical multi-temporal Landsat imagery and clipping data from the National Landcover Database. The landscape pattern is expressed means of metrics such as patch density, edge density, fractal distribution index, all of which were calculated by FRAGSTATS. The soil and water assessment tool (SWAT) was used to analyse and visualize the fate of NPS nitrogen and phosphorus loads in diverse formats from different land cover types in different years. Statistical analysis indicated that the grassland landscapes played a major role in NPS nutrient pollution dynamics and grassland patch edges benefited pollution control. However, the presence of more forest and farmland lead to more NPS nitrogen emissions. It was found that grassland areas reduced NPS nitrogen loss and had a multi-functional role in the nutrient pollution process. Farmland was the direct source of organic nutrients, but did not have great impacts on sediment P and soluble N loadings. Forest areas contributed NPS nutrients pollution loading. The statistical models derived in this study can be used to estimate watershed NPS nutrient pollution losses. These equations can help identify pollution sources and suggest appropriate and effective solutions for planning basin management practices.

Submitted as:
Ouyang Wei, Skidmore A.K., Toxopeus A.G., Hao Fanghua. Long-term landscape pattern with non-point source nutrient pollution in upper catchments of Yellow River basin. Journal of Hydrology, 2010, 389(3-4): 373-380.

7.1 Introduction

During the last several decades, and in spite of considerable efforts to reduce point source pollution, water quality often has not improved significantly. This may be due to the contribution of non-point sources (NPS) of pollution in both developed and developing countries (Leone et al., 2007). The major NPS pollutants are nitrogen (N) and phosphorus (P), and they are the leading causes of water degradation in rivers and lakes. Nutrient losses from farmland, grassland and forest are important factors limiting water quality (Ribarova et al., 2008; Munodawafa, 2007). Long-term NPS nutrient pollution modelling plays an important role in environmental management and for determining the value of vegetation in limiting NPS pollution.

With the increasing importance of prevention and protection of natural water resources, a number of studies have been carried out to assess NPS pollution (Duchemin and Hogue, 2009). The fate of NPS nutrient pollutants is the main content in water quality modelling. Nutrients are delivered to water bodies from multiple sources, each having different transport and composition characteristics. The variation of spatial-temporal patterns of NPS pollution produces different impacts (Edwards and Withers, 2008). Inputs of nitrogen in a watershed are derived from atmospheric deposition, mineral N pools of top soil, and fertilization. Furthermore, ammonia, mediated by microorganisms can mineralize from soil organic matter. NPS nutrient pollutants have two modes of transportation, namely by being dissolved in water and associated with the transportation of soil particles. Nitrogen can be found in various forms: molecular N, organic N, ammonium N, nitrite N and nitrate N (Maillard et al., 2008). N reduction and loss can result from denitrification, uptake of plants, percolation, lateral flow, and surface runoff. P is less mobile than nitrogen because it is less soluble, and, in general, losses via overland flow are affected by surface soil P concentrations and land management practices (Bowes et al., 2008).

Field research on NPS nutrient pollution is both expensive and time consuming. Because of the temporal and spatial variability in processes, regular monitoring requires a large investment. As a result, watershed-scale modelling of NPS pollution has become useful and popular (Easton et al., 2008). Physically based watershed modelling can take into consideration most of the factors that cause spatial and temporal variation in NPS pollutant loads. Several modelling systems can simulate hydrologic processes, soil erosion, and nutrient transport via surface runoff, interflow, and groundwater flow, as well as in-stream nutrient cycling at the catchment scale. Several models have been applied to estimate nutrient loadings in watersheds (Viotti et al., 2002; Cho et al., 2008). Among the NPS pollution simulation models, the soil and water assessment tool (SWAT) can integrate local weather variables, soil properties, topography, vegetation and land management scenarios.

Vegetation cover status has been recognized as major factor contributing to watershed NPS nutrient pollution movement (Bouldin et al., 2004). However, little attention has been paid to long-term watershed responses of NPS nutrient pollution on vegetation and landscape variations. We simulated watershed organic N, nitrate N, sediment P and organic P over four years and correlated them to the corresponding areas of the three major types of vegetation in the study area. This paper reports on a pilot attempt to employ the SWAT model system and other geospatial technologies to explore impacts of vegetation landscape patterns on NPS nutrient pollution loads. The findings demonstrate the influence of landscape patterns on NPS nutrient pollution dynamics provide insights into watershed NPS nutrients loss processes and allow to prediction of watershed NPS nutrient pollutant loads.

7.2 Materials and methods

7.2.1 Research framework

The analytical framework of the research comprises four steps. First, land cover was mapped by classifying multi-temporal Landsat images over four year periods, by clipping the data from national basic databases. Then, with the spatial databases, sensitive parameters were selected and the SWAT model was validated for water, sediment, and nutrient yields. The tempo-spatial distribution of watershed NPS nutrients pollution was simulated. Third, the area and landscape patterns of three vegetative covers were calculated and correlated with NPS nutrient pollution. Finally, correlations between NPS nutrient pollution loads and vegetation area and landscape patterns were identified.

7.2.2 Data process

Landscape metrics are the basic indicator used for landscape pattern calculation and assessment (Eric et al., 2006). The metrics reflect landscape structure and function and summarize the spatial and temporal distribution of land cover. In this paper, we applied three metrics to indicate landscape patterns, which characterize long-term variation of three principal types of vegetative covers. Patch density is patch number per 100 hectares, which reflects landscape fragmentation. Edge density is total length of all edge segments divided by total landscape area. Fractal distribution index equals 2 times the logarithm of the patch perimeter divided by the logarithm of the patch area, an index of patch shape complexity (McGarigal et al., 2002). FRAGSTATS is a set of spatial statistics that were implemented by ecologists to describe the characteristics of landscapes and components of those landscapes. These statistics facilitate the comparison of landscapes and the evaluation of processes (Raines, 2002).

With the landscape pattern and nutrient pollution loading from SWAT, the interactions of three kinds of vegetation' areas and landscape pattern with NPS pollution were analysed with SPSS software, respectively. In order to deepen the understanding the dynamics between them, the NPS pollutants were correlated as different formats.

7.3 Results

7.3.1 NPS nutrients pollution simulation

(1) Nitrogen simulation

The watershed NPS organic N, inorganic N, and total N yields were estimated by SWAT with four-year land covers (Table 7-1). Organic and inorganic N yields responded differently in each of the four years. The nitrate N load decreased from 0.05 kg/ha in 1977 to 0.03 kg/ha/yr in 2006. The organic N load increased from 0.106 to 0.27 kg/ha/yr in the period of 1977-2006.

Table 7-1 Watershed NPS nitrogen loss load in four simulated years (kg/ha/yr)

Year / Format	1977	1996	2000	2006
Organic N	0.11	0.17	0.21	0.27
Nitrate N	0.05	0.04	0.03	0.03
Total N	0.16	0.21	0.24	0.30

The spatial distribution of watershed NPS total N loss is shown in Fig. 7-1. The eastern sub-basins contributed most of NPS nitrogen loss in all four years.

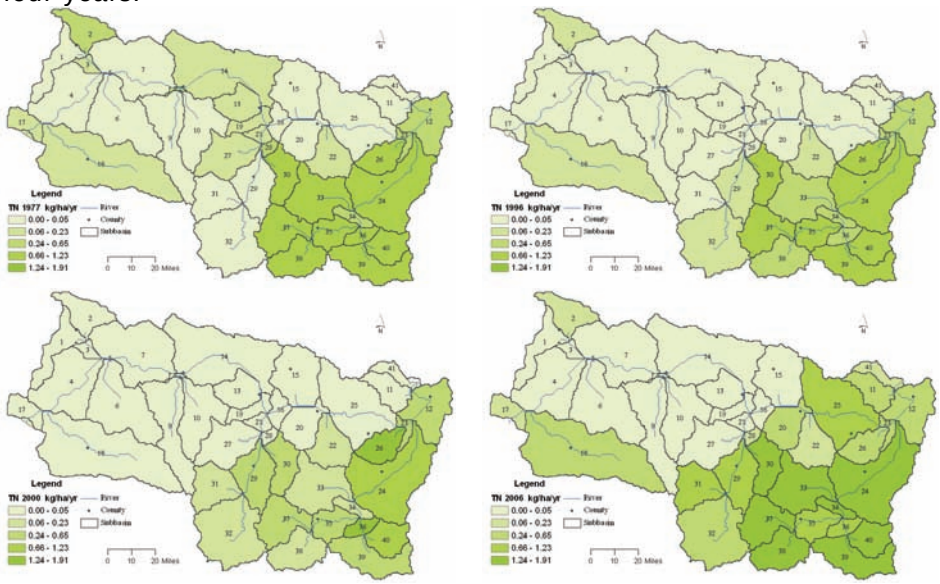

Fig. 7-1 Watershed NPS total nitrogen loss load distribution in four simulated years

(2) Phosphorus simulation

The losses of three main forms of P (organic P, soluble P and sediment P) were simulated, and their annual loads were calculated for the subsequent analysis (Table 7-2). The principal part of P is incorporated into organic matter or is adsorbed on clay particles. The load of sediment P fluctuated greatly in this period and reached a maximum in 2000. Organic P was another important source of P pollution and had the minimum load in 1996.

Table 7-2 Watershed P loss load in four simulated years (kg/ha/yr)

Format \ Year	1977	1996	2000	2006
Organic P	0.094	0.029	0.041	0.079
Soluble P	0.002	0.001	0.001	0.001
Sediment P	0.264	0.138	0.043	0.139
Total P	0.36	0.17	0.08	0.22

The spatial distributions of TP loadings in the four years simulated are shown in Fig. 7-2. Similar to TN losses, TP losses were greatest in the eastern sub-basins of the watershed, and TP losses were greatest in the year 1977. The watershed averaged loads in 1977, 1996, 2000, and 2006 were 1.20, 0.52, 0.88, and 1.02 kg/ha/yr, respectively.

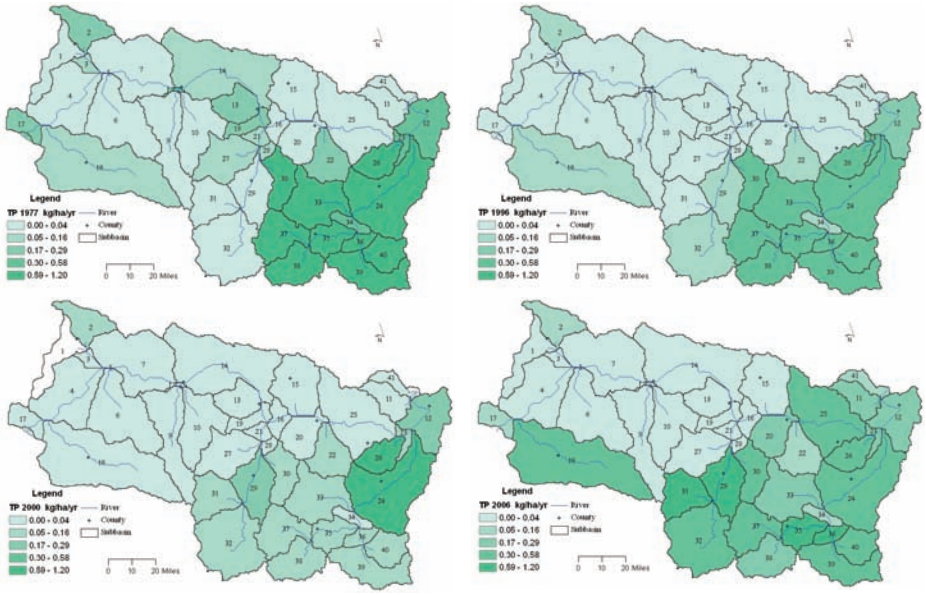

Fig. 7-2 Watershed NPS total phosphorus loss load distribution in four simulated years

7.3.2 Landscape pattern

Table 7-3 shows the variation of vegetation landscape pattern in the four years selected for this study. The area ratio of farmland, forest, and grassland in 2006 was 12.82%, 15.49%, 59.57% respectively. Among the four years, farmland area increased by 16%, forest areas by 8%, and grassland areas by 6 %. Forest had the greatest patch density (PD), increasing during the observation period. The largest change of PD was found in grassland, which increased from 0.06 to 0.09. The farmland PD had a similar trend to grassland, but it did not increase as much as the grassland PD over the last six years. Grassland had the largest edge density (ED), which was greatest in 1996 and decreased thereafter. The other two land covers had similar ED variation from 1977 to 2006. All vegetative covers had similar fractal distribution index (FI) values over the year considered in the study.

Table 7-3 Landscape pattern metrics of three vegetation types

Landscape	Year	Area (ha)	PD	ED	FI
Grassland	1977	2162346	0.06	14.48	1.06
	1996	2136788	0.06	22.61	1.08
	2000	2125454	0.06	22.59	1.08
	2006	2041691	0.09	20.46	1.08
Forest	1977	527936	0.10	10.11	1.08
	1996	491598	0.10	12.06	1.10
	2000	489799	0.10	12.01	1.10
	2006	530756	0.11	11.12	1.08
Farmland	1977	410355	0.01	2.47	1.09
	1996	384582	0.05	7.66	1.09
	2000	392696	0.05	7.61	1.09
	2006	445431	0.05	6.95	1.08

7.3.3 NPS nutrients pollution interaction with vegetation area

(1) Nitrogen loads respond to vegetation area

NPS nitrate N, organic N, organic P and sediment P are the main forms of nutrient pollutants from the watershed; therefore, their correlations with land cover over three decades were explored. The value of coefficient of correlation and F-test is listed in Table 7-4. Grassland was dominant land cover in the watershed, and its temporal area changes had different impacts on organic N and nitrate N losses. The negative correlation of grassland area with organic and nitrate N loss suggests that retained grassland prevents N NPS pollution. The R^2 value of organic N was much less than the nitrate N, which meant the grassland had low influence on organic N. Since organic N losses were larger than nitrate N losses, both

negative correlations proved that the increasing grassland area could substantially reduce total N losses from the watershed.

The forest area did not show any reliable correlation with nitrate N, but it was positively correlated with organic N loss, possibly due to losses in runoff of organic N from the decomposing biomass residues on the soil surface. The farmland area was significantly, although not strongly, correlated with nitrate N losses. With the comparison, farmland did not contribute to nitrate N pollution significantly. Considering all the correlation models of N losses with three vegetation types, it was concluded that organic N losses increased with increasing farmland and forest area. However, nitrate N losses, which were much smaller than organic N losses, were negatively correlated with grassland area.

Table 7-4 Correlation of vegetation area with N lodgings

x (area)	Correlation model of N	R^2	F
Forest	$N_{Organic}$=0.024x-0.966	0.849	1.414
	$N_{Nitrate}$=0.001x-0.021	0.035	0.091
Farmland	$N_{Organic}$=0.016x-0.4	0.539	2.346
	$N_{Nitrate}$= -0.0016x+0.105	0.109	0.214
Grassland	$N_{Organic}$=-0.0018x+0.617	0.028	0.057
	$N_{Nitrate}$=-0.002x-0.39	0.614	2.937
	Correlation model of P	R^2	F
Forest	$P_{Organic}$=0.0106x-0.5007	0.560	1.862
	$P_{Sediment}$=0.028x-1.2825	0.478	2.502
Farmland	$P_{Organic}$=-0.0042x+0.9305	0.478	1.301
	$P_{Sediment}$=0.0059x-1.1071	0.117	0.125
Grassland	$P_{Organic}$=0.0108x-0.3981	0.838	1.853
	$P_{Sediment}$=0.0081x-0.1859	0.059	0.264

The grassland area variation had a complex linear relationship with sediment and organic P losses. The negatively relationship with organic P suggests that grassland can reduce P pollution as expected. However, its impact on sediment P can be ignored. The correlation of organic P with farmland indicated that it was a stable source of organic P pollution. However, there were almost no sediment P come from farmland. The forest area had a moderately strong relationship with both formats of P. While, the positive correlation of two formats P indicated that forest was a contributor to P loss. In brief, expect for the grassland, which can prevent the organic P loading, other vegetation types were identified as contributor for both formats of P loadings.

7.3.4 NPS nutrients pollution interaction with vegetation landscape

(1) Nitrogen loads respond to vegetation landscape

After calculating the correlation of NPS nutrient loads with land cover area, the correlations with landscape pattern characteristics also was calculated (Table 7-5). By comparing all six correlation models, it appeared that forest landscape patterns were more closely related to organic N than nitrate N. The R^2 value of forest ED and FI with organic N were highly significant. The results also indicated that NPS nitrogen losses are more closely related to forest fractal distribution status than to edge area. Consideration of all three forest patch indicators meant that integration of forest patches can reduce NPS nitrogen loss.

Considering the correlation of six grassland landscape indicators with N loading, it was found that half of them were positive. The grassland FI had higher R^2 value than the grassland PD and ED, which suggests that grassland fractal distribution had more influence on organic N yield. Greater grassland fractal distribution was associated with less nitrate N pollution. It was found that nitrate N was negatively correlated with all three grassland landscape indicators. However, the organic N was positively correlated with the same three metrics, which indicates that the source of two formats of N was different.

The six correlation models of farmland metrics with two formats of N had much higher R^2 value than grassland. For these correlation models, farmland ED with nitrate N had the highest R^2 value, suggesting that farmland patch edges were principal contributors to N losses. The farmland FI had a greater correlation with organic N loss than with nitrate N loss. It is interesting to note that all three farmland landscape indicators had opposite correlation with two formats of N. The correlation analysis showed that two formats of N originated differently and the farmland landscape pattern had a different influence on NPS nitrogen pollutions.

Table 7-5 Correlation of vegetation landscape pattern and N pollution

x	Correlation model	R^2
Forest PD	$N_{Organic}$= 17.102-1.554	0.478
	$N_{Nitrate}$= -2.12x+0.2529	0.189
Forest ED	$N_{Organic}$=5.799x + 10.244	0.182
	$N_{Nitrate}$=-39.135x + 12.781	0.328
Forest FI	$N_{Organic}$= 0.625x-0.496	0.881
	$N_{Nitrate}$=-0.2258x + 1.10	0.092
Grassland PD	$N_{Organic}$= 2.8x+0.004	0.396
	$N_{Nitrate}$= -0.4435x + 0.0815	0.154
Grassland ED	$N_{Organic}$= 34.755x + 13.556	0.376
	$N_{Nitrate}$= -0.003x+0.089	0.529
Farmland PD	$N_{Organic}$= 2.868+0.76	0.635
	$N_{Nitrate}$= -0.598x+0.06	0.710
Farmland ED	$N_{Organic}$=25.987x + 1.331	0.499
	$N_{Nitrate}$= -0.004x+0.0633	0.618
Farmland FI	$N_{Organic}$= -173.4x+189.5	0.675
	$N_{Nitrate}$=0.0647x + 1.086	0.018
Grassland FI	$N_{Organic}$= 5.164x-5.347	0.502
	$N_{Nitrate}$= -1.120x+1.237	0.607

(2) Phosphorus loads respond to vegetation landscape

The correlations between vegetation landscape indicators and sediment P and organic P losses are summarized in Table 7-6. Except for the low correlation of forest PD with sediment P, the other five correlating models were negatively related to sediment and organic P. Forest was important in the watershed landscape, and it has been identified as contributors to P losses. The correlation models of forest ED and FI with P pollutants had a big R^2 value. The higher forest edge density can decrease both sediment P and organic P loads. The forest FI had the highest R^2 value with organic P. The analysis indicates that the more P pollutions result from the lower fractal forest landscape status.

The grassland landscape ED and FI had significant negative correlations with organic and sediment P loads. This suggests that landscapes with large amounts of grassland patches and grassland edges are associated with smaller amounts of NPS phosphorus loss. The positive correlations of grassland PD with two formats of P also coincide with this trend. Three farmland landscape indicators were all negatively correlated with the two forms of P loss. Based on these correlation equations, higher patch

density and more edges of farmland landscape was associated with smaller P loading. Since farmland was a source of NPS phosphorus losses, one solution may be to reduce patch edges and densities.

Table 7-6 Correlation of vegetation landscape with P pollution

x	Correlation model	R^2
Forest PD	$P_{Organic}$=-5.859x-0.536	0.275
	$P_{Sediment}$=3.379x-0.198	0.010
Forest ED	$P_{Organic}$=-0.032x+0.421	0.917
	$P_{Sediment}$=-0.086x+1.123	0.766
Forest FI	$P_{Organic}$=-2.991x+3.325	0.967
	$P_{Sediment}$=-6.851x+7.622	0.576
Grassland PD	$P_{Organic}$=0.3059x + 0.046	0.378
	$P_{Sediment}$=0.0294x + 0.06	0.031
Grassland ED	$P_{Organic}$=-0.07x+0.200	0.765
	$P_{Sediment}$=-0.21x+0.573	0.815
Grassland FI	$P_{Organic}$= -2.637x+2.886	0.643
	$P_{Sediment}$=-8.549x+9.307	0.767
Farmland PD	$P_{Organic}$= -1.161x+0.105	0.511
	$P_{Sediment}$=-4.183x+0.307	0.753
Farmland ED	$P_{Organic}$= -0.010x+0.122	0.650
	$P_{Sediment}$=-0.032x+0.346	0.791
Farmland FI	$P_{Organic}$= -3.944x+4.352	0.690
	$P_{Sediment}$=-6.064x+6.745	0.185

7.4 Discussion

7.4.1 NPS nutrient pollution with three types of vegetation's' area

Similar spatial distributions of TN loading were found for the four years (Fig. 7-1). This spatial distribution of TN loss helps identify the critical sub-basins for watershed NPS pollution. After comparing the TN loss distribution with land cover figures, it was concluded that farmland was the principal contributor to NPS nitrogen losses. The temporal variation of TP suggests that loads of TP have declined over the last thirty years. Among the three P pollutants, soluble P loads were less than 1% of total P loads. The sediment P was the dominant P pollutant, constituting more than half of TP load.

Increasing farmland area was associated with increases in organic N and organic P losses. Agricultural activity was major contributor of NPS pollution, and farmland can be a critical source of pollution (Behera and Panda, 2006). Increasing forestry was positively correlated with losses in organic N, organic P and sediment P. Increases in grassland area were positively correlated with the decrease of losses in nitrate N and organic P. The study of Gorsevski (2008) also noted the potential non-point source pollution in forested watersheds. With the correlation models, the function of grassland to reduce NPS pollution was identified. The slope in Table 5 and Table 6 is the feedback of vegetation area variation on pollution export of different nutrient formats. With this finding, it will be used to evaluate and predict the impact of potential land cover change on the nitrogen and phosphorus load. Such an understanding is critical in term of predicting how vegetation land cover may alert water quality in local ecosystem and the subsequent interactions between ecological and hydrological processes (Wood, 2007).

The export of nutrient is determined by land cover, climatic conditions, soil properties and topography (Beaulac and Reckhow, 1982). The latter two factors were not to vary in decade period. The climatic indicator, mainly about precipitation is covered in the simulation. The weakness in this paper is the limitation of monitored data, which could reduce the credibility of the analysis. However, we concentrated on the interactions of nutrients loading with vegetation area and landscape pattern. The comparative data was the basis for analysis, so the vegetative area and landscape pattern were kept as variables. With the calculated outcome, the aims of analysis were achieved. Mattikalli and Richards (1996) also successfully modelled the NPS pollutants loading and land cover was the variable.

7.4.2 Influence of vegetation landscape pattern on NPS nutrients pollution

The land cover landscape pattern has been point out with interaction with surface water quality in small area (Xiao and Ji, 2007). The role of vegetation's landscape pattern in influencing non-point source N and P pollution process of different formats at watershed sale was also established in this paper. The correlation equations of landscape indicators with N loading suggest that the three vegetation's landscape pattern had direct effect on watershed NPS nitrogen pollution. As right is expected, farmland metrics appear to have had greater effects on nitrate N losses (Borin and Tocchetto, 2007). The analysis indicated that more fractal farmland patches with more edges caused more NPS nitrogen losses, especially organic N. However, the pattern of forestry and grassland had greater impacts on organic N than nitrate N losses. More fractal forestry and farmland landscapes were associated with more N losses. In contrast, more grassland patch edges are associated with reduced N losses. Patch size and edge both had significant correlations

with N loss; therefore, integrating small farmland patches into bigger areas might decrease NPS nitrogen losses.

Although forestry was the contributor of NPS P pollution, simple and less fractal landscape patterns can decrease P losses. On the other hand, the landscape pattern of farmland can be applied in watershed NPS phosphors pollution preventions. The most important finding was that more factual and complex grasslands help minimize NPS P loadings.

Planting has been recognized as main solution to preventing the non-point source nutrients pollution (O'Geen et al., 2007). The study of Siepel also showed that the vegetation landscape had the function in adjusting hydrological conditions and affecting NPS nutrients pollution transportation to the water body (Siepel et al., 2002).When planting grass to prevent watershed NPS pollution, grass strips would be more effective and provide much valuable service with the consideration of landscape pattern. Bouldin (2004) also stated that the vegetative pattern in agricultural drainages had impact on nutrients pollution control.

7.5 Conclusions

The models correlated different landscape indicators and diverse formats of NPS nutrients loading. The correlations suggested that landscape pattern of vegetative cover had close effect on NPS nutrients pollution. The grassland with more patch edges may reduce NPS loads. Although forest was the partial contributor to NPS phosphorus pollution, a simple and less fractal forest landscape can decrease P loads. More fractal and complex grassland landscapes were also associated with smaller NPS phosphorus loads. These suggested effects of landscape design on NPS nutrient loads could lead to economic and efficient solutions to reduce NPS loading.

Naturally, there are limitations in this research. Based on the results obtained in this study, it was also found that grassland area had apparent effects on nutrient pollution control. Grassland strips appear to have significant impacts on NPS nitrate N or organic P pollution. Farmland contributed both organic N and P loads, but we did not find large impacts on sediment P or nitrate N losses. These correlation models can be used to simulate and predict the responses of vegetation area variation on watershed NPS nutrients pollution loading.

The SWAT modelling system simulated watershed nutrient pollutions with the consideration of land cover in different years, which enhanced modelling accuracy and provided the comparative data used in this study. The spatial distribution of NPS pollution loads is an important consideration in the control of watershed pollution. The different behaviour of forms of NPS nitrogen and phosphorus can be used to identify pollution sources and thus heightened cost-effective water quality management planning.

Chapter 8 Temporal-spatial dynamics of vegetation variation on non-point source nutrient pollution

Abstract

The temporal-spatial interaction of land cover and non-point source (NPS) nutrient pollution were analysed with the Soil and Water Assessment Tool (SWAT) to simulate the temporal-spatial features of NPS nutrient loading in the upper catchments of the Yellow River catchment. The corresponding land cover data variance was expressed by the normalized difference vegetation index (NDVI) that was calculated from MODIS images. It was noted that the temporal variation of land cover NDVI was significantly correlated with NPS nutrient loading. The regression analysis indicated that vegetation not only detained NPS nutrient pollution transportation, but also contributed to sustainable loading. The temporal analysis also confirmed that regional NDVI was an effective index for monthly assessment of NPS nitrogen and phosphorus loading. The spatial variations of NPS nutrient loading can be classified with land cover status. The high loadings of NPS nitrogen in high NDVI sub-basins indicated that forest and farmland are the main loss areas. Farmland contributed sustainable soluble N, but the loading of soluble and organic N from grassland sub-basins was much lower. Most P loading came from the areas covered with dense grassland and forest, which cannot directly discharge to local water bodies. However, some NPS phosphorus from suburban farmland can directly discharge into adjacent water bodies. The interactions among nutrient loading, NDVI, and slope were also analysed. This study confirmed that the integration of NPS modelling, geographic information systems and remote sensing is needed to understand the interactive dynamics of NPS nutrient loading. Understanding the temporal-spatial variation of NPS nutrients and their correlations with land cover will help NPS pollution prevention and water quality management efforts. Therefore, the proposed method for evaluating NPS nutrient loading by land cover NDVI can be an effective tool for pollution evaluation and watersheds planning.

Published as:
Ouyang Wei, Wang Xuelei, Hao Fanghua, Srinivasan R.. Temporal-spatial dynamics of vegetation variation on non-point source nutrient pollution. Ecological Modelling, 2009, 220(20): 2702-2713.

8.1 Introduction

The watershed-land cover variation and its impact on non-point source (NPS) nutrient pollution can lead to serious water quality concerns (George et al., 2008; Chang, 2008). The NPS nutrient pollutants, such as N and P, are significantly related to land cover status and are direct cause of eutrophication (Ahearn et al., 2006). Traditional monitoring cannot provide the necessary information for the environmental management of a river watershed. Furthermore, the NPS pollution simulation does not provide an effective description of land cover variation because it includes the impacts of temporal variation of land cover and is in need of diverse spatial and input data (Haregeweyn and Yohannes, 2003). The integration of the NPS simulation model and GIS can resolve these problems in river basin water quality management, and this combined system is an effective method for identifying the influence of land cover variation as at temporal-spatial scale (Ning et al., 2006). This paper is a pilot attempt to discover the temporal and spatial correlation between land cover and NPS nutrient pollution with GIS and a simulation model at the watershed scale and to explore the role of land cover zoning with different NDVI in dynamic NPS nutrient settings.

Several methods have been proposed for simulating nutrient loads in a water body, which is a great need in water pollution prevention and source identification (Xian et al., 2007). Most of the model systems can simulate the yield of TN and TP based on the summation of modelling cells and discharge rate (Gowda et al., 2008). However, the variation of land cover at the temporal-spatial scale cannot be considered. On the other hand, the loading differences of diverse land cover categories were measured in small areas, which cannot be applied in water quality control. Based on remote sensing data, the spatial relationship of land cover variation and the variance of nutrient yield has attracted some attention (Krause et al., 2008). In addition to the influence of land cover, precipitation is another significant factor for NPS nutrient yield. The NDVI was applied to express the land cover status, which is directly linked to precipitation (Brunsell, 2006).

In the past, regional land covers were investigated by remote sensing LANDSAT MSS and TM data (Oki and Yasuoka, 2008). In order to get consistent data from images in temporal scale, coarse resolution images were widely used. The NOAA AVHRR image was used to describe land cover transformations at a global or watershed scale (Vicente et al., 2006). In this study, land cover NDVI information was calculated with imagery from MODIS. The MODIS instrument on board NASA's Terra satellite is designed primarily for remote sensing the land surface with spatial resolutions of 250 m (William and Maik, 2005). Moreover, frequent temporal resolution can provide fine repeated data, providing a good method for monitoring and analysing vegetation processes. MODIS has been popularly applied in a variety of projects involving large scale

vegetation dynamics and land coverage research (Wardlow and Egbert, 2008).

Most of the NPS modelling systems have the ability to estimate the discharge of annual nitrogen and phosphorus loads (Flipo et al., 2007). However, the discharge sum of basin calculation cells can only evaluate the load of each watershed. In other words, it is not easy to simulate the temporal-spatial characteristics of NPS nutrient load, which is the basis for land cover variation correlation identification in watersheds.

8.2 Materials and methods

The general framework of the present study is followed. First, the SWAT-required spatial database was constructed then the model system was calibrated. Secondly, monthly and yearly NPS nutrient yields, in their different forms, were estimated at basin and sub-basin scales. Thirdly, the land cover dynamics in the same temporal-spatial scale were calculated with MODIS images using ArcGIS. With statistical analyses, the temporal correlations of land cover NDVI with NPS nutrient loadings from the whole basin were identified. Furthermore, the spatial interaction of land cover at the sub-basin level was calculated with corresponding NPS nutrient discharge.

8.3 Results

8.3.1 Temporal-spatial trends of the NDVI

(1) Spatial trends of the NDVI

With MODIS images, the yearly NDVI distributions in 2000, 2003, and 2006 are shown in Fig. 8-1. Comparing the three years, the NDVI distribution did not experience substantial variation. The western portion and areas along the river bank distinguished the lower NDVI from the area of higher NDVI which was spread mainly throughout the south-eastern region. The NDVI ranges during the three years were 0.9173, 0.9233, and 0.8921, respectively. In 2003, the largest NDVI range was impacted directly by a greater amount of precipitation. The spatial variation of NDVI was created by extracting the NDVI value in every sub-basin cell, assisted by the ArcGIS tool. At the sub-basin level, the NDVI range in 2000, 2003, and 2006 were 0.5347, 0.4690, and 0.5159, respectively. The NDVI in 2003 had the smallest range and standard deviation, which indicated that the sub-basin NDVI was more similar than in the other years. With the sub-basin mean NDVI data, the vegetation status in each cell can be expressed, which was the basis for interaction analysis.

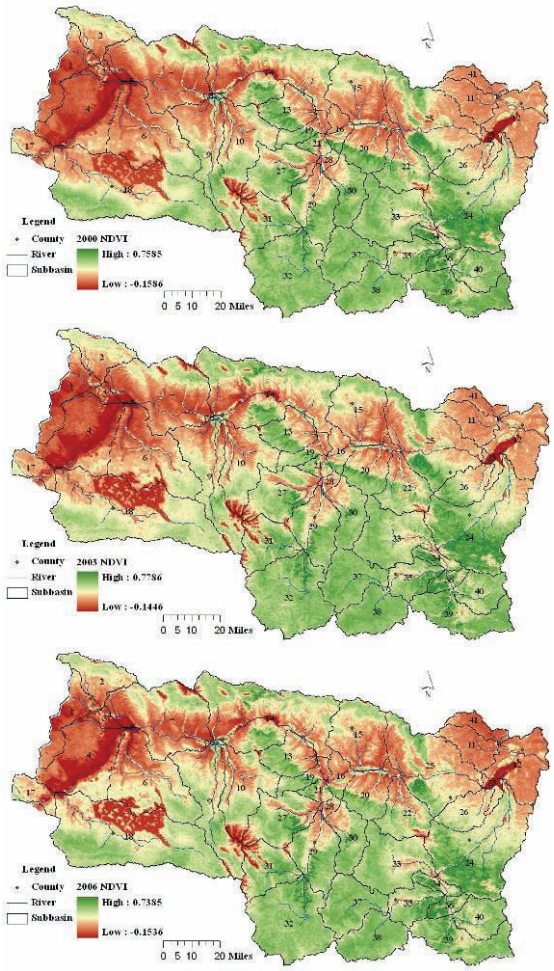

Fig.8-1 NDVI distribution of each sub-basin over three years

(2) Temporal trends in basin NDVI

The monthly NDVI data were averaged with MODIS data by ArcGIS (Table 8-1), which presented the temporal variation principle of watershed land cover. The monthly pattern showed similar trends during the three years, describing vegetation growth dynamics. The NDVI increased dramatically from April and reached its summit in July, then decreased slowly throughout the remainder of the year. Overall, the NDVI range during the three-year period dropped from 0.3669 to 0.3017, which also caused the standard deviation (Std. D) to continually decrease from 0.1342 to 0.1245. However, the mean NDVI value increased from 0.2885 to 0.3172 in the same period. The minimum NDVI in 2000 was 0.1228, which was significantly less than the other two years. The lower NDVI value in 2000 was consistent with the drought in that year. The

NDVI demonstrated the features of land cover and precipitation, which are the dominant factors for soil erosion formation and transportation.

Table 8-1 Watershed monthly NDVI value and statistical feature

Year / Month	2000	2003	2006
1	0.1228	0.2076	0.1904
2	0.1305	0.1948	0.1874
3	0.1884	0.1868	0.1943
4	0.2062	0.2143	0.2441
5	0.3945	0.3912	0.4186
6	0.4897	0.4507	0.4874
7	0.4579	0.5178	0.4891
8	0.4453	0.5028	0.4684
9	0.3661	0.3708	0.3927
10	0.2642	0.2741	0.2799
11	0.2195	0.2350	0.2568
12	0.1767	0.1584	0.1963
Range	0.3669	0.3594	0.3017
Mean	0.2885	0.3087	0.3171
Std. D	0.1342	0.1309	0.1245

8.3.2 Spatial trends of NPS nitrogen pollution

(1) Spatial trends of NPS nitrogen loss

The annual load of TN and TP during the three simulated years is shown in Fig. 8-2. NPS nitrogen loadings from different sub-basins showed significant spatial differences, showing an increasing trend from west to east in the observed watershed. In the northeast region, TP loadings ranged from 0.005 to 1.718 Kg/ha. The main loading sub-basins were distributed in the east, while the farmlands were distributed predominantly around the Liujiaxia reservoir and along the main stream of the Yellow River. The spatial distribution observed throughout the three years contained similar trends, and the sub-basins covered with more vegetation had a remarkable association with TN loading.

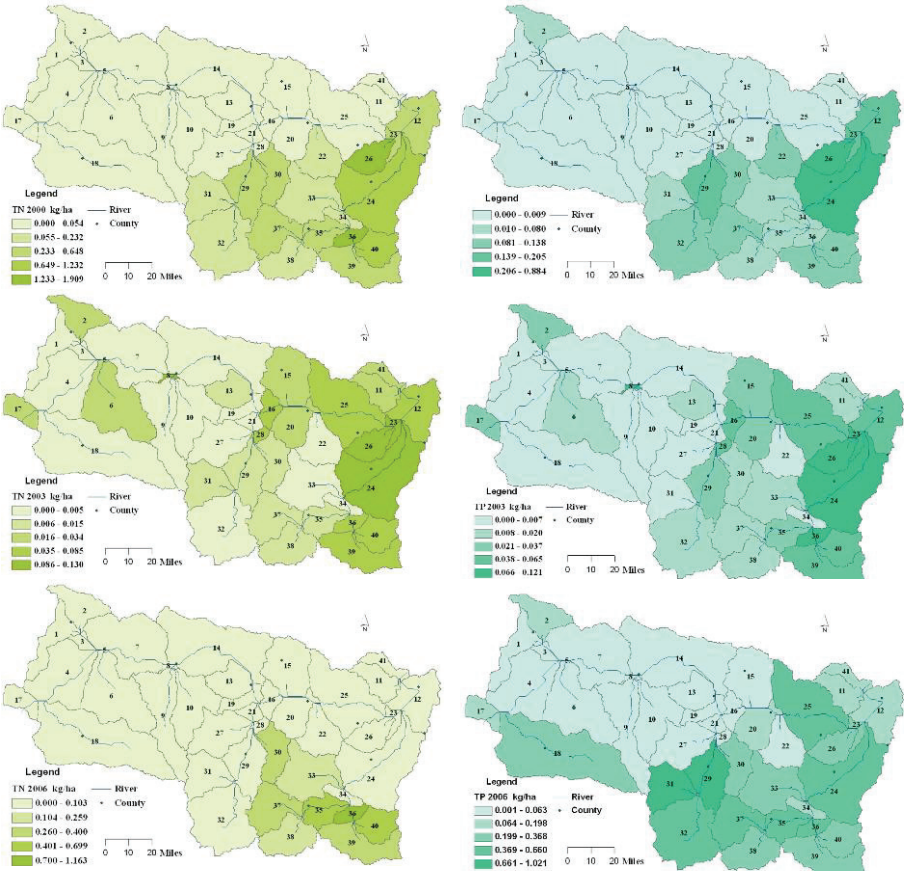

Fig.8-2 TN and TP loading distributions for each sub-basin during the three years

(2) Temporal trends of NPS nitrogen

The monthly TN loading for the three years is listed in Table 8-2. The monthly load had a significant temporal trend. The TN loading increased from Jan. to Jul. then declined, which paralleled the similar temporal pattern of vegetation growth. The maximum loadings were recorded in Jun. and Jul. as 0.105, 0.753 and 0.096 Kg/ha in 2000, 2003, and 2006, respectively. The annual loading of NPS nitrogen in 2003 was much more than the other two years. This may be due to the combined effects of land cover variation and storm rain. Although there were some variances in monthly loading, the temporal pattern was constant.

Table 8-2 Watershed monthly TN load (Kg/ha) and statistical features

Year / Month	2000	2003	2006
1	0.000	0.000	0.000
2	0.002	0.003	0.000
3	0.004	0.037	0.000
4	0.000	0.106	0.002
5	0.020	0.074	0.002
6	0.060	0.007	0.096
7	0.105	0.753	0.081
8	0.010	0.342	0.047
9	0.037	0.189	0.038
10	0.010	0.354	0.010
11	0.002	0.044	0.008
12	0.003	0.001	0.005
Range	0.105	0.753	0.096
Mean	0.021	0.159	0.024
Std. D	0.032	0.226	0.034

8.3.3 Spatial trends of NPS phosphorus pollution

(1) Spatial trends of NPS phosphorus loss

The watershed TP loadings in 2000, 2003, and 2006 were simulated and the annual distributions were shown in Fig. 3-5. NPS phosphorus yields from individual sub-basins had a high spatial variability, but the spatial distribution during the three years followed similar trends. Approximately half of the basin contributed fewer little P (0.008 Kg/ha) and did not impact water quality. However, some sub-basins in the eastern and southern areas contributed much more TP, which had loadings in excess of 0.1 Kg/ha. The No. 29 sub-basin in the middle reach had the most remarkable loss. The spatial distribution coincided with vegetation trends, indicating that vegetation, especially forest and dense grass, has a direct relationship with NPS phosphorus pollution. The spatial distribution of NPS phosphorus was also useful for identifying the transportation path.

(2) Temporal trends of NPS phosphorus

The estimated monthly TP load during the three years shared similar temporal patterns with TN. The TP loading exhibited an upward trend from Jan. to Aug. then decreased (Table 8-3). The highest yearly and monthly loads were both in 2006. The peak value of monthly loading in these years appeared in Jun. and Jul., which coincided with summit TN loadings. The maximum loads throughout the three years were 0.048, 0.042, and 0.088 Kg/ha, respectively, causing corresponding variation in the standard deviation.

Table 8-3 Monthly watershed TP loads (Kg/ha) and statistical features

Year / Month	2000	2003	2006
1	0	0	0
2	0.002	0	0
3	0.004	0.004	0
4	0	0.005	0.08
5	0.021	0.007	0.002
6	0.048	0.002	0.002
7	0.002	0.042	0.088
8	0.007	0.026	0.046
9	0.012	0.011	0.036
10	0.004	0.019	0.01
11	0	0	0.007
12	0.002	0	0.004
Range	0.048	0.042	0.088
Mean	0.009	0.010	0.023
Std. D	0.0139	0.0131	0.0322

8.4 Discussion

8.4.1 Influence of NDVI temporal variation on NPS nutrient loads

(1) NPS nitrogen

The monthly basin NDVI can be used as an indicator for NPS nitrogen loading, as the correlation between them shows (Fig. 8-3). It was concluded that the variation of TN loss had considerable connection with the temporal scale of watershed land cover. When watershed NDVI was less than 0.27, the NPS total nitrogen loading was much lower. Local vegetation NDVI increased quickly in the summer, so there was an NDVI gap during correlation analysis. However, the TN loss increased dramatically when land cover had an NDVI higher than 0.35. Previous studies have concluded that more vegetation can prevent NPS pollution (Maillard and Santos, 2006). The analysis indicated that vegetation not only disturbed pollutant transportation, but contributed sustainable NPS pollution. During the period of vegetation growth and maturity, the increasing NDVI and its associated precipitation intensified NPS loadings. This delivery certainly impacted the water quality and terrestrial ecosystem. The regression analysis indicated that the monthly NDVI was a good predictor for determining monthly NPS total nitrogen pollution load.

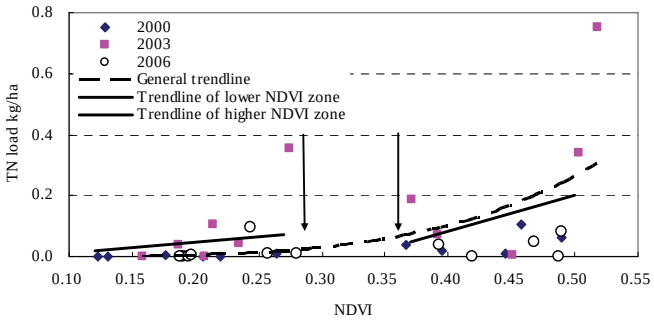

Fig.8-3 Temporal interaction between watershed NDVI and monthly TN loss

(2) NPS phosphorus

The temporal correlation pattern between the monthly variation in land cover on the formation and transportation of TP loadings was confirmed (Fig. 8-4). When the average watershed NDVI was lower than 0.28, much less NPS phosphorus pollution occurred. Watershed TP yields increased when the NDVI value was higher than 0.35. There was an obvious threshold point in TP loading at which watershed NDVI jumped from 0.28 to 0.35. In preventing NPS phosphorus pollution, the critical time period is the moment of higher NDVI. Human engineering solution should be applied during the time of higher NDVI, resulting in better water quality. The regression analysis also confirmed that regional NDVI was an effective index for monthly assessments of NPS total phosphorus discharges.

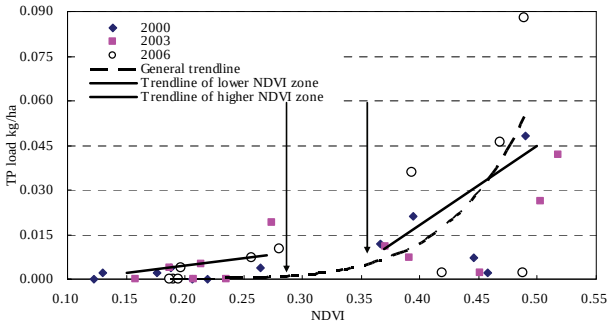

Fig.8-4 Temporal interaction of watershed NDVI with monthly TP loss

8.4.2 Sub-basin NDVI with NPS nitrogen pollution

In order to recognize the influence of land cover status on NPS nitrogen loading, the correlation between NDVI and TN, organic N, and soluble N was calculated at the sub-basin level (Fig. 8-5). It was found that sub-basin NDVI was a significant factor in NPS nitrogen yield. The sub-basins with an NDVI lower than 0.15 contributed almost no NPS nitrogen, differing from areas with high soil erosion. Preventing NPS nitrogen discharges from areas with dense vegetation was the highest priority for pollution control. Furthermore, forest and dense grass were found to

have more influence on NPS nitrogen loading than other land covers. After classifying the land covers by NDVI, the gathering plots were defined in five zones. In forested sub-basins (zone E), the NPS nitrogen load was much higher than other zones. The NPS nitrogen load discharged from bare land and grassland areas (zone A and zone C) was much lower. The cultivated sub-basins (zone B) contributed some NPS nitrogen. Based on an NDVI value from a predefined sub-basin, the NPS total nitrogen load from each sub-basin can be estimated, which was helpful for a quick assessment of pollution loads.

Furthermore, the correlation of land cover NDVI with soluble N and organic N were analysed. Soluble N loading was a small portion of TN loss, but it had a more significant link with sub-basin NDVI. As seen in Fig. 8-5b, the soluble N discharge was higher in zone B than organic N. The higher load in zone B was due to the loss of fertilizers. Soluble N discharged from forested areas was due to arboreal remains. However, the soluble N yield from sub-basins covered with dense grass was low due to the uptake by grass. The findings in this study confirm that grassland strips are an effective way to prevent NPS soluble N from discharging into the aquatic environment. Fig. 8-5c shows the relationship between organic N loading and NDVI. Unlike the remarkable load of soluble N in zone B, the organic N yield from this zone was relatively slight. On the other hand, the organic N discharge value was the same for both the grass and forested sub-basins. This was due to the fact that most organic N was transported with the soil particle. The sub-basin characterized with dense grass was still the key for organic N.

Overall more loading of NPS nitrogen in higher NDVI sub-basins indicated that forests and farmland were the loss sources. The key to preventing NPS nitrogen is to disturb the transportation paths, as demonstrated by the fact that the loading of soluble and organic N in the grassland sub-basins was much lower. In addition, other studies have shown that grassland can reduce particle movement and is more effective in detaining N (Merrill and Benning, 2006). Based on the findings of this study and the conclusion of the aforementioned study, setting aside grassland strips along the critical sub-basin is probably the most effective solution to reducing NPS nitrogen.

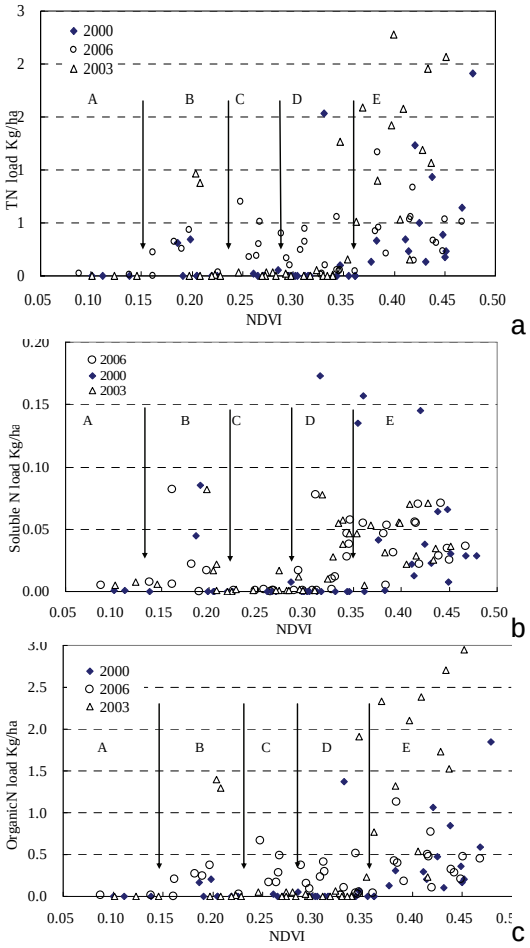

Fig.8-5 Interaction of annual sub-basin NDVI with N loss

8.4.3 Sub-basin NDVI with NPS phosphorus pollution

Following the same procedure, the impact of land cover NDVI on NPS phosphorus loss was analysed (Fig. 8-6). The hypothesized NPS phosphorus load differences among the sub-basins were confirmed consistently. The first notable trend was that the loading of NPS phosphorus increased with increasing NDVI. As shown in Fig. 8-6a, forested areas with higher NDVI in zone E contributed sustainable TP yield. The bare land with NDVI less than 0.15 produced almost no NPS phosphorus pollution. The agricultural land with NDVI between 0.15-0.23 had a positive association with P loading. The grassland with NDVI between 0.23-0.30 was the primary land cover that contributed much less TP loss. On the other hand, grassland has been proven as an effective buffer zone to prevent NPS phosphorus pollution (Bouldin, et al., 2004). These results suggested land cover with higher NDVI was the principal driving force for NPS phosphorus pollution.

The relationship between sub-basin NDVI and organic and sediment P loadings was further analysed (Fig. 8-6b and Fig. 8-6c). Both forms of P loadings had close linkages with forested areas. The spatial variation of organic P loading was accompanied by NDVI. There was urban sprawl moving into forested areas (zone E) and notable loading decreases from agricultural land (zone B) and dense grassland (zone D). This illustrates that forested areas increase NPS organic P pollution. Runoff from these densely covered sub-basins typically contained a high density of NPS phosphorus.

The correlation of NDVI with sediment P is shown in Fig. 8-6c. There were significant increases in sediment P yield in most sub-basins with an NDVI between 0.15 and 0.23 (zone B). This illustrated that agricultural cultivation had a major impact on NPS sediment P pollution. The surplus of P fertilizer and deposition of waste intensified sediment P loss. Unlike the scenario with organic P, the sub-basins covered with dense grassland (zone D) had higher loading. Equally, the forested sub-basins contributed significant sediment P loading. There were no significant differences between the yield of organic P and sediment P in zone E, which included higher NDVI sub-basins in the mountainous region.

Except NPS phosphorus from farmland, most P loading came from the area with dense grassland and forests, which cannot directly discharge into local water bodies. Engineering structures should be constructed along the forested sub-basins, effectively preventing phosphorus loading. Equally, most NPS phosphorus from suburban farmland discharges directly into adjacent water bodies. In riparian systems, the agricultural P loading can be prevented though best management practices.

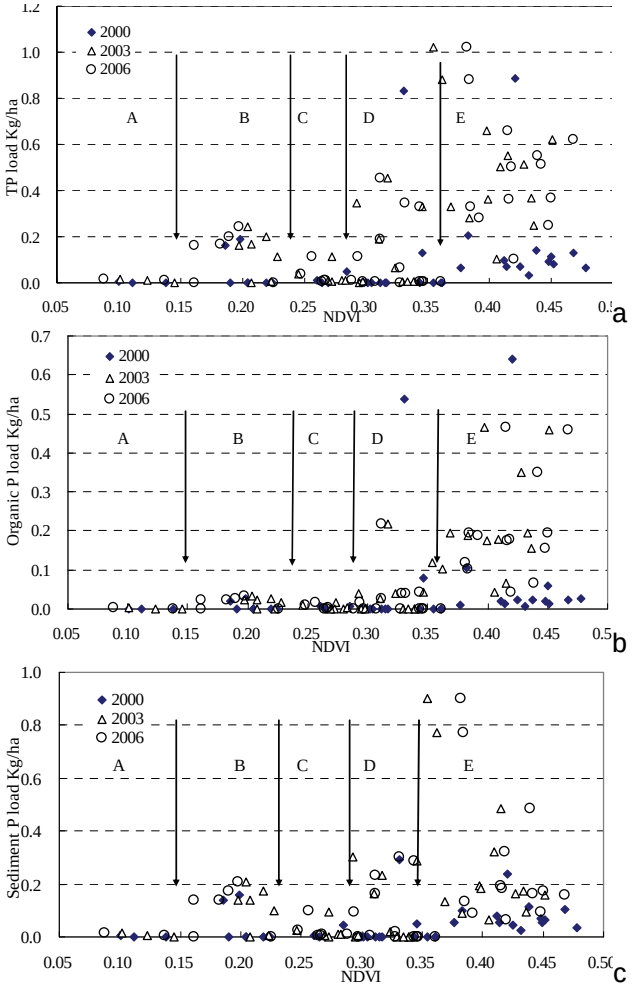

Fig.8-6 Interaction of annual sub-basin NDVI with P loss

8.4.4 Slope, NDVI and nutrients load

As seen in Fig. 8-5 and Fig. 8-6, there were some outlying points and clustered points. In order to explain this and the intensified impact of slope, the interrelationship of slope, annual NDVI, and yearly nutrient loads were analysed (Fig. 8-7). Slope was a compensatory signal for erosion. Consequently, the analysis demonstrated that the main TN loss area was the sub-basin with higher NDVI. The NDVI status had more direct impact on TN loss than the slope condition. The forested mountain area with the steepest slope was a TN discharge source. The forested sub-basins with a slope of 6-8 degrees contributed to TN loading. The discharge source of TP was much more complicated. The slope was more sensitive than NDVI in regard to TP loss. Therefore, the main areas had a slope higher than 10 degrees with an NDVI ranging from 0.32 to 0.47.

However, there was another zone that had a remarkable TP yield with an NDVI around 0.3 and a slope of 6 degrees. The analyses showed that most of the TP originated from steep, forested areas and dense grassland. The well-preserved, natural plantation was the main contributor of TP loading, not the human activity landscape.

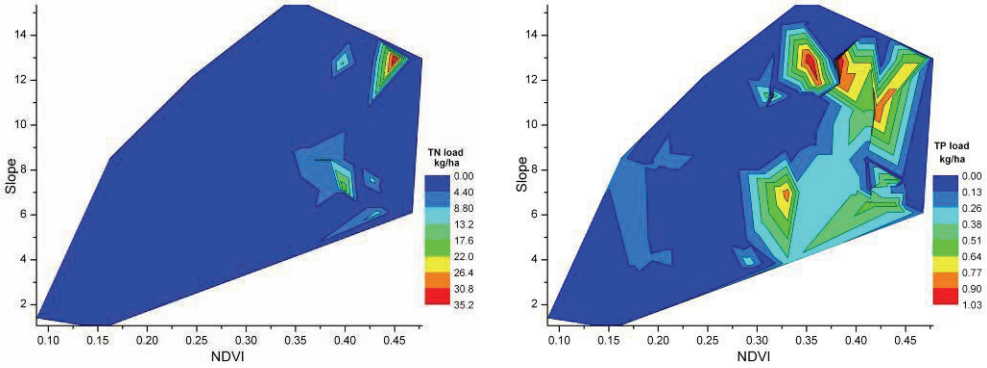

Fig.8-7 Interaction of sub-basin NDVI and slope with nutrient loads

8.5 Conclusions

In this paper, we estimated the annual and monthly NPS nutrient loads in the upper catchments of the Yellow River catchment using SWAT. The variation principle of land cover status was expressed by NDVI, calculated from MODIS imagery. The study demonstrated that temporal variation of land cover NDVI showed significant correlation with NPS nutrient loading. The regression analysis indicated that vegetation not only prevented NPS nutrient pollution transportation, but also contributed sustainable NPS nitrogen and phosphorus pollution. In the period of vegetation growth and maturity, the increasing NDVI and associated precipitation increased NPS nutrient loadings, which certainly impacted the water quality and terrestrial ecosystem once delivered. The temporal analysis confirmed that regional NDVI was an effective index for the monthly assessment of NPS nitrogen and phosphorus loadings.

The spatial variations of NPS nutrient loads were associated with land cover status. Greater loading of NPS nitrogen in higher NDVI sub-basins indicated that forest and farmland are main loading areas. Farmland contributed sustainable soluble N, but the discharge of soluble and organic N in the grassland sub-basins was much lower. The spatial analysis demonstrated that most P loadings came from the area covered with dense grassland and forests that cannot directly discharge to local water bodies. On the other hand, some NPS phosphorus from suburban farmland can easily discharge into adjacent water bodies. Setting aside riparian habitat along the critical sub-basin, adjacent to farmland and forests, will be the most effective solution for reducing NPS nutrients.

The interaction of slope, NDVI, and nutrient loading identified the

nutrient discharge source deeply. The analysis demonstrated that the area with steeper slope and higher NDVI contributed most of the nutrient loadings. The remote, natural plantation was the main source of NPS nutrient pollution in the study watershed rather than being human activity oriented.

This study supports the integration of NPS modelling and land cover monitoring by remote sensing to understand the interactive dynamics of NPS nutrient loading. Understanding the temporal-spatial variation of NPS nutrients and their correlation with land cover will help NPS pollution prevention and water quality management efforts. Therefore, the proposed method for evaluating the NPS nutrient loadings by land cover NDVI is a helpful and effective tool for pollution evaluation and watershed planning.

Chapter 9 Synthesis

9.1 Introduction

Soil erosion and pollution from non-point source nutrients pollution are common issues in regional environmental protection and management (Ni et al., 2008). These issues are especially important in the upper Yellow River, where the natural environment is fragile as a result of the continental climate and increasing pressure by human disturbance (Wang et al., 2006). The long-term land cover and landscape pattern variations are the basic index for analysis of terrestrial environmental processes. Furthermore, these changes impact the formation and transport of soil erosion, as well as pollution from non-point source nutrient pollution, which subsequently influences water quantity and quality not only in local watersheds, but also downstream in the Yellow River basin.

This research was proposed because of the fact that an understanding of soil erosion and non-point source pollution control would allow an assessment an understanding of the environmental processes in watershed. Moreover, the long-term land cover and landscape response to hydroelectric cascade exploitation in China are beginning to attract the attention of policy makers and politicians. Tools to achieve such an understanding are remote sensing and geographical information systems, as they have potential to acquire and analyse the land cover data effectively and at a low cost (Carlson and Arthur, 2000; Loboda et al., 2007).

We found that the proposed modelling, remote sensing and geographical information systems in this thesis are effective solutions to achieving these goals. In this final chapter, we summarize the main results and their interactions in this study and highlight the needs of future work. The detailed problem statement, study objectives and study area description were stated in Chapter 1.

9.2 Main results and their interrelationships

9.2.1 Identifying long term land cover and landscape variation

The eco-environmental quality, especially vegetation cover status in the upper catchments of the Yellow River, is important for the whole watershed (Neal et al., 2003). Climatic and intensive human activities have influenced regional land cover condition and eco-environment quality (McAlpine et al., 2007). Because grassland and forest are the two types of dominant vegetation, we consider therefore that there is possibility to identify the interactions between vegetation NDVI with climatic variables. Our first research question is:

- Is vegetation NDVI derived from MODIS related with climatic variables in the upper catchments of the Yellow River? If so, does a statistically significant difference exist between the climatic variables and the vegetation status?

In Chapter 2, we examine the vegetation dynamics and connections with climatic variables. The Moderate Resolution Imaging Spectroradiometer (MODIS) has the advantage of high temporal resolution and appropriate spatial resolution for regional scale analysis (William and Maik, 2005). MODIS has been widely used in land cover monitoring (Pflugmacher et al., 2007). Vegetation is the dominant land cover in the upper catchments of the Yellow River, which affect the ecological stability of the whole watershed. So, MODIS was used to monitor land cover dynamics and its connection with climatic characteristics.

With the normalized difference vegetation index (NDVI), the responses of inter-annual grassland and forest to three climatic indices (i.e. yearly precipitation, highest and lowest temperature) were analysed. As expected, there were strong positive correlations between them (larger than 0.733). The analysis at monthly scale provided the threshold value for three climatic indictors, which were used to assess growth of grassland and forest under different climate features.

The results confirmed the utility of NDVI as an index to express vegetation variability in a watershed with continental climate at high latitude and with little precipitation. It was also found that the lowest monthly temperature has the most pronounced impact on land cover change. The response of NDVI of regional vegetation to climate feature can be assessed much more accurately with climatic data, which is helpful for terrestrial environment assessment.

Over the last several decades, the Yellow River has experienced a dramatically decreasing water flow discharge since the construction and operation of large reservoirs, which are mainly located in the upstream catchments (Ta et al., 2007). Studies have demonstrated that remotely sensing (RS) data can provide spatial information for land cover monitoring and analysis which is difficult to monitor using conventional techniques, especially at a watershed scale over long periods of time (Adel and Ryutaro, 2007). After understanding the spatial distribution of vegetation, the temporal variation was the next research task. So our second research question is

- Is it possible to identify the long-term land cover variation in the upper catchments of the Yellow River based on remote sensing and GIS?

After spatial land cover variation with MODIS series was analysed in Chapter 2, the long-term land cover variation was analysed in Chapter 3. The temporal variation in land cover can be assessed from remote sensing (RS) data as the Landsat satellite was launched in 1974. Landsat Multispectral Scanner (MSS) and Thematic Mapper (TM) data were applied to produce land cover maps for the years 1977 and 2006. In combination with data from the national Chinese land cover database

from 1996 and 2000, the data in these four years were applied to analyse land cover dynamics over three decades.

Three-decades of successive hydropower exploitation has occurred in the study area. It was noted that the area of grassland decreased and other five types of land covers increased. The grassland area decreased 120 000 ha over 30 years. After eight dams came into operations, the water area increased from 53919 ha to 78124 ha. The largest annual rate of land cover change was found for construction land, whose annual increase rate was about 17.4%. The analytical technique has proven to be an effective procedure for identifying long-tern land cover impacts induced by hydroelectric cascade exploitation.

Landscape ecology has been defined as the study of land cover pattern change from the perspective of ecology (Turner, 1989). One major landscape change resulting from hydroelectric cascade exploitation is the development of successive dams in a watershed. One systematic approach to assess the accumulated impact of hydroelectric cascade exploitation on ecosystems is to observe the ecosystem pattern changes with methods derived from landscape ecology (Sternberg, 2006). In particular, the combination of GIS and the FRAGSTATS model greatly increase the efficiency of landscape analysis (Tinker et al, 2003). Our third research question, therefore, is

- Are there the accumulated impacts of landscape pattern variation with hydroelectric cascade exploitation? If so, how to calculate and express them?

The change of land cover over three decades was analysed in Chapter 3. The landscape pattern was analysed from an ecological prospective. With land cover data in a time-series of four dates from 1977 to 2006, the temporal and spatial landscape characteristics when exploiting hydroelectric dam (cascades) were analysed. According to the metrics applied, the regional landscape changed into more fragmented zones, especially the grassland, farmland and open water. The regional landscape shape characteristics became more complex after three decades. Three landscape diversity simulators proved that regional landscape diversity levels increased in the period between 1977 and 2006.

Grassland and open water were selected as two typical landscapes to describe the relationship with hydroelectric cascade exploitation. Correspondingly, the summed dam heights and accumulated hydroelectric generator capacities were selected to express the degree of hydroelectric cascade exploitation from 1977 to 2006. The regression models between the two indicators revealed that landscape fragmentation variation had a strong relationship with hydroelectric cascade exploitation. The coefficient of determination between three landscape fragmentation metrics and two independents ranged from 0.65

to 0.95. The six exponential models of three diversity metrics also gave logical results as demonstrated by their high correlation coefficients, between 0.75 and 0.99.

In conclusion, landscape fragmentation, shape and diversity appeared have a strong connection with the degree of hydroelectric cascade exploitation development. The landscape pattern can be predicted under different scenarios of hydroelectric cascade exploitation, which is helpful for regional environmental management.

The impact of a single dam on land cover and landscape pattern has been studied. To the best of our knowledge, it is the first successful case in which the accumulated impacts from a cascade of dams over a long period has been studied. Hence, we believe that this work presents a step forward in the application of remote sensing and GIS techniques.

9.2.2 Soil erosion dynamics response to landscape pattern and vegetation

Regional landscape variation often results from the transformation of land cover and hydrological conditions, which in turn affects the amount of soil erosion initiation and transportation to the water body (Bakker et al., 2008). Understanding the spatial distribution and long-term dynamic principles of soil erosion is the basis for effective regional land cover management and soil erosion prevention (Irvem et al., 2007). Soil erosion research requires regular field experiments or long-term monitoring, which is both expensive and time consuming (Siegrist, et al., 1998). In this context, the application of a watershed simulation model may be useful. A physically based watershed modelling approach may consider many factors, leading to the temporal and spatial quantification of soil erosion load. Our fourth research question is

- Is long-term land cover and landscape pattern changes interacting with soil erosion? Is there any possibility that landscape pattern can be used to prevent erosion

As Chapter 3 indicated, the area of grassland decreased and other five types of land cover increased, and such changes have impacts on soil erosion. With the four-year land cover, a Soil Water Assessment Tool (SWAT) model led to an accurate assessment of erosion in the upper watershed of the Yellow River between 1977 and 2006. Using water flow and sand density data as parameters, the regional soil erosion load was simulated. Chapter 5 showed that the decadal decrease of grassland area did not pose a significant threat to soil erosion load, while the continual increase of bare land, water area and farmland increased soil erosion. When the impact of precipitation was considered, the land cover types had significant relationship with treated soil erosion. Forest and grassland fit a positive correlation model while the other four types fit negative equations. Most of land cover types had close relation with soil erosion,

which allowed us to conclude that watershed erosion was the integrated result of diverse land cover types.

The landscape patterns of different land covers in a watershed also affect the soil erosion process. The patch correlation indicated that contagious grassland patches reduced soil erosion yields. The increase in the number of grassland patches led to more patch edges, which in turn increased the sediment transportation from the patch edges. Correlation of patch level characteristics with soil erosion was also analysed. The grassland patch density and edge density analysis demonstrated that smaller patch size and more patch edge led to lower load because erosion was a function of patch edge, and not of the whole patch area. These findings enhance our understanding of the temporal variation in soil erosion processes, which is the basis for preventing local pollution. A principal component analysis showed that grassland and open water were the principal variable dependents in six landscapes.

Soil erosion is considered to deteriorate on-site soil quality in an irreversible way and is quantified by the average amount of soil removed from a defined area over a given period (Munro et al., 2008). Sediment yield is the amount of soil removed to rivers and lakes in a given period over a defined area, which is an important process in catchment soil erosion (Tripathi et al., 2003; Sutherland and Ziegler, 2007). Among the factors influencing soil erosion, soil properties and topography can be considered constant in the short term, so that land cover and climatic features are the dominant variables influencing the erosion process in the short term (Marques et al., 2007). Consequently, a vegetation index (such as NDVI) can be used to integrate land cover and climatic features, which influence watershed soil erosion and sediment yield. Our fifth research question is

- What are the temporal-spatial interactions of soil erosion loading and sediment yields with vegetation NDVI dynamics?

Chapter 6 presented the temporal-spatial correlation of soil erosion with NDVI. The vegetation zones of higher NDVI not only prevent sediment transportation, but also are the main source of soil erosion. Based on the outcomes of the present modelling, it appears that regional soil erosion was concentrated on the eastern farmlands and southern mountain areas. At a monthly scale, correlation analysis indicated that the vegetation NDVI peak period was the proper period for soil erosion conservation. With the threshold point in the trend-line of general correlation equations, soil erosion and sediment transportation can be assessed and conserved. Storm rain run-off has intense impacts on soil erosion processes, but cannot be expressed in the slow NDVI variation, which decreases the coefficient of determination.

9.2.3 Non-point source pollution dynamics response to landscape pattern and vegetation

With the increasing importance of protecting natural water resources, a number of studies have been carried out to assess non-point source pollution (Duchemin and Hogue, 2009). Non-point source pollution has increased in concentration in river basins and has attracted wide attention (McFarland and Hauck, 2001). Because of the temporal and spatial variability in processes, regular monitoring requires a large investment. As a result, watershed-scale modelling of non-point source pollution has become useful and popular (Easton et al., 2008). Vegetation cover status has been recognized as major factor contributing to watershed non-point source nutrient pollution movement (Bouldin et al., 2004). With the four-year land cover data and results in Chapter 3, the SWAT model system can provide more accurate results about nitrogen and phosphorus pollutions. Our sixth research question is

- Are land cover and landscape pattern changes correlated with non-point source nutrient pollution variation? Is there any possibility that an understanding of the function of vegetation landscape pattern can be used in preventing pollution?

In Chapter 7, we examine the interactions of grassland, forest and farmland areas, landscape pattern with the non-point source nitrogen and phosphorus loading. The models correlating different landscape indicators and diverse formats of non-point source nutrient pollution loading suggest that landscape pattern of vegetative cover had a direct effect on non-point source nutrient pollution. The grasslands with more patch edges may reduce non-point source loads. Although forest was the partial contributor for non-point source phosphorus pollution, a simple shape of forest landscape can decrease P loads. These results suggest effects of landscape design on non-point source nutrient loads could lead to economic solutions to reduce non-point source loading.

The watershed-land cover variation and its impact on non-point source nutrient pollution can lead to serious water quality problems (George et al., 2008). Most non-point source modelling systems have the ability to estimate the discharge of annual nitrogen and phosphorus loads (Flipo et al., 2007). MODIS has been popularly applied to a variety of projects involving large scale vegetation dynamics and land coverage research (Wardlow and Egbert, 2008). The integration of the non-point source simulation model and GIS can accelerate the procedures for water quality management in a river basin, and this combined system is an effective method for identifying the influence of land cover variation as at temporal-spatial scale (Ning et al., 2006). Our seventh research question is

- What are the temporal-spatial interactions of non-point source nutrient pollution loading with vegetation NDVI dynamics?

Chapter 8 explores the integration of non-point source modelling and land cover monitoring by remote sensing to understand the interactive dynamics of non-point source nutrient loading. A Soil Water Assessment Tool (SWAT) model was enhanced and the non-point source nutrient pollutants estimated. The results in this chapter confirmed that: (i) the area with steeper slopes and higher NDVI contributed most to the non-point source (NPS) nutrient load. (ii) Managing the temporal-spatial variation of nutrients discharges by manipulating land cover could prevent non-point source (NPS) pollution and improve water quality.

At the watershed scale, the first step in pollution control is to identify the temporal-spatial feature of the pollution sources. The analysis indicated that, during the period of vegetation growth and maturity, increased NDVI and associated precipitation increased non-point source pollution loadings, which certainly impacted the water quality.

The findings in this study imply that during the design of soil erosion and non-point source pollution control, the vegetation status should first be investigated. The role of landscape pattern in soil erosion and non-point source pollution transportation should be identified. The remote sensing and modelling based approach discussed in this study can be applied in regular pollution assessment and environmental management.

9.3 Future work

Temporal-spatial dynamics of watershed land cover, landscape characteristic with their influences on soil erosion and non-point source nutrients pollution were the emphasis of this study. However, this study has not covered all the environmental processes related to regional environmental assessment. There are some important aspects that need to be studied with more data; some issues need be assessed objectively with field monitoring in future. Future works related to this study are suggested as follows:

(1) Validating the hydroelectric cascade exploitation impacts

With the two indicators of hydroelectric cascade exploitation, the land cover and landscape variation principles were analysed. The model developed can be used to predict landscape variation with future hydro-exploitation. Now, several hydropower stations are under construction. The land cover and landscape pattern can be analysed by remote sensing images in near future. Then, the predictions made in this thesis may be validated.

(2) Assess the spatial scale effect

Landscape pattern is found to play an important role in soil erosion and nutrients pollution transportation. Actually, the landscape pattern is different at different spatial scales. The calculation at watershed scale,

land cover scale, or patch level will lead to different results. The corresponding soil erosion and nutrients pollution at these spatial scales therefore need to be estimated. The influence of different spatial scales could then be identified, which will widen the potential application of landscape function.

(3) Predicting the climate change impact of non-point source pollution

In this study, the model system works with different land cover and climatic inputs,. However, this study area may be sensitive to global climate changes. If the vegetation variation can be predicted using a climate change model, then the soil erosion and non-point source pollution can be simulated. Such results may help in our understanding of long-term environmental change and its impact on water quality in future.

9.4 Conclusions

This chapter summarizes the research hypotheses tested in this study, and the relations between these hypotheses. Future work related to this study are proposed. The results and conclusions of this study may provide support and advice for the responsible authorities, hydropower exploitation groups and regional environmental protection agencies. The negative and positive impacts of landscape and their impacts on terrestrial environment need to be considered in the management of the regional environment.

Bibliography

Achim Röder, Tobias Kuemmerle, Joachim Hill, 2005. Extension of retrospective datasets using multiple sensors. An approach to radiometric intercalibration of Landsat TM and MSS data. Remote Sensing of Environment, 95(2): 195-210.

Adel Shalaby, Ryutaro Tateishi, 2007. Remote sensing and GIS for mapping and monitoring land cover and land-use changes in the Northwestern coastal zone of Egypt. Applied Geography, 27(1): 28-41.

Ahearn S Dylan., Sheibley W. Richard, Randy A. Dahlgren, Anderson Michael, Johnson Joshua, Tate Kenneth W., 2005. Land use and land cover influence on water quality in the last free-flowing river draining the western Sierra Nevada, California. Journal of Hydrology, 313(3-4): 234-247.

Arnaev J., Larrea V., Ortigosa L., 2004. Surface runoff and soil erosion on unpaved forest roads from rainfall simulation tests in northeastern Spain. CATENA, 57(1): 1-14.

Arnold J.G., Srinivasan R., Muttiah R.S., Williams J.R., 1998. Large area hydrologic modelling and assessment Part I: model development. Journal of the American Water Resources Association 34 (1), 73-89.

Arsenault E, Bonn F, 2005. Evaluation of soil erosion protective cover by crop residues using vegetation indices and spectral mixture analysis of multispectral and hyperspectral data. CATENA**,** 62(2-3): 157-172.

Ashraf M., Kahlown M.A., Ashfaq A., 2007. Impact of small dams on agriculture and groundwater development: A case study from Pakistan. Agricultural Water Management, 92(1-2): 90-98.

Bakker Martha M., Govers Gerard, van Doom Anne, Quetier Fabien, Chouvardas Dimitris, Rounsevell Mark, 2008. The response of soil erosion and sediment export to land-use change in four areas of Europe: The importance of landscape pattern. Geomorphology, 98(3-4):213-226.

Beaulac, M.N., Reckhow K.H., 1982. An examination of land use-Nutrient export relationships. Water Resources Bulletin 18:1013-1024.

Behera S., Panda R.K., 2006. Evaluation of management alternatives for an agricultural watershed in a sub-humid subtropical region using a physical process based model. Agriculture, Ecosystems & Environment, 113(1-4): 62-72.

Belda F., Melia J., 2000. Relationships between climatic parameters and forest vegetation: application to burned area in Alicante (Spain). Forest Ecology and Management, 135(1-3), 195-204.

Borin Maurizio, Tocchetto Davide, 2007. Five year water and nitrogen balance for a constructed surface flow wetland treating agricultural drainage waters. Science of total environment. 380(1-3): SI:38-47.

Bouldin J.L., Farris J.L., Moore M.T., Cooper C.M., 2004. Vegetative and structural characteristics of agricultural drainages in the Mississippi Delta landscapes. Environmental Pollution, 132(3): 403-411.

Bowes Michael J., Smith Jim T., Jarvie Helen P., Neal Colin, 2008. Modelling of phosphorus inputs to rivers from diffuse and point sources. Science of The Total Environment, 395(2-3):125-138.

Brunsell N.A., 2006.Characterization of land-surface precipitation feedback regimes with remote sensing. Remote Sensing of Environment, 100(2): 200-211.

Bunkei Matsushita, Ming Xub, Takehiko Fukushima, 2006. Characterizing the

changes in landscape structure in the Lake Kasumigaura Basin, Japan using a high-quality GIS dataset. Landscape and Urban Planning, 78: 241–250.

Carlson T.N., Arthur S.T., 2000. The impact of land use - land cover changes due to urbanization on surface microclimate and hydrology: a satellite perspective. Global and planetary change, 25 (1-2): 49-65.

Carrera-Hernandez J.J., Gaskin S.J., 2007. Spatio temporal analysis of daily precipitation and temperature in the Basin of Mexico. Journal of Hydrology, 336(3-4), 231-249.

Chang Heejun, 2008. Spatial analysis of water quality trends in the Han River basin, South Korea. Water Research, 42(13):3285-3304.

Chen J.S., He D.W., Cui S.B., 2003. The response of river water quality and quantity to the development of irrigated agriculture in the last 4 decades in the Yellow River Basin, China. Water Resources Research, 39(3):1047.

Corry R.C., 2005. Characterizing fine-scale patterns of alternative agricultural landscapes with landscape pattern indices. Landscape Ecology, 20(5): 591-608.

Coulson R.N., Pinto M.A., Tchakerian M.D., Baum K.A., Rubink W.L., Johnston J.S., 2005. Feral honey bees in pine forest landscapes of east Texas. Forest Ecology and Management, 215 (1-3): 91-102.

Cumming S., Vernier P., 2002. Statistical models of landscape pattern metrics, with applications to regional scale dynamic forest simulations. Landscape Ecology, 17(5): 433-444.

Davison P., Hutchins M.G., Anthony S.G., Betson M., Johnson C., Lord E.I., 2005. The relationship between potentially erosive storm energy and daily rainfall quantity in England and Wales. Science of The Total Environment, 344(1-3):15-25.

de Vente Joris, Poesen Jean, Verstraeten Gert, Van Rompaey Anton, Govers Gerard, 2008. Spatially distributed modelling of soil erosion and sediment yield at regional scales in Spain. Global and Planetary Change, 60(3-4):393-415.

del Mar Lopez Tania, Aide T. Mitchell, Scatena F. N., 1998. The effect of land use on soil erosion in the Guadiana watershed in Puerto Rico. Caribbean Journal of Science, 34 (3-4): 298-307.

Duchemin Marc, Hogue Richard, 2009. Reduction in agricultural non-point source pollution in the first year following establishment of an integrated grass/tree filter strip system in southern Quebec(Canada). Agriculture, Ecosystems & Environment, 131(1-2), SI: 85-97.

Easton Zachary M., Fuka Daniel R., Walter M. Todd, Cowan Dillon M., Schneiderman Elliot M., Steenhuis, Tammo S., 2008. Re-conceptualizing the soil and water assessment tool (SWAT) model to predict runoff from variable source areas. Journal of Hydrology, 348(3-4): 279-291.

Edwards A.C., Withers P.J.A., 2008. Transport and delivery of suspended solids, nitrogen and phosphorus from various sources to freshwaters in the UK. Journal of Hydrology, 350(3-4), 144-153.

Engel F.L., Bertol I., Ritter S.R., Gonzalez A.Paz, Paz-Ferreiro J., Vazquez E. Vidal, 2009. Soil erosion under simulated rainfall in relation to phenological stages of soybeans and tillage methods in Lages, SC, Brazil. Soil & Tillage Research. 103(2): 216-221.

Fabio Maselli, 2004. Monitoring forest conditions in a protected Mediterranean coastal area by the analysis of multiyear NDVI data. Remote Sensing of

Environment**,** 89(4): 423-433.

Fearer M. Todd, Prisley P. Stephen, Stauffer F. Dean, Keyser D. Patrick, 2007. A method for integrating the Breeding Bird Survey and Forest Inventory and Analysis databases to evaluate forest bird–habitat relationships at multiple spatial scales. FOREST ECOL MANAG, 243(1): 128-143.

Feng J.M., Wang T., Qi S.Z., Xie C.W., 2005. Land degradation in the source region of the Yellow River, northeast Qinghai-Xizang Plateau: classification and evaluation. Environmental geology, 47 (4):459-466.

Fensholt R., Sandholt I., Rasmussen M.S., 2004. Evaluation of MODIS LAI, fAPAR and the relation between fAPAR and NDVI in a semi-arid environment using in situ measurements. Remote Sensing of Environment, 91 (3-4): 490-507.

Flipo Nicolas, Jeannée Nicolas, Poulin Michel, Even Stéphanie, Ledoux Emmanuel, 2007. Assessment of nitrate pollution in the Grand Morin aquifers (France): Combined use of geostatistics and physically based modelling. Environmental Pollution, 146(1): 241-256.

Fox D.M., Bryan R.B., 2000. The relationship of soil loss by interrill erosion to slope gradient CATENA, 38(3): 211-222.

Fritts H.C., 1974. Relationships of ring widths in arid-site conifers to variations in monthly temperature and precipitation. Ecological Monographs, 44, 411-440.

Garrigues S., Allard D., Baret F., 2008. Modelling temporal changes in surface spatial heterogeneity over an agricultural. Site. Remote Sensing of Environment, 112(2): 588-602.

Gordon Eric, Meentemeyer Ross K., 2006. Effects of dam operation and land cover on stream channel morphology and riparian vegetation. Geomorphology, 82(3-4): 412-429.

George N. Zaimes, Richard C. Schultz, Thomas M. Isenhart, 2008. Total phosphorus concentrations and compaction in riparian areas under different riparian land-uses of Iowa. Agriculture, Ecosystems & Environment, 127, Issues (1-2): 22-30.

Gorsevski Pece V., Boll Jan, Gomezdelcampo Enrique, Brooks Erin S, 2008. Dynamic riparian buffer widths from potential non-point source pollution areas in forested watersheds. Forest Ecology and Management, 256(4): 664-673.

Gowda H. Prasanna, Mulla J. David, Jaynes B Dan, 2008. Simulated long-term nitrogen losses for a midwestern agricultural watershed in the United States. Agricultural Water Management, 95(5): 616-624.

Han S.Y., Kwak SeungJun, Yoo SeungHoon, 2008. Valuing environmental impacts of large dam construction in Korea: An application of choice experiments. Environmental Impact Assessment Review, 28(4-5): 256-266.

Hansen M.C., DeFries R., Townshend S., Sohlberg R., Dimiceli C., Carroll M., 2002. Towards an operational MODIS continuous field of percent tree cover algorithm: Examples using AVHRR and MODIS data. Remote Sensing of Environment, 83(1-2), 303-319.

Haregeweyn Nigussie, Yohannes Fekadu, 2003. Testing and evaluation of the agricultural non-point source pollution model (AGNPS) on Augucho catchment, western Hararghe, Ethiopia. Agriculture, Ecosystems & Environment, 99(1-3): 201-212.

Hartanto H., Prabhu R., Widayat A.S.E., Asdak C., 2003. Factors affecting runoff and soil erosion: plot-level soil loss monitoring for assessing sustainability of forest management. Forest Ecology and Management, 180(1-3): 361-374.

Hefting MM, de Klein JJM, 1998. Nitrogen removal in buffer strips along a lowland stream in the Netherlands: a pilot study. Environmental Pollution, 102: 521-526.

Hessel Rudi, Jetten Victor, 2007. Suitability of transport equations in modelling soil erosion for a small Loess Plateau catchment. Engineering Geology, 91(1): 56-71.

Hogarth W.L., Parlange J.Y., Rose C.W., Sander G.C., Steenhuis T.S., Barry A., 2004. Soil erosion due to rainfall impact with inflow: an analytical solution with spatial and temporal effects. Journal of hydrology, 295(1-4):140-148.

Hooke J.M., 2006. Human impacts on fluvial systems in the Mediterranean region. Geomorphology, 79(3-4): 311-335.

Huang C.C., Pang J., Su H., Yang Q., Ha Y., 2007. Climatic and anthropogenic impacts on soil formation in the semiarid loess tablelands in the middle reaches of the Yellow River, China. Journal of Arid Environments, 71(3): 280-298.

Ierodiaconou D., Laurenson L., Leblanc M., Stagnitti F., Duff G., Sralzman S., Versace V., 2005. The consequences of land use change on nutrient exports: a regional scale assessment in south-west Victoria, Australia. Journal of Environmental Management, 74(4): 305-316.

Irvem Ahmet, Topaloglu Fatih, Uygur Veli, 2007. Estimating spatial distribution of soil loss over Seyhan River Basin in Turkey. Journal of Hydrology, 336(1-2):30-37.

İrvema Ahmet, Topaloğlub Fatih, Uygur Veli, 2007. Estimating spatial distribution of soil loss over Seyhan River Basin in Turkey. Journal of Hydrology, 336 (1-2):30-37.

Jeffrey S.J., Carter J.O., Moodie K.B., Beswick A.R., 2001. Using spatial interpolation to construct a comprehensive archive of Australian climate data. Environmental Modelling & Software, 16(4): 309-330.

Jiao Nianzhi, Zhang Yao, Zeng Yonghui, et al., 2007. Ecological anomalies in the East China Sea: Impacts of the Three Gorges Dam? Water Research, 41(6): 1287-1293.

John K. Maingi, Stuart E. Marsh, 2002. Quantifying hydrologic impacts following dam construction along the Tana River, Kenya. Journal of Arid Environments, 50(1): 53-79.

Johnes, P. J., 1996. Evaluation and management of the impact of land use change on the nitrogen and phosphorus load delivered to surface waters: The export coefficient modelling approach. Journal of Hydrology, 183(3-4): 323-349.

Jørn Stave, Gufu Oba, Nils Chr. Stenseth, et al., 2005. Environmental gradients in the Turkwel riverine forest, Kenya: Hypotheses on dam-induced vegetation change. Forest Ecology and Management, 212: 184-198.

Kjærland Frode, 2007. A real option analysis of investments in hydropower-The case of Norway. ENERG POLICY, 35(11): 5901-5908.

Klaver Gerard, Bertil van O.S., Philippe Negrel, Emmanuelle Petelet Giraud, 2007. Influence of hydropower dams on the composition of the suspended and riverbank sediments in the Danube. ENVIRON POLLUT,

148(3): 718-728.
Koulouri M., Giourga Chr., 2007. Land abandonment and slope gradient as key factors of soil erosion in Mediterranean terraced lands. CATENA, 69(3): 274-281.
Krause Stefan, Jacobs Joerg, Voss Anja, Bronstert Axel, Zehe Erwin, 2008. Assessing the impact of changes in landuse and management practices on the diffuse pollution and retention of nitrate in a riparian floodplain. Science of The Total Environment, 389(1): 149-164.
Leonard B. Lerer, Thayer Scudder, 1999. Health impacts of large dams. Environmental Impact Assessment Review, 19(2), 113-123.
Leone A., Ripa M. N., Uricchio V., Deak J., Vargay Z., 2009. Vulnerability and risk evaluation of agricultural nitrogen pollution for Hungary's main aquifer using DRASTIC and GLEAMS models. Journal of Environmental Management, 90(10): 2969-2978.
Lin G., Phillips S.L., Ehleringer J.R., 1996. Monsoonal precipitation responses of shrubs in a cold desert community on the Colorado Plateau. Oecologia, 106(1): 8-17.
Liu Jiyuan, Liu Mingliang, Tian Hanqin, 2005. Spatial and temporal patterns of China's cropland during 1990–2000: An analysis based on Landsat TM data . Remote Sensing of Environment**,** 98(4): 442-456.
Loboda T.V., Csiszar I.A., 2007. Reconstruction of fire spread within wildland fire events in Northern Eurasia from the MODIS active fire product. Global and planetary change, 56 (3-4): 258-273.
Long H., Mao L.Q., Che Z.X., Yang G.W., 2006. Impact on water resources in Yellow River with climatic change. Journal of Water Resources and Water Engineering, 17(4), 74-77.
Lorenzo Busetto, Michele Meroni and Roberto Colombo, 2008. Combining medium and coarse spatial resolution satellite data to improve the estimation of sub-pixel NDVI time series. Remote Sensing of Environment, 112(1): 118-131.
Maillard Philippe, Pinheiro Santos Nádia Antônia, 2008. A spatial-statistical approach for modelling the effect of non-point source pollution on different water quality parameters in the Velhas river watershed–Brazil. Journal of Environmental Management, 86(1):158-170.
Maillard Philippe, Santos Nádia Antônia Pinheiro, 2008. A spatial-statistical approach for modelling the effect of non-point source pollution on different water quality parameters in the Velhas river watershed – Brazil. Journal of Environmental Management, 86(1): 158-170.
Marques Maria Jose, Bienes Ramon, Jimenez Luis, Perez-Rodriguez Raquel, 2007. Effect of vegetal cover on runoff and soil erosion under light intensity events. Rainfall simulation over USLE plots. Science of the Total Environment, 378(1-2): 161-165.
Matti Kummu, Olli Varis, 2007. Sediment-related impacts due to upstream reservoir trapping, the Lower Mekong River.Geomorphology, 85(3-4): 275-293.
Mattikalli Nandish M., Richards Keith S., 1996. Estimation of surface water quality changes in response to land use change: Application of the export coefficient model using remote sensing and geographical information system. Journal of Environmental Management, 48(3): 263-282.
McAlpine C.A., Syktus J., Deo R.C., Lawrence P.J., McGowan, H.A., Watterson I.G., Phinn S.R., 2007. Modelling the impact of historical land cover

change on Australia's regional climate. Geophysical Research Letters, 34(22): L22711.

McConchie Jack A., Ma Huan-cheng, 2002. A discussion of the risks and benefits of using rock terracing to limit soil erosion in Guizhou Province. Journal of Forestry Research (Harbin). 13(1): 41-47.

McFarland A.M.S., Hauck L.M., 2001. Determining nutrient export coefficients and source loading uncertainty using in stream monitoring data. Journal of the American Water Resources Association, 37(1):223-236.

McGarigal K, Tagil S, Cushman SA, 2009. Surface metrics: an alternative to patch metrics for the quantification of landscape structure LANDSCAPE ECOL, (3):433-450.

McGarigal K., Cushman S.A., Neel M.C., Ene E., 2002. FRAGSTATS: Spatial Pattern Analysis Program for Categorical Maps. Computer software program produced by the authors at the University of Massachusetts, Amherst.

Melville N., Morgan R.P.C., 2001. The influence of grass density on effectiveness of contour grass strips for control of soil erosion on low angle slopes. Soil Use and Management. 17(4): 278-281.

Merrill A.G., Benning T.L., 2006. Ecosystem type differences in nitrogen process rates and controls in the riparian zone of a montane landscape. Forest Ecology and Management, 222(1-3): 145-161.

Misgana K. Muleta, John W. Nicklow, 2005. Sensitivity and uncertainty analysis coupled with automatic calibration for a distributed watershed model. Journal of Hydrology, 306(1-4): 127-145.

Mulungu Deogratlas M.M., Munishi Subira E., 2007. Simiyu River catchment parameterization using SWAT model. Physics and Chemistry of the Earth, Parts A/B/C, 32(15-18): 1032-1039.

Munodawafa Adelaide, 2007. Assessing nutrient losses with soil erosion under different tillage systems and their implications on water quality. Physics and Chemistry of the Earth, 32(15-18): 1135-1140.

Munro R. Neil, Deckers J., Haile Mitiku, Grove A.T.,Poesen J., Nyssen J., 2008. Soil landscapes, land cover change and erosion features of the Central Plateau region of Tigrai, Ethiopia: Photo-monitoring with an interval of 30 years. CATENA, 75(1):55-64.

Neal C., Reynolds B., Neal M., Hughes S., Wickham H., Hill L., Rowland P., Pugh B., 2003. Soluble reactive phosphorus levels in rainfall, cloud water, through fall, stem flow, soil waters, stream waters and ground waters for the Upper River Severn area, Plynlimon, mid Wales. Science of the total environment, 314(10): 99-120.

Neel M.C., McGarigal K., Cushman S.A., 2004. Behavior of class-level landscape metrics across gradients of class aggregation and area. Landscape ecology, 19 (4): 435-455.

Ning S.K., Chang N.B., Jeng K.Y., Tseng Y.H., 2006. Soil erosion and non-point source pollution impacts assessment with the aid of multi-temporal remote sensing images. Journal of Environmental Management, 79(1): 88-101.

Nyakatawa E.Z., Jakkula V., Reddy K.C., Lemunyon J. L., Norris B. E., Jr., 2007. Soil erosion estimation in conservation tillage systems with poultry litter application using RUSLE 2.0 model. Soil and Tillage Research, 94(2):410-419.

O'Geen A.T., Maynard J.J., DahlgrenR.A., 2007. Efficacy of constructed wetlands to mitigate non-point source pollution from irrigation tailwaters

in the San Joaquin Valley, California, USA. Water Science and Technology. 55(3): 55-61.

Oki Kazuo, Yasuoka Yoshifumi, 2008. Mapping the potential annual total nitrogen load in the river basins of Japan with remotely sensed imagery. Remote Sensing of Environment, 112 (6): 3091-3098.

Okin G.S., Murray B., Schlesinger W.H., 2001. Degradation of sandy arid shrubland environments: observations, process modelling, and management implications. Journal of Arid Environments, 47(2): 123-144.

Ouyang Wei, Hao Fanghua, Wang Xuelei, 2008. Regional non point source organic pollution modelling and critical area identification for watershed best environmental management. Water, Air, & Soil Pollution, 187(1-4): 251-261.

Ouyang Wei, Hao Fanghua, Wang xuelei, Cheng Hongguang, 2008. Non point source pollution responses simulation for conversion cropland to forest in mountains by SWAT in China. Environmental Management, 41(1): 79-89.

Ouyang Wei, Skidmore, A.K., Hao Fanghua, Toxopeus A.G., Abkar Ali, 20009. Accumulated effects on landscape pattern by hydroelectric cascade exploitation in the Yellow River basin from 1977-2006. Landscape and Urban Planning, 93(3-4): 163-171.

Ouyang Wei, Wang Xuelei, Hao Fanghua, Srinivasan R., 2009. Temporal-spatial dynamics of vegetation variation on non-point source nutrient pollution. Ecological Modelling, 220(20): 2702-2713.

Palmer James F., 2004. Using spatial metrics to predict scenic perception in a changing landscape: Dennis, Massachusetts. Landscape and Urban Planning, 69 (2-3): 201-218.

Pamo E. Tedonkeng, Tchamba M.N., 2001. Elephants and vegetation change in the Sahelo-Soudanian region of Cameroon. Journal of Arid Environments, 48(3): 243-253.

Patrick Hostert, Röder Achim, Hill Joachim, 2003. Coupling spectral unmixing and trend analysis for monitoring of long-term vegetation dynamics in Mediterranean rangelands. Remote Sensing of Environment, 87(2-3): 183-197.

Pflugmacher D., Krankina O.N., Cohen W.B., 2007. Satellite-based peatland mapping: Potential of the MODIS sensor. Global and planetary change, 56 (3-4): 248-257.

Piao S.L., Fang J.Y., He J.S., 2006. Variations in vegetation net primary production in the Qinghai-Xizang Plateau, China, from 1982 to 1999. Climatic change, 74 (1-3): 253-267.

Pinho Paulo, Maia Rodrigo, Monterroso Ana, 2007. The quality of Portuguese Environmental Impact Studies: The case of small hydropower projects. ENVIRON IMPACT ASSES, 27(3): 189-205.

Pontus Olofsson, Lars Eklundh, Fredrik Lagergren, Per Jönsson, Anders Lindroth, 2007. Estimating net primary production for Scandinavian forests using data from Terra/MODIS. Advances in Space Research, 39(1): 125-130.

Prasad A.K., Sarkar S., Singh R.P., Kafatos M., 2007. Inter-annual variability of vegetation cover and rainfall over india. Advances in Space Research, 39(1): 79-87.

Qian W.H., Xu T., Quan L.S., 2004. Regional characteristics of dust storms in China. Atmospheric Environment, 38(29): 4895-4907.

Raines, GL, 2002. Description and comparison of geologic maps with

FRAGSTATS-a spatial statistics program. Computers & Geosciences, 28(2): 169-177.

Rasmus Houborg, Eva Boegh, 2008. Mapping leaf chlorophyll and leaf area index using inverse and forward canopy reflectance modelling and SPOT reflectance data. Remote Sensing of Environment, 112(1): 186-202.

Renard, K.G., Foster, G.A., Weesies, G.A., McCool, D.K., 1997. Predicting soil erosion by water: a guide to conservation planning with RUSLE. USDA. Agriculture Handbook No. 703. Washington, DC.

Ribarova Irina, Ninov Plamen, Cooper David, 2008, Modelling nutrient pollution during a first flood event using HSPF software: Iskar River case study, Bulgaria. Ecological Modelling, 211(1-2):241-246.

Running S.W., Justice C.O., Salomonson V., Hall D., Barker J., Kaufmann Y.J., Strahler A.H., Huete A.R., Muller J.-P., Vanderbilt V., Wan Z.M., Teillet P., Carneggie D., 1994. Terrestrial remote sensing science and algorithms planned for EOS/MODIS. International Journal of Remote Sensing, 15(17): 3587-3620.

Ruysschaert G., Poesen J., Verstraeten G., Govers G.., 2007. Soil loss due to harvesting of various crop types in contrasting agro-ecological environments. Agriculture, Ecosystems & Environment, 120(2-4): 153-165.

Sahin S., Kurum E., 2002. Erosion risk analysis by GIS in environmental impact assessments: a case study—Seyhan Köprü Dam construction. Journal of Environmental Management, 66(3): 239-247.

Schob Annekatrin, Schmidt Juergen, Tenholtern Rolf, 2006. Land abandonment and slope gradient as key factors of soil erosion in Mediterranean terraced lands. CATENA, 68(2-3): 153-160.

Seaquist J.W., Olsson L., Ardö J., 2003. A remote sensing-based primary production model for grassland biomes. Ecological Modelling, 169(1): 131-155.

Siegrist S., Schaub D., Pfiffner L., Mader P., 1998. Does organic agriculture reduce soil erodibility? The results of a long-term field study on loess in Switzerland Agriculture, Ecosystems & Environment, 69(3):253-264.

Siepel A.C., Steenhuis T.S., Rose C.W., Parlange J.Y., McIsaac G.F., 2002. A simplified hillslope erosion model with vegetation elements for practical applications. Journal of Hydrology, 258(1-4): 111-121.

Siepel A.C., Steenhuis T.S., Rose C.W., Parlange J.Y., McIsaac G.F., 2002. A simplified hillslope erosion model with vegetation elements for practical applications. Journal of Hydrology, 258(1-4): 111-121.

Sternberg R., 2006. Damming the river: a changing perspective on altering nature. RENEW SUST ENERG REV, 10(3): 165-197.

Sutherland Ross A., Ziegler Alan D., 2007. Effectiveness of coir-based rolled erosion control systems in reducing sediment transport from hillslopes. Applied Geography, 27(3-4): 150-164.

Ta W.Q., Xiao H.L., Dong Z.B., 2008, Long-term morphodynamic changes of a desert reach of the Yellow River following upstream large reservoirs' operation. Geomorphology. 97(3-4):249-259

Thórhallsdóttir Ellen Thóra, 2007. Strategic planning at the national level: Evaluating and ranking energy projects by environmental impact. Environmental Impact Asses, 27(6): 545-568.

Thwaites N. Robin, Slater K. Brian, 2000. Soil–landscape resource assessment for plantations—a conceptual framework towards an explicit multi-scale approach. Forest Ecology and Management, 138(1-3):123-138.

Tinker D.B., Romme W.H., Despain D.G., 2003. Historic range of variability in landscape structure in subalpine forests of the Greater Yellowstone Area, USA. Landscape Ecology, 18 (4): 427-439.

Tripathi M. P., Panda R. K., Raghuwanshi N. S., 2003. Identification and Prioritisation of Critical Sub-watersheds for Soil Conservation Management using the SWAT Model. Biosystems Engineering, 85(3): 365-379.

Turner M.G., 1989. Landscape ecology: the effect of pattern on process. ANNU REV ECOL EVOL S, 20, 171–197.

Uuemaa Evelyn, Jüri Roosaare, Arno Kanal, Ülo Mander., 2008. Spatial correlograms of soil cover as an indicator of landscape heterogeneity. ECOL INDIC, 8(6): 783-794.

Vanacker, V., Govers, G., Barros, S., Poesen J., Deckers J., 2003. The effect of short-term socio-economic and demographic change on landuse dynamics and its corresponding geomorphic response with relation to water erosion in a tropical mountainous catchment, Ecuador. Landscape Ecology 18: 1-15.

Vicente Serrano S.M., Cuadrat Prats J.M., Romo A., 2006. Aridity influence on vegetation patterns in the middle Ebro Valley (Spain): Evaluation by means of AVHRR images and climate interpolation techniques. Journal of Arid Environments, 66(2): 353-375.

Vienneau D., de Hoogh K., Briggs D., 2009. A GIS-based method for modelling air pollution exposures across Europe. Science of The Total Environment, 408(2): 255-266.

Viotti P., Liuti G., Di Genova P., 2002. Atmospheric urban pollution: applications of an artificial neural network (ANN) to the city of Perugia. Ecological Modelling, 148(1): 27-46.

Vrieling Anton, de Jong Steven M., Sterk Geert, Rodrigues Silvio C., 2009. Timing of erosion and satellite data: A multi-resolution approach to soil erosion risk mapping. International Journal of Applied Earth Observation and Geoinformation, 10(3): 267-281.

Wang D., Fu B.J., Zhao W.W., Hu H.F., Wang Y.F., 2008. Multifractal characteristics of soil particle size distribution under different land-use types on the Loess Plateau, China. CATENA, 72(1): 29-36.

Wang G.X., Cheng G.D., Shen Y.P., Qian J., 2003. Influence of land cover changes on the physical and chemical properties of alpine meadow soil. Chinese science bulletin, 48 (2): 118-124.

Wang H.J., Yang Z.S., Yoshiki Saito, Liu J. Paul, Sun X.X., Wang Y., 2007. Stepwise decreases of the Huanghe (Yellow River) sediment load (1950–2005): Impacts of climate change and human activities. Global and Planetary Change, 57(3-4): 331-354.

Wang X.D., Li M.H., Liu S.Z., Liu G.C., 2006. Fractal characteristics of soils under different land-use patterns in the arid and semiarid regions of the Tibetan Plateau, China. Geoderma, 134(1-2): 56-61.

Wardlow D. Brian, Egbert L. Stephen, 2008. Large-area crop mapping using time-series MODIS 250 m NDVI data: An assessment for the U.S. Central Great Plains. Remote Sensing of Environment, 112(3): 1096-1116.

Weiss, J.L., Gutzler, D.S., Gutzler D.S., Coonrod J.E.A., Dahm C.N., 2004. Long-term vegetation monitoring with NDVI in a diverse semiarid setting, central New Mexico, USA. Journal of Arid Environments, 58(2): 249-272.

Weng YenChu, 2007. Spatiotemporal changes of landscape pattern in

response to urbanization. Landscape and Urban Planning, 81(4): 341-353.
William L Stefanov., Maik Netzband, 2005. Assessment of ASTER land cover and MODIS NDVI data at multiple scales for ecological characterization of an arid urban center. Remote Sensing of Environment, 99(1-2): 31-43.
Williams, J.R. 1995. Chapter 25. The EPIC Model. In Computer Models of Watershed Hydrology. Water Resources Publications. Highlands Ranch, CO. p. 909-1000.
Wilson G.V., Cullum R.F., Römkens M.J.M., 2008. Ephemeral gully erosion by preferential flow through a discontinuous soil-pipe. CATENA, 73(1): 98-106.
With K.A., King A.W., 1999. Dispersal success on fractal landscapes: a consequence of lacunarity thresholds. LANDSCAPE ECOL, 14:73-82.
Wood Pal. J., 2007. Hydroecology and ecohydrology: Past, Present and Future. John Wiley and Sons, Ltd. ISBN: 978-0-470-01017-4.
Worrall F., Burt T. P., 2001. Inter-annual controls on nitrate export from an agricultural catchment — how much land-use change is safe? Journal of Hydrology, 243(3-4): 228-241.
Xian George, Crane Mike, Su Junshan, 2007. An analysis of urban development and its environmental impact on the Tampa Bay watershed. Journal of Environmental Management, 85(4): 965-976.
Xiao H., Ji W., 2007. Relating landscape characteristics to non-point source pollution in mine waste-located watersheds using geospatial techniques. Journal of Environmental Management, 82: 111-119.
Xiao H.G., Ji W., 2007. Relating landscape characteristics to non-point source pollution in mine waste-located watersheds using geospatial techniques. Journal of Environmental Management, 82(1):111-119.
Xu J.X., Yan Y.X., 2005. Scale effects on specific sediment yield in the Yellow River basin and geomorphological explanations. Journal hydrology, 307(1-4): 219-232.
Yang J.P., Ding Y.J., Chen R.S., 2006. Spatial and temporal of variations of alpine vegetation cover in the source regions of the Yangtze and Yellow Rivers of the Tibetan Plateau from 1982 to 2001. Environmental Geology, 50(3): 313-322.
Yang S.T., Cheng H.G., Bu Q.S., Zhang J.Y., Shi X.X., 2006. Estimation of soil erosion and its application in assessment of the absorbed nitrogen and phosphorus load in China. Acta Scientiae Circumstantiae, 26(3): 366-374.
Yuksek Omer, Komurcu Murat Ihsan, Yuksel Ibrahim, Kamil Kaygusuz, 2006. The role of hydropower in meeting Turkey's electric energy demand. ENERG POLICY, 34(17): 3093-3103.
Zaharescu, Dragos G., Hooda Peter S., Soler Antonio P., Fernandez Javier, Burghelea Carmen I., 2009. Trace metals and their source in the catchment of the high altitude Lake Respomuso, Central Pyrenees. Science of The Total Environment, 407(11): 3546-3553.
Zeng Y.N., Feng Z.D., Cao G.C., 2003. Land cover change and its environmental impact in the Upper reaches of the Yellow River, Northeast Qinghai-Tibetan Plateau. Mountain research and development, 23(4): 353-361.
Zhang N., He D.W., Chen J.S., Cui S.B., 2003. A preliminary study on nitrogen contamination in the Yellow River system, China. Environmental Chemistry, 2(22): 105-110.
Zhang Y., Yang Z.F., Wang X.Q., 2006. Methodology to determine regional

water demand for instream flow and its application in the Yellow River Basin. Journal of Environmental Sciences, 18(5); 1031-1039.

Zhou D.W., Fan G.Z., Huang R.H., Fang Z.F., Liu Y.Q., Li H.Q., 2007. Interannual variability of the normalized difference vegetation index on the Tibetan plateau and its relationship with climate change. Advance in atmospheric science, 24 (3): 474-484.

Author’s biography

Ouyang Wei was born in November 1980 in Jiangxi Province, China.

In 2002 he got the Bachelor Degree on Agricultural Environmental Protection from the Chinese Agricultural University (CAU). He acquired Professional Master Degree on Environmental Engineering for School of Environment, Beijing Normal University (BNU) in 2005. After that, he become a Ph.D. candidate in School of Environment, Beijing Normal University. In November 2006, he was awarded a scholarship by the Faculty of Geo-Information Science and Earth Observation (ITC), University of Twente, Enschede, The Netherlands to pursue a PhD Degree (Sandwich) in the Netherlands.

He works at the School of Environment, BNU, China since 2008. He teaches watershed environmental modelling course. His research interests cover watershed environmental management, non-point source pollution simulation, application of 3S tech in environmental management.

Summary

The status of the vegetation in the upper catchments of the Yellow River, of which the dominant cover types are grassland and forest, is critical for the ecological stability of the whole watershed. It can influence strongly the eco-environmental quality, of which soil erosion and non-point source (NPS) pollutants such as nitrogen (N) and phosphorus (P) are the main concerns in regional environmental protection and management. This is especially critical in the upper catchment of the Yellow River, where the original environment is fragile and is subject to increasing human disturbance, particularly hydroelectric cascade exploitation. The long-term land use and landscape pattern variations form a basic index for regional environmental assessment. Furthermore, the changes in land use and landscape pattern variations have impacts on the formation and transport of soil erosion and non-point source nutrient pollutants, which has direct influence on the water quantity and quality in the local watershed (of the upper catchment), but also downstream in the Yellow River basin. The results achieved in this research are now summarized.

Vegetation in the upper catchment of the Yellow River is critical for the ecological stability of the whole watershed. The dominant vegetation cover types in this region are grassland and forest which can influence strongly the eco-environmental quality of the whole watershed. The responses of the NDVI values of the inter-annual grassland and forest condition to three climatic indices (i.e. yearly precipitation, maximum and minimum temperature) were analysed. It is shown that yearly precipitation and maximum temperature had strong correlations with the NDVI values of the two vegetation communities. The NDVI values and the three climatic indices also had strong positive correlations. The monthly correlations provided the threshold values for the three climatic indictors, to be used for simulating vegetation growth in the regional grassland and forest under the climatic indices.

The eco-environmental impacts for dam constructions are a main concern for regional environmental managers. However, there is a widespread lack of detailed data to support systematical assessments of hydropower cascade exploitation induced over long periods. During the period of 1977–2006, the variations of land cover in the upper catchments of Yellow River for successively eight dam constructions were investigated using remote sensing. Landsat imagery were used to produce land cover maps in 1977 and 2006. In combination with data from national land cover database in 1996 and 2000, the data in these four years are applied to analyse land cover dynamics over

three decades. The grasslands have reduced considerably, while the area of the other five categories of land cover increased during the three decades. Furthermore, the conversion area was mapped using transformation matrix analysis, which can assess the impact range for the dam disturbances.

The accumulated impacts of hydroelectric cascade exploitation on the landscape are greater than the simple sum of the impacts from a single dam. The spatial–temporal landscape characteristics resulting from the accumulated impacts of hydroelectric cascade exploitation from 1977 to 2006 in Longliu Watershed, a part of the Yellow River basin, were investigated. Landscape indices were calculated, characterizing landscape in term of its fragmentation, shape and diversity. The analysis revealed that landscape fragmentation depends on the magnitude of exploitation.

Simulating soil erosion variation with a temporal land cover database reveals long-term fluctuations in the landscape pattern. The application of a multi-year land cover database led to an accurate assessment, from 1977 to 2006, of erosion in the upper watershed of the Yellow River. At same time, the impacts of land cover and landscape features on soil erosion load were assessed. A series of supervised land cover classifications of Landsat images characterized variations in land cover and landscape patterns over three decades. A database was constructed with soil properties, climate and elevation data and using water flow and sand density data as parameters, allowing regional soil erosion load to be simulated. The results indicated that decadal decrease of grassland areas did not pose a significant threat to soil erosion, while the continual increase of bare land, water area and farmland increased soil erosion. Regional landscape variation also had a strong relationship with erosion. Patch level landscape analyses demonstrated that larger water areas led to more soil erosion.

Simulations with the use of the Soil and Water Assessment Tool (SWAT) revealed that the annual soil erosion and sediment yield showed spatial distribution patterns, but the monthly variation fluctuated significantly. The inter-annual simulation focused on the spatial difference and interaction with the corresponding vegetation NDVI value for every sub-basin. It was concluded that, for this continental monsoon climate basin, the higher NDVI vegetation zones prevented sediment transportation.

The interaction of landscape transformation with the simulated non-point source pollutants (i.e. nitrogen and phosphorus) has been

studied and the influence of vegetation cover on NPS and transportation identified. The regional vegetative cover in 1977, 1996, 2000 and 2006 was determined using historical multi-temporal Landsat imagery and data from the National Landcover Database. The landscape pattern is expressed by means of metrics such as patch density, edge density, and fractal distribution indices. Statistical analysis indicated that the grassland landscapes played a major role in NPS nutrient pollution dynamics. However, the presence of forest and farmland lead to more NPS nitrogen emissions. It was found that grassland areas reduced nitrogen NPS. Farmland was a direct source of organic nutrients, but did not have a great impact on sediment P and soluble N loadings.

It was noted that the temporal variation of land cover NDVI was significantly correlated with NPS nutrient loading and that vegetation prevented NPS nutrient pollution transportation. High loadings of NPS nitrogen in sub-basins with high NDVI indicated that forest and farmland are the main contributing land covers. Most P loadings came from the areas covered with dense grassland and forest, which cannot directly discharge to local water bodies. The interaction of slope, NDVI, and nutrient loading identified that the area with steeper slopes and higher NDVI contributed most of the nutrient loadings.

It is anticipated that these results can provide some supports and provide management advices for the responsible authorities, hydropower exploitation group companies, as well as regional environmental protection agencies.

Samenvatting

De status van de vegetatie in de bovenste stroomgebieden van de Gele Rivier, waar grasland en bos dominant zijn, is van cruciaal belang voor de ecologische stabiliteit van het gehele stroomgebied. Het kan een sterke invloed hebben op de eco-kwaliteit van het milieu, waarvan bodemerosie en diffuse (NPS) nutriënten vervuiling zoals stikstof (N) en fosfor (P) de belangrijkste zorgen zijn voor het regionale milieu bescherming. Deze kwesties zijn vooral belangrijk in het bovenstroomse gebied van de Gele Rivier, waar het oorspronkelijke ecosysteem erg kwetsbaar is door toenemende menselijke verstoring, vooral het bouwen van waterkracht centrales. Variaties in lange termijn landgebruik en landschaps patronen vormen de basis voor de beoordeling van regionale milieueffecten. Bovendien hebben de veranderingen in het landgebruik en in de variaties in het landschaps patroon effect op bodemerosie en op het transport van bodemerosie producten en verontreiniging door nutriënten. Dit heeft rechtstreekse invloed op de waterkwantiteit en-kwaliteit in de lokale waterscheiding (van het bovenstroomse gebied), maar ook stroomafwaarts in het bekken van de Gele Rivier. De in dit onderzoek bereikte resultaten kunnen als volgt worden samengevat:

Vegetatie in de bovenste stroomgebieden van de Gele Rivier is cruciaal voor de ecologische stabiliteit van het gehele stroomgebied. De dominante vegetatie klassen in deze regio, die de milieukwaliteit van het geheel sterk kunnen beïnvloeden, zijn grasland en bos. De inter-jaarlijkse NDVI waarden van grasland en bos samen met drie klimatologische indices (jaarlijkse neerslag en maximum- en minimum temperatuur) werden geanalyseerd. Hieruit bleek dat jaarlijkse neerslag en maximum temperatuur sterke correlaties vertoonden met de NDVI waarden van de twee onderzochte vegetatie klassen (grasland en bos). De NDVI van de vegetatie en de drie klimatologische indices hadden een sterke positieve correlatie. De maandelijkse correlaties gaven de drempelwaarden voor de drie klimatologische indicatoren, die gebruikt kunnen worden voor het simuleren van de vegetatie groei in regionaal grasland en bos onder verschillende klimaat-variabelen.

De milieu effecten, veroorzaakt door dam constructies, zijn de belangrijkste zorgen voor regionaal milieu-management. Er is echter een groot gebrek aan gedetailleerde gegevens om een systematische beoordeling van door waterkracht centrales geïnduceerde effecten gedurende langere periodes te ondersteunen. Daarom zijn gedurende de periode van 1977-2006 de variaties van de bodembedekking in de bovenstroomse gebieden van de Gele Rivier bij acht dam constructies onderzocht met behulp van remote sensing data. Landsat beelden

werden gebruikt voor de productie van vegetatie kaarten voor de situatie in 1977 en 2006. In combinatie met gegevens uit de Nationale Landbedekking Databank van 1996 en 2000 zijn de gegevens van deze vier jaren gebruikt om de vegetatie dynamiek te analyseren voor meer dan drie decennia. De graslanden blijken aanzienlijk in omvang te zijn verminderd, terwijl de overige vijf categorieën bodembedekking groter geworden zijn gedurende deze drie decennia. Bovendien werd het conversie gebied in kaart gebracht door middel van transformatie matrix-analyse, waarin het effect van de verstoringen door de dam constructies kon worden beoordeeld.

De geaccumuleerde effecten van de waterkracht centrales op het landschap zijn groter dan de eenvoudige som van de effecten van een enkele dam. De ruimtelijk-temporele landschappelijke kenmerken die voortvloeien uit de geaccumuleerde effecten van de waterkracht centrales van 1977 tot 2006 in Longliu Watershed, een deel van het stroomgebied van de Gele Rivier, werden onderzocht. Landschap indices, die het landschap karakteriseren in termen van versnippering, vorm en diversiteit, zijn berekend. Uit de analyse bleek dat variaties in de fragmentatie van het landschap sterk afhankelijk waren van de grootte van de waterkracht centrales.

Simulaties van de variatie in bodem erosie met behulp van de Nationale Landbedekking Database onthulde lange termijn schommelingen in de landschappelijke patronen. Het toepassen van de Nationale Landbedekking Database van 1977 tot 2006 heeft geleid tot een nauwkeurige evaluatie van de mate van erosie in het bovenstroomse gebied van de Gele Rivier. Eveneens werden de effecten van de vegetatie en andere landschaps kenmerken op de mate van bodemerosie beoordeeld. Classificatie van de Landsat beelden gaf variaties aan in vegetatie en landschap patronen over meer dan drie decennia. Er werd een database aangelegd met diverse bodem eigenschappen, klimaat en hoogte gegevens, en gebruik makend van gegevens over waterafvoer en bodem structuur waardoor de bodemerosie gesimuleerd kon worden op regionaal niveau. De resultaten toonden aan dat decadale vermindering van de weidegebieden geen toename veroorzaakte in bodem erosie, terwijl bij een toename van bouwrijpe grond en water gebied en een toename van landbouwgrond ook de bodemerosie toenam. Regionale variaties in het landschap hadden ook een sterke relatie met erosie. Landschaps analyses op kleinere schaal toonden aan dat grotere water gebieden leidden tot meer bodemerosie.

Uit simulaties met behulp van de Bodem en Water Assessment Tool (SWAT) is gebleken dat de jaarlijkse bodemerosie en sedimentlast in

het Longliu Bekken ruimtelijke verdelings patronen laten zien, maar dat de maandelijkse variatie sterk schommelde. De inter-jaarlijkse simulatie richtte zich op het ruimtelijke verschil en interactie met de bijbehorende vegetatie NDVI waarde voor elk deelstroom gebied. Geconcludeerd kan worden dat voor het Longliu Bekken, met een continentaal moesson klimaat, de vegetatiezones met een hogere NDVI sediment transport verhinderen.

De veranderingen in het landschap onder invloed van gesimuleerde NPS stikstof en fosfor hoeveelheden werden onderzocht en de invloed van vegetatie op NPS verontreiniging en het afvoer daarvan werd ook vastgesteld. De regionale vegetatieve bedekking in 1977, 1996, 2000 en 2006 werd bepaald met behulp van historische multi-temporele Landsat beelden en gegevens van de Nationale Landbedekking Database. Het landschaps patroon werd uitgedrukt in eenheden zoals patch dichtheid, rand-dichtheidswaarden en/of fractale distributie-index. Statistische analyses gaven aan dat grasland een belangrijke rol speelde in de NPS nutriënten verontreiniging. De aanwezigheid van bos en landbouwgrond leidde echter tot meer NPS stikstof emissies. Verder bleek dat weidegebieden NPS stikstof hadden. Landbouwgrond was de directe bron van organische voedingsstoffen, maar had geen grote gevolgen voor de hoeveelheid fosfor en.

De temporele variatie in NDVI van de bodembedekking was significant gecorreleerd met de hoeveelheid NPS nutriënten en dat de afvoer van de verontreinigende NPS nutriënten door vegetatie werd verminderd. Hoge belastingen van NPS stikstof in het deelstroomgebieden met hoge NDVI waarden gaven aan dat bos en landbouwgrond de belangrijkste gebieden waren waar nutriënten verloren gingen. Het meeste fosfor kwam uit die gebieden, die bedekt zijn met grasland en bos met hoge NDVI waarden en die niet direct konden afwateren aan de lokale waterlichamen. Verder bleek dat gebieden met een steilere helling en een hogere NDVI voor het merendeel verantwoordelijk waren voor het nutriënt gehalte.

Verwacht wordt dat bovengenoemde resultaten gebruikt kunnen worden ter ondersteuning van adviezen voor de verantwoordelijke autoriteiten, waterkracht exploitanten en voor regionale bureaus voor milieubescherming.

ITC Dissertation List

http://www.itc.nl/Pub/research/Graduate-programme/Graduate-programme-PhD_Graduates.html